# Experimental and Numerical Investigation on Sustainable Machining of Ti6Al4V using Micro-Pillar Texture Tools

Doctoral Thesis

by

Gaurav Saraf

2020MEZ0006



Department of Mechanical Engineering

INDIAN INSTITUTE OF TECHNOLOGY ROPAR

March 2025

# Experimental and Numerical Investigation on Sustainable Machining of Ti6Al4V using Micro-Pillar Texture Tools

A Thesis Submitted

In Partial Fulfillment of the Requirements

for the Degree of

## DOCTOR OF PHILOSOPHY

by

Gaurav Saraf 2020MEZ0006



Department of Mechanical Engineering

INDIAN INSTITUTE OF TECHNOLOGY ROPAR

March 2025

Gaurav Saraf: Experimental and Numerical Investigation on Sustainable Machining of Ti6Al4V using Micro-Pillar Texture Tools
Copyright © 2025, Indian Institute of Technology Ropar All Rights Reserved
ii

# DEDICATED TO FRIENDS AND FAMILY

# **Declaration of Originality**

I hereby declare that the work which is being presented in the thesis entitled **Experimental and Numerical Investigation on Sustainable Machining of** Ti6Al4V using Micro-Pillar Texture Tools has been solely authored by me. It presents the result of my own independent investigation/research conducted during the time period from September 2020 to August 2024 under the supervision of Dr. Chandrakant Kumar Nirala, Associate Professor in the Department of Mechanical Engineering. To the best of my knowledge, it is an original work, both in terms of research content and narrative, and has not been submitted or accepted elsewhere, in part or in full, for the award of any degree, diploma, fellowship, associateship, or similar title of any university or institution. Further, due credit has been attributed to the relevant state-of-the-art and collaborations with appropriate citations and acknowledgements, in line with established ethical norms and practices. I also declare that any idea/data/fact/source stated in my thesis has not been fabricated/ falsified/ misrepresented. All the principles of academic honesty and integrity have been followed. I fully understand that if the thesis is found to be unoriginal, fabricated, or plagiarized, the Institute reserves the right to withdraw the thesis from its archive and revoke the associated Degree conferred. Additionally, the Institute also reserves the right to appraise all concerned sections of society of the matter for their information and necessary action (if any). If accepted, I hereby consent for my thesis to be available online in the Institute's Open Access repository, inter-library loan, and the title & abstract to be made available to outside organizations.

Signature

Name: Gaurav Saraf

Gawan Saraf

Entry Number: 2020MEZ0006

Program: PhD

Department: Mechanical Engineering Indian Institute of Technology Ropar

Rupnagar, Punjab 140001

Date: 28th March 2025



# Acknowledgements

I would like to express my sincere gratitude to the following organizations and personals for their support (technical or personal) for my research work and stay at IIT Ropar during my PhD tenure.

- ❖ Supervisor: Dr. Chandrakant Kumar Nirala (Associate Professor, Mechanical Engineering, IIT Ropar).
- ❖ Doctoral Committee Members: Dr. Ekta Singla (DC-Chairperson), Dr. Anupam Agrawal, Dr. Anshu Dhar Jayal, Dr. Balwinder Sodhi and Dr. Ravi Kant.
- Faculties from Dept. of Mechanical Engineering at IIT Ropar: Prof. Harpreet Singh, Dr. Navaneet K. Marath, Dr. Himanshu Tyagi and Dr. Jitendra Prasad.
- Lab Staff at IIT Ropar: Mr. Varinder Kumar, Mr. Pankaj Thakur, Mr. Rajeev Kumar.
- Workshop Staffs at IIT Ropar: Mr. Rambeer, Mr. Jaswinder, Mr. Girdhari, Mr. Jograj, Mr. Bhupinder, Mr. Randhir, and Mr. Jashkaran.
- Lab Members at IIT Ropar: Mr. Mainak Pal, Mr. Sharib Imam, Mr. Gaurav Sharma, Mr. Anandhu Suresh, Mr. Varun Bhola, Mr. Pranay Kumar, Mr. Rajnish Kumar Mishra, Mr. Dheeraj Singh, Mr. Ninad Hari Sutrave, Mr. Shyamalin Saikia, Mr. Sujit Kadam, Mr. Ishan Arora, Mr. Abhishek Gupta, Mr. Mohd Usama, Mr. Ajit Kumar and Dr. Sohaib Raza.
- Friends and Colleagues at IIT Ropar: Dr. Rakesh Kumar, Dr. Neeraj Deswal, Dr. Dhruva Goyal, Mr. Vinay Gidla, Mr. Sumit Rathor, Mr. Dasari Yogeshwar, Mr. Vikalp Sharma, Mr. Pulak Gupta, Mr. Rajat Dhiman, Mr. Himanshu Shekhar, Mr. Varun Sarkar, Mr. Rahul Kumar and Dr. Nishant Gupta.
- ❖ Institute and PhD Hockey team at IIT Ropar.
- Thanks to all my friends for their motivation and time-to-time support.
- Special thanks should go to my parents and family members, who gave me enormous support. Thank you for your understanding and for providing me with the freedom and time to carry out my Ph.D.

Thank you all... Gaurav Saraf March 2025



## Certificate

This is to certify that the thesis entitled **Experimental and Numerical Investigation on Sustainable Machining of Ti6Al4V using Micro-Pillar Texture Tools**, submitted by **Gaurav Saraf (2020MEZ0006)** for the award of the degree of **Doctor of Philosophy** of Indian Institute of Technology Ropar, is a record of bonafide research work carried out under my guidance and supervision. To the best of my knowledge and belief, the work presented in this thesis is original and has not been submitted, either in part or full, for the award of any other degree, diploma, fellowship, associateship or similar title of any university or institution.

In my opinion, the thesis has reached the standard fulfilling the requirements of the regulations relating to the Degree.

Chandrakant la jurda

Signature of the Supervisor Name- Dr. Chandrakant Kumar Nirala Department- Mechanical Engineering Indian Institute of Technology Ropar Rupnagar, Punjab 140001

Date: 28th March 2025



## **Lay Summary**

Conventional machining is the most widely used manufacturing process for material removal. Generally, every manufactured component undergoes machining as its last finishing operation. High heat and forces are the major challenges associated with this process. The plastic deformation and shearing of the workpiece material generate excessive heat in the machining region. This heat, added to the high compressive forces, leads to tool wear, affecting the efficiency of the process. Generally cutting fluids are used to cool and lubricate the machining region. However, the economic and environmental burden associated with the use of cutting fluids has led the research in the direction of sustainable machining. Machining without the use of cutting fluids is referred to as dry machining. However, the complete adoption of dry machining is challenging due to the aforementioned challenges. A small quantity of cutting fluid mixed with pressurized air, referred to as Minimum Quantity Lubrication (MQL) has emerged as an alternative solution to dry machining. Modifying the surface design of the cutting tools, referred to as textured tools, has also demonstrated the potential for reducing the usage of cutting fluids.

In this thesis, a novel texture tool pattern is proposed, referred to as micro-pillar textured tools. A detailed study of the fabrication of these textures on the surface of cutting tools has been performed. The performance of these tools is explored during the machining of a titanium alloy, with and without the use of cutting fluids. A series of experiments led to a fundamental understanding of the positive alterations introduced in the machining zone due to the presence of these textures. The textures helped reduce the interaction between the fast-moving chips produced during the process and the tool surface. This reduced interaction resulted in improved frictional condition as reflected in the measured forces. Micro-pillar textures also resulted in lower tool temperature due to reduced heat input to the tool and enhanced heat dissipation from the surface of the tool. The improved performance of the textured cutting tools under dry and near-dry conditions is influential in promoting sustainability in metal cutting. It is expected that the knowledge gained from this fundamental study will lead to the development of advanced cutting tools.

## **Abstract**

Continuous shearing of the chip under the condition of seizure at the tool-chip interface has been recognized as a significant source of heat input to the tool. This heat negatively affects the tool as it exhibits high plastic deformation of the sharp cutting edge under high compressive stresses, leading to tool wear. To diminish the severity of this condition, it seems necessary to decrease the chip-tool interface contact and enhance cutting fluid penetration and retention into this seizure zone. However, the use of cutting fluids in metal cutting is questioned due to environmental and biological impacts, encouraging the adoption of dry and near-dry machining to minimize these effects. However, dry machining accelerates tool wear, particularly in difficult-tomachine materials like Titanium and Nickel alloys. Approaches, such as rake surface texturing, address this challenge and promote sustainability in metal cutting. This work proposes a novel texture pattern fabricated on the rake face of tungsten carbide inserts using the Reverse micro electrical discharge machining process. A series of machining experiments under dry, compressed air, minimum quantity lubrication, and wet conditions revealed the potential of this micro-pillar textured tool to enhance its cutting performance. The textured tools can restrict the tool-chip contact area by disrupting the chip flow momentum and inducing tighter curling of the chips. Enhanced capillary suction through these developed texture patterns mitigates work material adhesion on the tool's rake face. The reduced heat input to the tool results in prolonged sharpness retention of the cutting edge, which controls flank wear and surface finish of the machined component. A theoretical estimation based on the minimum energy approach established the occurrence of the rate of total work done minima at a higher shear plane angle compared to a plain tool. A CFD-based numerical approach for inverse estimation of the tool tip temperature revealed the capability of textured tools to restrict the tool temperature, especially under dry condition. The same study further determines the effect of micro-pillar size on heat dissipation capability, revealing that smaller diameter, closed-spaced, and higher-depth textures perform better. It is expected that the knowledge gained from this fundamental study will lead to the development of advanced cutting tools.

**Keywords**: Cutting tools; Surface texture; Machining; Sustainability; RμΕDM; Micro-pillars



#### **List of Publications from Thesis**

#### **Publication in Peer-Reviewed Journals**

1. **Saraf Gaurav**, and Chandrakant K. Nirala. "Novel texture pattern on WC inserts fabricated using Reverse-μEDM for enhanced cutting of Ti6Al4V." *Manufacturing Letters* 36 (2023): 72-75.

https://doi.org/10.1016/j.mfglet.2023.04.001

- 2. **Saraf Gaurav**, Ninad Hari Sutrave, and Chandrakant K. Nirala. "Sustainable approach for machining of Ti6Al4V using micro-pillar textured turning tool insert." *Sustainable Materials and Technologies* 40 (2024): e00929. <a href="https://doi.org/10.1016/j.susmat.2024.e00929">https://doi.org/10.1016/j.susmat.2024.e00929</a>
- 3. **Saraf Gaurav**, and Chandrakant K. Nirala. "Experimental investigation of micropillar textured WC inserts during turning of Ti6Al4V under various cutting fluid strategies." *Journal of Manufacturing Processes* 113 (2024): 61-75. https://doi.org/10.1016/j.jmapro.2024.01.065
- 4. **Saraf Gaurav**, Sharib Imam, and Chandrakant K. Nirala. "Machinability analysis of additively manufactured Ti6Al4V using micro-pillar textured tool under various cutting fluid strategies." *Wear* (2024): 205514. https://doi.org/10.1016/j.wear.2024.205514
- 5. **Saraf Gaurav**, Sharma Gaurav, Kumar Rahul, and Chandrakant K. Nirala. "Experimental and numerical investigation on heat dissipation capability of micropillar textured cutting tools" (Accepted in Scientific Reports)



# **Contents**

Declaration of Originality	v
Acknowledgements	vii
Certificate	ix
Lay Summary	xi
Abstract	xiii
List of Publication from Thesis	XV
Contents	xvii
List of Figures	xxi
List of Tables	XXV
Abbreviations	xxvii
Chapter 1	
Introduction	1
1.1 Sustainable machining	1
1.2 Machining of titanium alloys	4
1.3 Surface texturing of cutting tools	5
1.4 Motivation	6
1.5 Organization of the dissertation	7
Chapter 2	
Literature Survey	9
2.1 Sustainable machining.	9
2.1.1 Dry machining	9
2.1.2 Strategies to adopt sustainable machining	10
2.2 Textured cutting tools	14
2.2.1 Machining performance of textured tools	15
2.2.2 Types of texture patterns	19
2.2.3 Conclusion from the literature	21
2.3 Research gaps	21
2.4 Research Objectives	22
2.5 Research methodology	23
Chapter 3	
Design and development of the novel texture pattern	25
3.1 Design of texture pattern	25
3.2 Development of the texture pattern	26
3.2.1 Preliminary fabrication tests	28
3.2.2 Textured tools	32

<b>3.3 Chap</b>	ter conclusion	. 34
Chapter 4	4	
	nal machining of Ti6Al4V using textured tool under dry	. 35
	rimental plan	
4.1.1	Orthogonal machining	
4.1.2	Selection of process parameters	. 36
4.1.3	Measurement and characterization of output responses	. 38
4.2 Resu	lts and discussion	. 42
4.2.1	Rake surface morphology	43
4.2.2	Chip morphology	46
4.2.3	Flank surface morphology	48
4.2.4	Force analysis	50
4.2.5	Tool temperature	53
4.3 Theo	retical estimation of shear plane angle	56
4.4 Chap	ter conclusions	60
Chapter 5	5	
Turning conditio	of Ti6Al4V using textured tool under different machining ns	63
5.1 Expe	rimental plan	63
5.1.1	Turning operation	63
5.1.2	Selection of process parameters	64
5.1.3	Measurement and characterization of output responses	65
5.2 Resu	lts and discussion	65
5.2.1	Rake surface morphology	65
5.2.2	Chip morphology	7
5.2.3	Flank face morphology	73
5.2.4	Force analysis	76
5.2.5	Surface roughness analysis	78
5.3 Mach	inability of additively manufactured titanium alloy	79
5.3.1	Tool-chip contact area and force analysis	82
<b>5.4</b> Chap	ter conclusions	84
Chapter	6	
Numeric	al Modeling of tool temperature	85
6.1 Back	ground	85
6.2 Simu	lation procedure and boundary conditions	86
6.2 Gove	rning equations	Q٠

6.4 Results and discussion	89
6.4.1 Temperature measurement at a distant location	89
6.4.2 Analysis of cutting tool temperature using CFD	90
6.5 Chapter conclusion	95
Chapter 7	
Summary, conclusion and future scope	97
7.1 Summary	97
7.1 Conclusions	99
7.2 Future Scope	99
References	101

# **List of Figures**

<b>Figure 1.1</b> Schematic illustration of different shear zones and velocities in orthogonal machining
Figure 1.2 MQL delivery system
<b>Figure 1.2</b> Textured tools: (a) Micro-pillars; (b, c) Micro-grooves: Perpendicular and parallel to cutting edge
Figure 2.1 Benefits and challenges associated with dry machining 10
Figure 2.2 Strategies to adopt sustainable machining
Figure 2.3 Methodology for literature survey
Figure 2.4 Year-wise distribution of articles from various databases
Figure 2.5 Factors contributing to the machining performance improvement of textured tools
Figure 2.6 Research methodology overview
Figure 3.1 Schematic representation of the proposed texture pattern 25
Figure 3.2 Schematic illustration of the fabrication of planar electrode in step I 26
<b>Figure 3.3</b> Schematic illustration of the fabrication of micro-pillars on the cutting tool inserts in step II
Figure 3.4 Experimental setup for LBμM - RμEDM process
<b>Figure 3.5</b> Measured discharge voltage at 100 nF: (a) 90 V; (b) 100 V; (c) 110 V; (d) Magnified view of the capacitor charging and discharging at 110 V
Figure 3.6 Average discharge gap measured at different input voltages 30
<b>Figure 3.7</b> Measured discharge voltage at 110 V: (a) 68 nF; (b) 100 nF; (c) 120 nF; (d) 150 nF
<b>Figure 3.8</b> RμEDM machined surface at 110 V: (a) 68 nF; (b) 100 nF; (c) 120 nF 32
<b>Figure 3.9</b> (a, b) Plain tool; (c, d) Texture tool with dimensioning parameters 33
Figure 3.10 Different depths of the fabricated micro-pillar textures
Figure 4.1 Orthogonal machining setup (a) schematic view; (b) actual setup 35
Figure 4.2 Schematic representation of force measurement setup
<b>Figure 4.3</b> Data processing of the acquired force signal using a low-pass filter 39
<b>Figure 4.4</b> Microscopic image of chip segment used to measure its curl radius 40
Figure 4.5 Measurement of tool-chip contact length on the rake face 40
Figure 4.6 Measurement of flank wear width
<b>Figure 4.7</b> Schematic illustration of thermocouple mounting holes on the tool inserts

<b>Figure 4.8</b> Thermocouple arrangement in preliminary temperature test for correlating cutting edge temperature to the temperature of the thermocouples a locations A, B and C
<b>Figure 4.9</b> Rake surface morphology under dry condition: (a) Plain tool (PT); (b-f Textured tool (TT) of 8, 15, 30, 55 and 80 μm micro-pillar depth
Figure 4.10 Schematic illustration of chip curling: (a) Plain tool; (b) Textured too
Figure 4.11 Average tool-chip contact length for plain tool and textured tools o different texture depth
Figure 4.12 Chips obtained during machining operation using plain and textured tools
Figure 4.13 Average chip curl radius for plain tool and textured tool of different depths
<b>Figure 4.14</b> Flank face morphology under the dry condition: (a) Plain tool (PT); (b-f Textured tool (TT) pf 8, 15, 30, 55 and 80 μm micro-pillar depth
Figure 4.15 Average flank wear width for plain tool and textured tool of different depths
Figure 4.16 Average force variation against different texture orientations 5
Figure 4.17 Average measured forces for plain tool and textured tool of different depths
<b>Figure 4.18</b> Measured temperature at the tool tip and locations A, B and C for plain tool and textured tool from preliminary test
<b>Figure 4.19</b> Correlation between measured tool tip temperature and rake surface temperature at locations A, B and C
<b>Figure 4.20</b> Measured rake surface temperature and estimated tool tip temperature during the actual machining operation for plain and textured tool
<b>Figure 4.21</b> Measured rake surface temperature variation with texture depth 56
<b>Figure 4.22</b> (a) 2D representation of an orthogonal cutting process (width b constant); (b) Corresponding hodograph
Figure 4.23 Shear plane angle from the intersection of P and Q 59
<b>Figure 4.24</b> Rate of work done vs shear plane angle for plain tool and textured tools of different depths
Figure 5.1 Turning process setup: (a) Schematic illustration; (b) Machine tool and setup

<b>Figure 5.2</b> Rake surface morphology of textured tool (TT) and plain tool(PT) under dry, compressed air, MQL, and wet conditions
<b>Figure 5.3</b> Schematic illustration of cutting fluid penetration for plain tool into the tool-chip interface
<b>Figure 5.4</b> Schematic illustration for cutting fluid penetration for textured tools unto the tool-chip interface
<b>Figure 5.5</b> (a) Measurement of tool-chip sticking area; (b) Average sticking contact area under different machining conditions
<b>Figure 5.6</b> Chip form obtained under various machining conditions for textured (TT) and plain tools (PT)
Figure 5.7 Chip curl radius under various machining conditions for plain and textured tools
<b>Figure 5.8</b> (a) Measurement of flank wear width; (b) Average width of the flank wear under different machining conditions for TT and PT
<b>Figure 5.9</b> Flank surface morphology of textured tool (TT) and plain tool (PT) under dry, compressed air, MQL and wet conditions
<b>Figure 5.10</b> Measured forces under all the machining environments for textured (TT) and plain tool (PT)
Figure 5.11 Average roughness (Ra) of the machined surface under different conditions
Figure 5.12 Microstructure (a) SLM Ti6Al4V; (b) Wrought Ti6Al4V
Figure 5.13 (a) Measurement of tool-chip sticking area; (b) Average sticking contact area under different machining conditions
<b>Figure 5.14</b> Average measured forces for plain and textured tools under different machining conditions
Figure 6.1 (a) Isometric view of the CFD model indicating the fluid control volume, turning insert, and the input heat flux; (b) Top view of the model illustrating fluid inlet and outlet
Figure 6.2 Schematic illustration of thermocouple mounting
Figure 6.3 Measured tool temperature at a distant location A under various machining conditions
<b>Figure 6.4</b> Mesh convergence results for maximum tool temperature of plain and textured tools

_	6.5 Temperature contours under dry, compressed air and wet conditions not
f	<b>6.6</b> Temperature contours for textured tools with varying micro-pillar depth from 40 $\mu$ m to 100 $\mu$ m beyond the contact area under dry condition (dia = 300 $\mu$ m, Pitch = 100 $\mu$ m)
d	<b>6.7</b> Temperature contours for textured tools with varying micro-pillar liameter from 200 $\mu$ m to 50 $\mu$ m beyond the contact area under dry condition Depth = 100 $\mu$ m, Pitch = 100 $\mu$ m)
f	<b>6.8</b> Temperature contours for textured tools with varying micro-pillar pitch from 200 $\mu$ m to 25 $\mu$ m beyond the contact area under dry condition (Depth = .00 $\mu$ m, dia = 100 $\mu$ m)
_	<b>6.9</b> Effect of variation in micro-pillar depth, diameter and pitch beyond the contact area on the tool temperature under dry condition

# **List of Tables**

Table 1.1 Properties of Ti6Al4V vs medium carbon steel    5
Table 2.1 Summary of sustainable strategies with their effects    13
Table 2.2 Performance of different texture patterns    19
Table 3.1 LBμM parameters   28
Table 3.2 RμEDM parameters
Table 3.3 Composition of cutting tool inserts    28
<b>Table 4.1</b> Trial process parameters and machine behavior during turning operation         37
<b>Table 4.2</b> Trial process parameters and machine behavior during turning operation         38
<b>Table 4.3</b> Final parameters for orthogonal machining    38
<b>Table 5.1</b> Details of machining conditions    63
<b>Table 5.2</b> Final parameters for turning operation    65
<b>Table 5.3</b> Properties of SLM and wrought Ti6Al4V    82
<b>Table 5.4</b> Machining performance comparison: % reduction in TT compared to PT
<b>Table 5.5</b> Machining performance of TT: % difference compared to wet condition         84
Table 6.1 Material properties in CFD analysis    87



# Abbreviations

GDP	Gross Domestic Product
SDG	Sustainable Development
	Goal
MRR	Material Removal Rate
SEM	Scanning Electron
	Microscopy
BUE	Built-Up Edge
LBμM	Laser Beam Micro
	Machining
RμEDM	Reverse Micro Electrical
	Discharge Machining
PT	Plain Tool

CF	Cutting Fluid
MQL	Minimum Quantity
	Lubrication
CM	Conventionally
	Manufactured
AM	Additively Manufactured
SLM	Selective Laser Melting
CFD	Computational Fluid
	Dynamics
CAD	Computer Aided Drawing
TT	Texture Tool



## CHAPTER 1 INTRODUCTION

The manufacturing sector significantly contributes to the global economy, representing 16% of the world's GDP [1], advancing societal well-being and economic prosperity. However, this progress comes with a significant environmental impact, accounting for one-fifth of global carbon emissions and consuming 54% of the world's energy [2]. Hence, adopting sustainable practices in manufacturing is of utmost importance.

Several definitions of sustainable manufacturing are available in the literature. According to the United States Environmental Protection Agency, sustainable manufacturing is 'The creation of manufacturing products through economically sound processes that minimizes negative environmental impacts while conserving energy and natural resources' [3] It is a comprehensive approach toward manufacturing that caters to the product, the process, and the manufacturing systems across all levels of the product life cycle [4] Two of the 17 United Nations Sustainable Development Goals (UN SDGs) are manufacturing-related. SDGs 8 and 12 emphasize the crucial areas of decent work, economic growth, responsible consumption, and production in the manufacturing sector [5].

### 1.1 Sustainable machining

Metal cutting or machining is an integral part of a manufacturing process. Typically, it represents the final step in any manufacturing process. Automobiles, railways, aircraft, shipbuilding, consumer electronics, home appliances, construction industries, and many more depend on machining to manufacture their final products. A substantial 15% of the overall manufacturing cost is allocated to machining expenses, highlighting the economic significance of the process [6]. A thorough analysis of all the input factors in the machining process is necessary to adopt sustainable practices without compromising efficiency.

In machining, metal is removed in the form of chips due to the shearing action induced by the sharp cutting edge of the tool. In the primary shear zone, the material undergoes severe plastic deformation during chip formation, and most of the energy expended in the process is converted into heat. The chips carry away a significant fraction of the heat generated in the primary shear zone, while the remaining is conducted into the workpiece, raising its temperature. Due to the minimal tool-chip contact area for a brief period, this part of the heat makes a negligible contribution to heating the cutting

tool. The tool-chip interface on the rake face forms the secondary shear zone. The contact between the moving chips and the rake surface of the tool is so nearly complete that sliding is almost impossible over a large portion of the total contact interface. To sustain a continuous chip flow under this seizure condition, excessive shearing of the chip underside is witnessed, confined to a thin region adjacent to the interface. The heat generated from this additional plastic deformation is conducted directly into the tool, raising its temperature. The classical friction theory turns invalid in this zone, as the contact area between the chip and the workpiece is an essential parameter in metal cutting. Similarly, heat generation is observed in the tertiary shear zone, formed at the tool-workpiece interface on the flank face. Although the contact region is relatively smaller than the secondary shear zone, it can be detrimental as the adhered workpiece is sheared at the cutting velocity, contrary to the rake face, where the adhered chip is sheared at chip velocity. The three shear zones for an orthogonal machining condition are schematically illustrated in Figure 1.1.

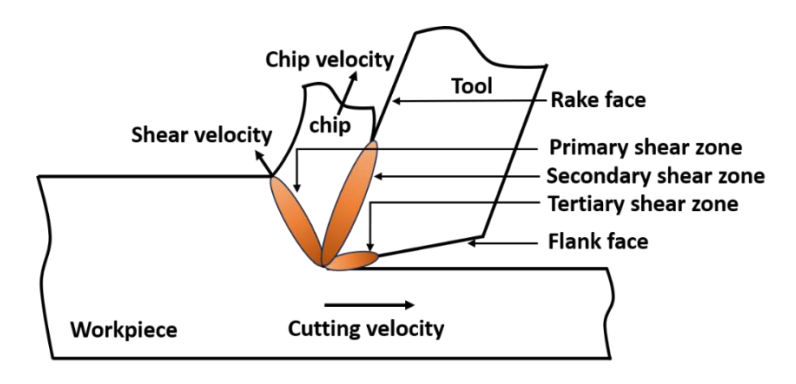


Figure 1.1. Schematic illustration of different shear zones and velocities in orthogonal machining

The high cutting tool temperature imposes a severe constraint on the material removal rate of the process due to rapid tool wear. Traditionally, cutting fluids are employed to tackle this enormous heat generation and lubricate the tool-chip contact area. These fluids control tool temperature, wear, and machined surface integrity, such as roughness, residual stresses, and dimensional accuracy. However, these benefits come with an economic and ecological burden. Using and maintaining a cutting fluid system can cost up to 17 % of the machined component cost [7]. The cost of purchasing and disposing of cutting fluids far exceeds the labor and overhead costs [8]. The annual usage of cutting fluids is reported to exceed 2 billion liters [9]. Since cutting fluids are diluted before use, the waste produced is expected to be ten times higher. Untreated disposal of the cutting fluids poses a high risk of contamination and ecological damage [10,11]. Toxic metal particles and microorganisms in the used cutting fluids lead to severe occupational diseases in the workers [12]. Long-term exposure to cutting fluids

can lead to severe skin and pulmonary disorders in the operators [13]. 80 % of occupational skin diseases are reported to be caused by cutting fluids [14]. Based on the studies of asthma and diminished lung function, an exposure limit of 0.4 mg/m<sup>3</sup> thoracic particulate (0.5 mg/m<sup>3</sup> total particulate) in cutting fluid aerosols for a new 8hour time-weighted average was recommended in the USA [15]. While acknowledging the benefits cutting fluids bring to the machining industry, it is imperative to recognize their negative impact. Therefore, it becomes necessary to mitigate the use of cutting fluids without compromising the productivity of the process. The primary challenge in implementing sustainability in machining is to preserve tool life and part quality under dry or near-dry conditions. In dry machining, cutting is performed in natural air, and cutting fluids are eliminated. In near-dry machining, also called Minimum Quantity Lubrication (MQL), a small quantity of lubricant is mixed with an air supply to form an atomized spray. The mist is supplied at the cutting zone to produce cooling and lubrication. Typically, the cutting fluid usage ranges from 10 to 100 ml/hour. The MQL system can reduce fluid consumption by 10,000 times compared to the conventional flooding strategy [16]. The MQL delivery system can be categorized as external and internal delivery, see Figure 1.2. In the external system, a mixture of CFs and compressed air is supplied through an external nozzle to the machining zone. On the contrary, the mixture is supplied through internal channels provided within the spindle, tool holder, and the tool, in the internal delivery system. The external systems are typically used for low length-to-diameter ratio (L/D < 3) operations such as turning and milling. While internal systems are used for drilling, reaming, and tapping, where typically L/D is greater than 3 [17].

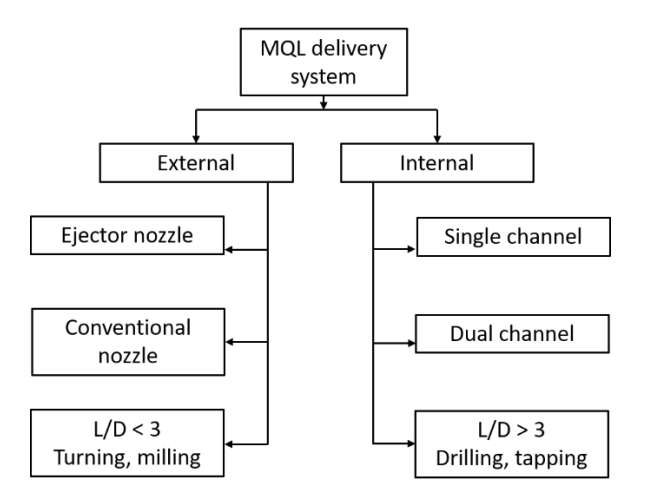


Figure 1.2. MQL delivery system

Based on the stage at which CF and compressed air are mixed, the external and internal systems are further classified [18].

#### External system:

- Ejector nozzle: Cutting fluid and compressed air are separately supplied to the nozzle. The mixing takes place just before its application to the cutting region.
- Conventional nozzle: The mixture is generated in a separate atomizer, and then it is supplied to the nozzle.

## Internal System:

- Single channel: Similar to the conventional nozzle, a mixture is supplied to the delivery channel.
- Dual channel: Similar to the ejector nozzle, separate channels are used to supply CF and compressed air, and mixing takes place in the tool holder.

## 1.2. Machining of titanium alloys

High strength-to-weight ratio retention at elevated temperatures, biocompatibility with the human body, and excellent corrosion resistance have made titanium alloys an established material for aerospace, defense, chemical, automobile, and medical applications [19,20]. Mainly, Ti6Al4V is used in gas turbine engine components, aircraft frames, and dental surgical implants, contributing to around 75 % of the total titanium alloy consumption [21,22]. Other grades of titanium alloys have commercial applications in petrochemical refineries, pollution control, food processing, etc. Despite the recognized potential, the usage of these alloys is still limited due to the soaring fabrication and machining costs.

Titanium alloys are labeled difficult to cut due to their strong chemical reaction with the cutting tool and low thermal conductivity, typically 1/6<sup>th</sup> of steel, refer to Table 1.1. The low thermal conductivity causes the concentration of heat in the machining region, leading to significant adhesion and chip segmentation [23]. Moreover, the low elastic modulus, typically half of Steel, refer to Table 1.1, induces chatter in the work material, leading to poor surface finish. Researchers have pointed out that these inherent issues in titanium machining will persist no matter the technique used [24]. However, with the optimized process parameters [25], availability of superior grade tool materials, self-lubricating and multi-layer coating [26], incorporation of non-conventional methods like ultrasonic [27] and laser-assisted [28] machining, and advanced cooling and lubrication strategies such as minimum quantity lubrication and liquid nitrogen [29], continuous attempts are in progress to ease titanium alloy's machinability

alongside promoting sustainability in machining. Surface texturing is one such research area that needs to be explored in conjunction with sustainable approaches like dry and MQL for the machining of titanium alloy.

Table 1.1. Properties of Ti6Al4V vs medium carbon steel [23]

Properties ↓ / Material →	Ti6Al4V	AISI-1045
Tensile strength (MPa)	895	625
Yield strength (MPa)	825	530
Modulus of elasticity (GPa)	110	207
Hardness (H <sub>v</sub> )	340	179
Density (g/cm³)	4.43	7.84
Thermal conductivity (W/ m-k)	7.3	50.7

## 1.3. Surface texturing of cutting tools

Surface texturing refers to modifying the surfaces of mechanical components via some externally controlled technique to improve their tribological performance at the contact interface. It involves the production of surfaces with regular patterns of predetermined shape and size. Cylinder liners, piston rings, mechanical seals, journal bearings, etc, are a few of the broad application areas of surface texturing [30]. Among the various application areas, researchers are widely exploring surface textures in the domain of metal-cutting tools. The available work sets a positive precedent for adopting surface texture on cutting tools to improve machining performance. Texture tools have been reported to improve the frictional condition at the tool-chip interface by reducing the contact area between the chip and tool surface [31-33] and by enhancing the cutting fluid penetration and retention in the region [34–37]. Texturing of the cutting tools has led to the overall improvement of the cutting process, but it also has its limitations. The most widely adopted texture patterns are shown in Figure 1.3. The performance of the textured tools is reported to be highly dependent on texture pattern and orientation [35,38-40], slowing down its wider adoption. Another problem observed with certain texture tools is an additional cutting of the chip underside as it moves over the sharp edges of the textures [32,41,42]. This results in hindrance to chip flow and increased forces. Therefore, surface texturing needs to be extensively explored in the context of cutting tools to further improve its machining performance by overcoming the existing associated challenges.



Figure 1.3. Textured tools (a) Micro-pillars; (b, c) Micro-grooves: Perpendicular and parallel to cutting edge [43]

## 1.4. Motivation

In machining, the tool-chip interface typically experiences nearly complete contact, with sliding being nearly impossible under most conditions. The underside of the freshly generated chip and the rake face are strongly bonded, which is termed a condition of seizure. To maintain the relative movement between the chip and tool surface under seizure, additional shearing of chips is witnessed in a very thin region near the interface. This condition is analogous to a highly viscous fluid flow over a solid surface, referred to as a flow zone. The strains in this region are several orders higher than those in the shear plane. The flow zone's high strain and strain rate generates continuous heat. This heat results in a significant rise in temperature in the tool.

Cutting fluids can significantly alter the seizure zone and tool temperature. However, the ability of the cutting fluids to penetrate the seizure zone is questionable. It was observed in a study that the application of cutting fluids could only reduce the heat-affected zone, while the maximum tool temperature was equal to that in dry machining. This implies that the cutting fluids are adequate only in the area surrounding the seizure zone but not in the region of high temperature [44].

Natural air can also act as a lubricant to some extent and restrict the seizure zone locally. Machining in the presence of oxygen reduces contact area and tool forces as opposed to when machining in a vacuum. Oxygen from the air can penetrate some distance under the chip and restrict the bonding between the tool and chips to some localized area. However, inside the chip body, the seizure is continuous [45,46].

Using high-pressure jets directed toward the position where it breaks contact with the tool is reported to reduce the seizure and, thus, the feed and cutting forces. The large curvature chips are reduced to short, curled segments. It is due to the mechanical stress exerted by the jet rather than any lubrication action [47].

From the above observations, it can be concluded that the effectiveness of cutting fluid or air mainly depends on the extent to which it can penetrate the seizure zone. The further it penetrates the tool-chip contact area, the lower the seizure zone. A smaller seizure zone indicates lower heat input into the tool. In titanium alloy machining, significantly high temperatures are observed. Therefore, there is a need to restrict the heat input into the tool and promote heat dissipation under dry and MQL conditions to promote sustainability in its machining. Thus, modification of the machining tools' rake surface may be exploited to limit the tool-chip contact area and enhance heat dissipation from the tool.

This research focuses on exploring novel micro-pillar textures on the rake face of machining tools as a potential solution. By modifying the surface of the tool, it is hypothesized that the tool-chip contact area can be reduced, promoting better heat dissipation, and improving the overall machinability of titanium alloys under various atmospheric, pressurized air, and MQL conditions.

## 1.5. Organization of the dissertation

Chapter 1 introduces the research work. It highlights the challenges associated with the metal-cutting process and presents a brief state of the art in overcoming those challenges. The motivation behind this work is all outlined.

Chapter 2 provides a systematic review of the previously carried out studies and its intriguing findings by various brilliant researchers. A detailed review is performed on the available types of texture patterns and the capabilities of these textures in improving the machining performance. The literature review led to identifying research gaps, based on which the research objectives are finalized. An overview of the adopted methodology is also presented here.

Chapter 3 presents the design and development of a novel texture pattern on the cutting tool inserts. It includes the details of the preliminary fabrication test, which led to selecting suitable process parameters for texture fabrication.

Chapter 4 presents the experimental plan and findings of the dry orthogonal machining performed using the developed textured tools. The capabilities of the textured tools are investigated based on (i) tool surface morphology, which includes tool-chip contact area and flank wear width measurement; (ii) cutting forces measurement; (iii) an indirect temperature measurement technique is adopted to measure the tool tip temperature; (iv) the chip morphology; (v) an analytical model based on minimum energy principle is adopted to determine the effect of contact length on the shear plane angle.

Chapter 5 investigates the effect of tool texturing under compressed air and MQL machining conditions during the turning operation. Dry and wet conditions are also

used for reference. The evaluation is based on the rake and flank face morphology, cutting forces, chip morphology, and workpiece surface roughness.

Chapter 6 presents a CFD-based numerical approach to estimate the cutting tool temperature under dry, compressed air, and wet machining conditions. Tool temperature measured at a distant location is used for inverse estimation of the tool tip temperature. The effect of texture size is also investigated based on tool temperature.

Chapter 7 presents the overall conclusions of each objective proposed in Chapter 2. The reasons for the improved performance of the proposed texture pattern are summarised. A few future scopes are also mentioned to extend the current study further.

This chapter systematically reviews and summarises the literature on sustainable machining techniques and surface-textured metal cutting tools. It covers the challenges associated with adopting sustainability in machining. It also examines the existing textured tools with respect to their machining performance, types of texture patterns, location of the textures, and various techniques adopted for texture generation. Based on this review, the research gaps are identified, followed by finalizing the research objectives.

## 2.1. Sustainable machining

Reduction in energy consumption, waste generation and environmental damage is the way to achieve sustainable machining [48]. The reported ecological and economic damage associated with the use of cutting fluids calls for a reduction in its usage.

#### 2.1.1. Dry machining

Machining performed in the absence of cutting fluids is termed dry machining. It is believed to be more sustainable than conventional wet machining because it eliminates the negative environmental and economic impact caused by cutting fluids. Occupational health hazards are reduced, and job satisfaction is promoted among the workers. It also eliminates the cost and the associated power consumption involved in cleaning the CF residue on the final components and the generated chips [49]. However, machining without cutting fluids has its challenges. Strong chip adhesion, poor heat dissipation, and accelerated tool wear contribute to poor surface integrity in dry machining. High temperatures cause the cutting edge to become blunt due to the thermal softening of the tool. Additionally, excessively high temperatures adversely affect the workpiece, leading to dimensional inaccuracy and altering sub-surface properties [26,50]. The benefits and challenges associated with dry machining are summarized in Figure 2.1. The successful implementation of dry machining relies heavily on machining material. While dry machining of cast iron is successful, machining aluminium poses severe challenges due to excessive chip adhesion at the tool-chip interface [51]. Implementing dry machining becomes more challenging with titanium and nickel-based superalloys due to their superior mechanical properties and poor thermal properties [52].

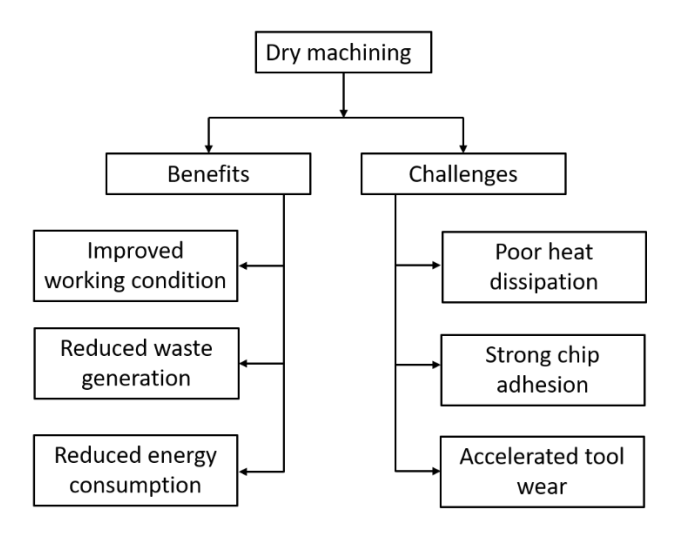


Figure 2.1. Benefits and challenges associated with dry machining

## 2.1.2. Strategies to adopt sustainable machining

To overcome the restrictions imposed during dry machining, different strategies are adopted to reduce the usage of cutting fluids in machining operations. These strategies are presented in Figure 2.2.

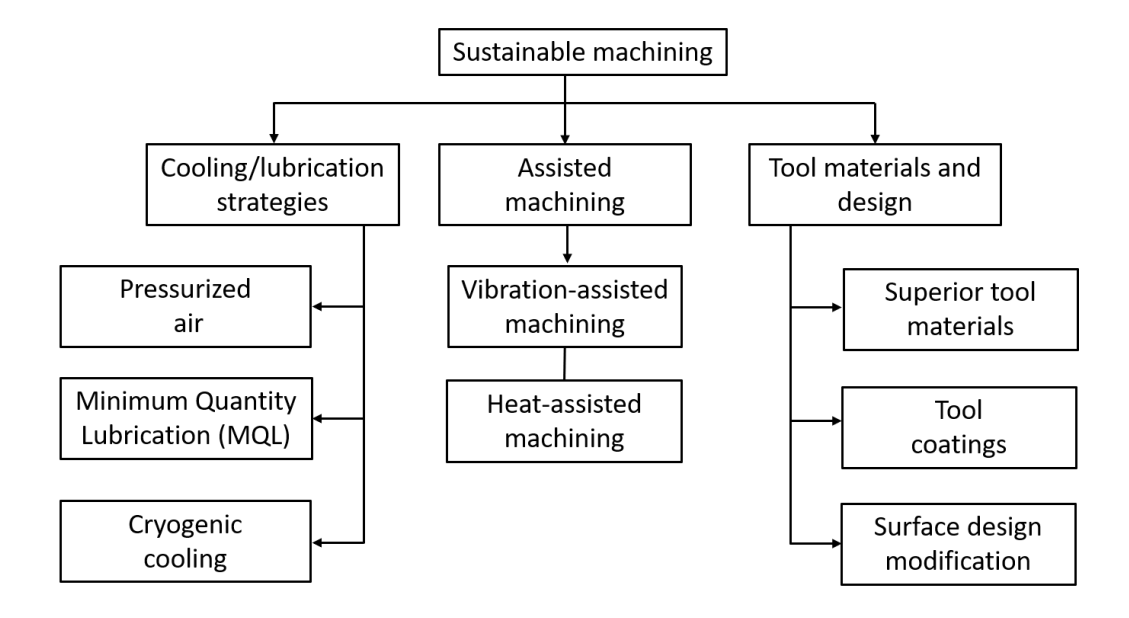


Figure 2.2. Strategies to adopt sustainable machining

#### (a) Cooling/lubrication strategies

Dry machining is the optimal solution, but only if it does not affect process productivity. Therefore, in situations where dry machining is not feasible, a near-dry alternative is utilized. In this approach, a small amount of lubricant is mixed with pressurized air to create an atomized spray, also known as minimum quantity lubrication. The atomized spray is precisely applied to the machining area, keeping the

surrounding workpiece, tool, and chips almost dry. Due to the minute quantity of lubricant consumption and its effectiveness in improving the machining performance, MQL is an economical, environmentally friendly alternative to flood machining [53]. The results obtained from MQL machining in terms of forces, finished surface, and tool wear are comparable to those of wet machining [54-56]. MQL-based cooling has exhibited a significant energy consumption reduction of up to 20 % compared to dry machining [57]. CFs mixed with nano-particles have been reported to possess superior thermo-physical and frictional properties compared to plain CFs, which leads to lower cutting temperatures and forces [58,59]. The presence of nano-particles at the interface zone improves the load-bearing capacity of the cutting tools by uniformly distributing the high compressive force. It also improves the tribological condition by forming a protective film at the interface [60,61]. Given the small quantity requirement of nano-particles in MQL, makes it economical to use in machining operations. A nanographite MQL machining condition is reported to produce a superior finish compared to flood condition [62]. The use of hybrid nano-cutting fluids has also been reported, which involves the mixing of different nano-particles in a fixed proportion with the CFs to enhance their performance [63].

Cryogenic cooling is reported to improve the machining performance due to the effective extraction of heat from the machining region. Liquid Nitrogen (LCO<sub>2</sub>) and liquid carbon dioxide (LCO<sub>2</sub>) are the widely used cryogenic medium in machining [64,65]. A comparative study between dry and cryogenic machining revealed the superiority of cryogenic cooling in terms of tool wear and surface roughness. Furthermore, the results of LN<sub>2</sub> are found to be better than LCO<sub>2</sub> during the machining of a titanium alloy at high MRR [66]. Similar results are reported during the machining of nickel alloy under dry and LN<sub>2</sub> conditions [67]. The effect of dry, flood and cryogenic cooling on surface roughness, tool wear and energy consumption are explored during the machining of Inconel 718 [68]. Severe abrasion is observed in dry machining, whereas, adhesion and edge chipping are reported for wet and cryogenic conditions. Additionally, cryogenic cooling reduced the flank wear width and energy consumption compared to other conditions. Cryogenic jet parameters like flow rate, pressure and nitrogen phases are studied to optimize the machining of titanium alloy [69]. The surface roughness is least for the liquid phase, followed by gaseous and two-phase flow. This is attributed to the suppressed plastic deformation due to the higher heat transfer ability of LN<sub>2</sub>. After the nitrogen phase, pressure proved to be an important parameter followed by flow rate.

It can be concluded that MQL and cryogenic conditions are capable of improving the machinability of materials with the added advantage of improved working conditions for the operators and reduced energy consumption and waste generation.

#### (b) Assisted machining

Researchers have achieved notable advancement in dry machining by leveraging external assistance mechanisms like laser and vibration. The interrupted contact at the tool-chip interface induced by high-frequency, low-amplitude vibrations in vibration-assisted machining improves the tribological condition in the region [70,71]. Improvement in the machining performance is demonstrated by a reduction in chip thickness and higher chip curling while using vibration-assisted machining [72]. The amplitude of the vibration has been reported as a significant factor to supress residual stresses in machined components [73]. A reduction in surface roughness and plastic deformation is observed at the interface using elliptical mode of vibration [74]

Exposing the material to be cut to an external heat source has proven beneficial in dry machining through localized heating and thermal softening [75]. A reduction in cutting force is reported using laser-assisted machining, which eventually reduces the specific cutting energy of the process [76,77]. Additionally, it is also observed that laser-assisted machining led to better surface finish and more uniform deformation of the chips [78]. A combination of both these techniques has also been adopted to improve machinability. A combination of ultrasonic and plasma yielded better surface quality and lower forces compared to these techniques used individually [79]. Another study utilizing a combination of ultrasonic vibrations and laser observed better surface finish and lower chip segmentation. However, the recorded machining temperature was high [80]. It can be concluded that external-assisted machining is a potential alternative to implementing dry machining.

#### (c) Tool material and design

The constraints imposed by the cutting temperatures have stimulated tool material development, from cast steel in 1742 to Mushet's tool steel in 1868, followed by High-Speed Steel (HSS) in 1906 [81]. HSS allows cutting speeds twice that of Mushet's steel and four times that of cast steel. The development of superior metals led to the adoption of cemented carbides in the mid-1920s. The adoption of sintered cubic boron nitride and sintered polycrystalline diamond as tool materials was reported in 1969 and the early 1970s [82]. The high hardness and chemical inactiveness of Cubic Boron Nitride (CBN) at elevated temperatures makes is suitable for dry machining. The high thermal conductivity and abrasive wear resistance of diamond make it a suitable

candidate for cutting tools. However, its strong affinity towards carbon typically restricts its usage to only non-ferrous materials.

Apart from the development of the tool materials, considerable research has been carried out on the surface coating of the tools. Coated carbide tools were first reported in the 1970s [82]. Modern-day cutting tools have three or more layers of generally used materials like TiC, TiN, Al<sub>2</sub>O<sub>3</sub>, etc [26,82]. Coatings facilitate the reduction of friction, which retards wear at the interface. Materials with low thermal conductivity are also used to create a thermal barrier at the interface [26]. Solid lubricants like MoS<sub>2</sub> and CaF<sub>2</sub> used in conjunction with coated tools have been reported to reduce friction considerably during machining [83]. The material removal rate has improved significantly with these superior cutting materials and coating techniques. However, the problem of high-temperature generation persists, especially for heat-resistant superalloys, which are still machined at a comparatively lower speed than steel [84].

Surface texturing of the tool inserts has also gained much popularity in this context. The textures on the rake and flank surfaces of the tool limit the tool-chip contact area. It slows the chemical interaction between the newly formed chip underside and the tool surface by allowing air/lubricant to penetrate up to the cutting edge [85]. The effects of the various sustainable strategies are summarized in Table 2.1.

Table 2.1: Summary of sustainable strategies with their effects

Strategy	Effect/Properties		
Cooling/lubricat	Cooling/lubrication		
Pressurized air,	Improved tribological condition at the interface due to		
Minimum	the formation of protective film; restricted tool-chip contact.		
quantity			
lubrication			
Cryogenic cooling	Enhanced heat dissipation		
Assisted machining			
Heat assisted	Thermal softening due to localized heating of the workpiece		
Vibration assisted	Improved tribological conditions at the tool-chip interface due		
	to interrupted contact.		
Tool materials a	Tool materials and design		
Material	Cemented carbides:		
	Ultra-fine grain size for hardness and wear resistance.		
	Cubic boron nitrides:		
	Chemical inertness and hardness at high temperatures.		

	Diamond:	
	Hardest known material, high thermal conductivity, and	
	abrasive wear resistance.	
Coatings	Reduced friction and wear at the interface; act as a thermal	
	barrier.	
Surface textures	Restricted tool-chip interaction and promotes air/CF	
	penetration closer to the cutting edge.	

## 2.2. Textured cutting tools

The methodology for conducting a scientific review on textured cutting tools is presented in Figure 2.3.

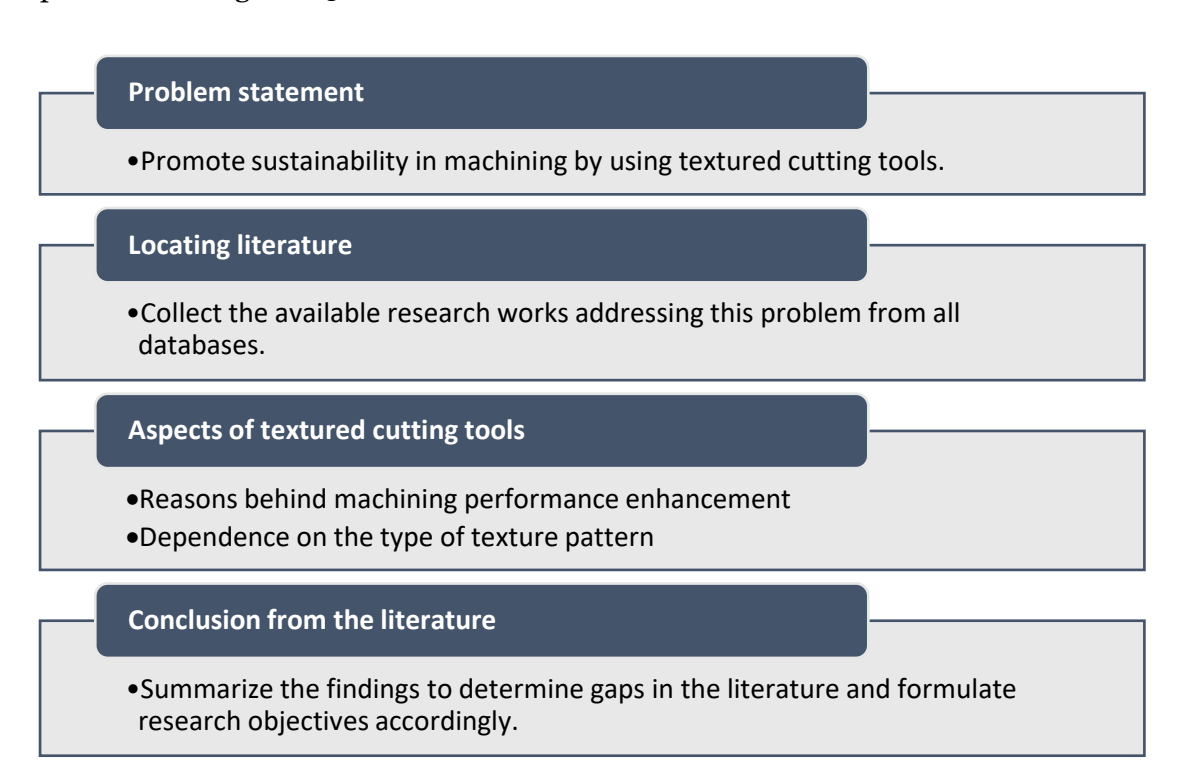


Figure 2.3. Methodology for literature survey

An extensive search is performed to collect all the literature related to the problem statement. Two electronic databases, namely, Scopus and ScienceDirect, are used to search the articles. The used keywords are Cutting tools, Surface textures and machining.

A total of 202 articles are in the database related to using textured cutting tools in machining, of which 151 are journal articles while the rest are conference proceedings. The year-wise distribution of the articles is summarized in Figure 2.4. It can be

observed that the surfaced texturing of cutting tools has gained much momentum in the scientific community since 2018.

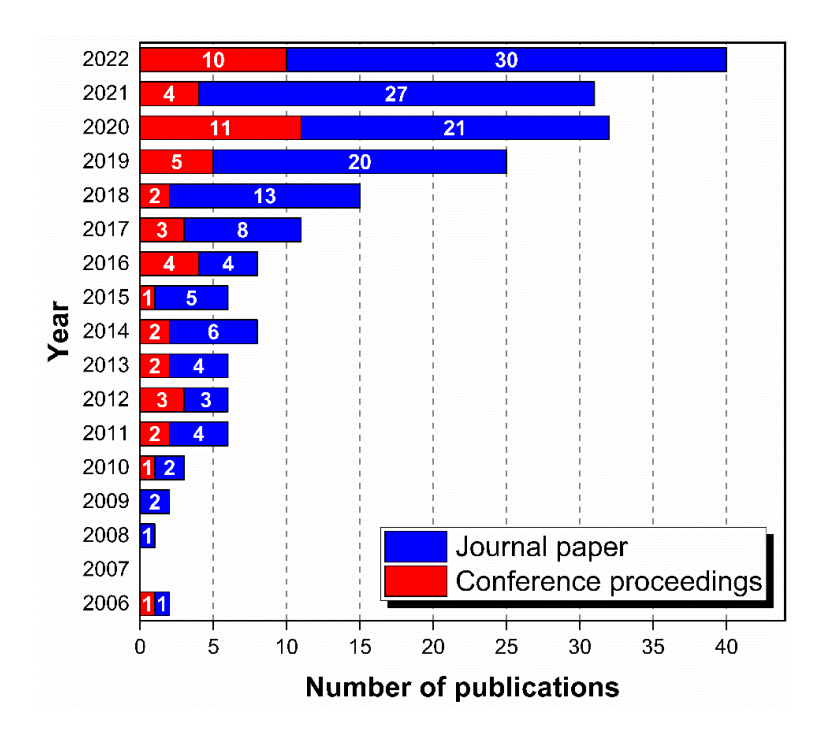


Figure 2.4. Year-wise distribution of articles from various database

## 2.2.1. Machining performance of textured tools

The performance of textured tools is primarily evaluated based on tool wear, cutting forces and cutting temperature of the machined components.

## (a) Tool wear

To understand the performance of the cutting tools it is crucial to study the rake and flank face morphology of the tools.

Better retention of cutting fluids in the presence of sine-wave shaped nano/micro-grooves on cemented carbide inserts resulted in the reduction of aluminium adhesion. However, these tools became ineffective under dry condition and during the machining of steel [86,87]. To improve the capabilities of textured tools, micro-grooves were developed. The reduction in contact area achieved by this texture pattern improved the anti-adhesion of aluminium even under dry condition [88]. The wear resistance of this texture pattern is reported to be effective even for the machining of steel. Micro-reservoirs for CF retention and micro-traps for debris entrapment are the prime functions of these textures [89,90]. Grooves oriented parallel to the cutting edge are more effective due to intermittent interaction with the flowing chips. A comparative analysis of micro-grooves and micro-dimples revealed the basic features of these textures. Micro-grooves, due to their long continuous nature, enable better penetration

of CFs into the seizure zone, but retention is challenging, whereas micro-dimples, due to their closed discontinuous nature, are capable of better retention, but penetration is challenging [39].

A comparative study amongst micro-dimples and micro-grooves parallel and perpendicular to the chip flow revealed the influence of texture patterns. Micro-dimples exhibited stable BUE yielding lower flank and corner radius wear. This is attributed to mechanical interlocking between the built-up layers and micro-dimple edges. However, these BUE are also responsible for poor surface finish of the machined surface. Maximum wear is observed in perpendicular micro-grooves due to unstable BUE and high chip embedment into the channels [43].

In a study, micro-grooves at 90° and 30° to the cutting edge were explored. The 30° micro-grooves yielded more stable machining due to reduced tool wear and chattering. This highlights the importance of aligning the chip direction perpendicular to the texture orientation such as to maintain intermittent contact between them during turning operation [38]. Further, textures in the shape of micro-pyramids were evaluated. The converging top experienced rapid wear possibly due to excessive weakening of the tool.

To handle the high seizure during the machining of Ti6Al4V, a dual combination of perpendicular grooves in the sticking region and dimples in the sliding region is explored. These tools are reported to experience lower adhesive wear compared to plain tools. Low adhesive wear, wear debris entrapment inside the texture and reduced contact area resulted in improved tribological condition at the interface. It also led to higher chip curling and lower chip segmentation compared to plain tools [91].

#### (b) Machining forces

Machining forces are the most widely used measure for the performance evaluation of the machining process. The cutting force is related to the shearing of the workpiece in the primary shearing zone, the feed force quantifies the frictional condition at the toolchip interface, and the radial component of the force tends to push the tool away from the workpiece. Thus, a reduction in these forces is a good indicator of improved machining conditions. Several studies have been reported in the context of cutting force measurement of textured tools.

Sustainable machining performed using a combination of micro-dimple texture tools and MQL revealed the capability of textures to improve machining performance. Improvement in capillary suction and formation of high vacuum space due to the texture aids in better penetration of MQL into the interface. This helps in improving

the frictional condition at the interface, which is reflected in the measured thrust forces. Severe adhesion has been reported for these textures under dry condition due to derivative cutting [36,92]. Chevron-shaped textures are reported to improve coating life due to mechanical interlocking and shear stress reduction. Coated textures are instrumental in reducing derivative cutting [93].

Micro-dimple and micro-groove textures are explored in combination with molybdenum disulphide (MoS<sub>2</sub>). All the textured tools exhibited lower machining forces compared to plain tools. The improvement in uncoated texture tools is due to reduced contact length, while the addition of MoS<sub>2</sub> further lowers the forces due to the formation of a self-lubricating film at the interface. Micro-grooves perpendicular to the cutting edge with MoS<sub>2</sub> yielded the best overall performance [40]. The effectiveness of nano-green cutting fluids is reported to improve in the presence of textured tools due to better infiltration of the CFs. This combination has demonstrated a maximum reduction in contact length and, hence, low machining forces [94].

Overlapping craters are explored as a texture pattern, and their performance is compared with micro-grooves. A significant reduction in machining forces is reported which is attributed to better CF penetration at the tool-chip interface than the micro-grooves [95]. Micro-grooves fabricated on the rake face of diamond cutting tools were evaluated during the machining of aluminium and nickel phosphorous. The study reported a significant reduction in the thrust force and chip thickness due to smaller contact lengths and enhanced air infiltration. Textures fabricated away from the cutting edge yielded better surface finish [33,96].

Two contrasting effects are identified while machining with micro-groove textured tools: (i) reduced forces due to shorter tool-chip contact and (ii) increased forces due to derivative cutting of the texture edges [32]. Contrary to this, derivative cutting is not severe for micro-dimples, except for unusually larger diameters [97]. To mitigate derivative cutting, micro-grooves are shifted away from the cutting edge to avoid the filling of texture cavities with the flowing chips. Furthermore, rounded texture edges and lower uncut chip thickness are recommended to replace derivative cutting with ploughing and sliding [41,42].

#### (c) Tool temperature

A significant part of the energy spent in machining is converted into heat. The excessive shearing of the chip in the secondary shearing zone is responsible for raising the tool temperature, which is detrimental to its performance. Researchers have explored the capability of texture in controlling the tool temperature. The tool temperature of

micro-groove textures fabricated on the rake face of cutting tools was measured during the machining of Ti6Al4V. The study revealed that micro-grooves can enhance heat dissipation from the cutting edge of the tools compared to plain tools [98]. This can be attributed to the increased surface area provided by the micro-grooves. A CFD-based study reported that textures fabricated on the flank face of the tools aid in surface expansion turbulence promotion and guide the coolant toward the cutting edge, leading to better heat transfer [34].

Machining of Ti6Al4V was performed using spot and dimple texture patterns on the rake face of HSS tools. The spot textures exhibited the minimum temperature followed by dimple textures and non-textured tools. This is attributed to the early separation of the chip from the rake face and the increased surface area due to the spot textures protruding from the rake face, unlike the dimple textures [35]. This also highlights the dependency of texture performance on its pattern type. Micro-groove textures fabricated parallel and perpendicular to the chip flow direction were examined during the machining of titanium alloy. The perpendicular orientation demonstrated the minimum temperature. This is attributed to improved frictional conditions at the interface [99].

The effect of tool texturing on the different output responses is summarized in Figure 2.5.

## Tool wear

- •Reduction in chip adhesion due to restricted interaction between the chip and tool.
- •Reduced chemical reactivity of the freshly generated chip due to better penetration of air/CFs.

#### **Machining forces**

- Substantial reduction in thrust force due to improved tribological conditions at the interface
- Reduction in cutting force due to the positive effect of shorter contact length on the shear plane.

#### **Cutting tool temperature**

- •Lower heat input to the tool due to restricted shearing of the chips in the seizure zone.
- •Better heat dissipation from the textured surface due to increased surface area.

Figure 2.5. Factors contributing to the machining performance improvement of textured tools

## 2.2.2. Types of texture patterns

The improvement in the machining performance of textured tools mentioned in Figure 2.5 is subject to the type of texture pattern employed in the process. Different texture patterns are reported to interact differently with the flowing chips during the machining operation, which significantly alters its effect on the output responses. The merits and demerits associated with each texture pattern are highlighted in Table 2.2.

Table 2.2. Performance of different texture patterns

Texture pattern	Effects
Micro-grooves: Perpendicular to the cutting edge [34,38,40,43,87–89,91,96,100]	<ul> <li>The chips flowing parallel to these textures (possible only in orthogonal cutting) get easily embedded in the cavities, creating adverse conditions at the interface.</li> <li>Significant wear is reported for this texture pattern due to the very small curling of the chips.</li> </ul>
Micro-grooves: Parallel to the cutting edge [32-34,39-43,88-90,96,100]	<ul> <li>Significant improvement in overall machining performance due to intermittent contact at the interface.</li> <li>The long shape edges of the textures result in derivative cutting.</li> <li>In everyday practice, it is not possible to maintain chip flow perpendicular to textures (possible only in orthogonal machining).</li> </ul>
Micro-grooves: At an angle to the cutting edge [38,98]	<ul> <li>To maintain the chip flow along and normal to texture direction, textures must be fabricated at an angle equal to the tool's inclination angle.</li> <li>Directionally dependent design.</li> </ul>

Texture pattern	Effects
Micro-grooves: Chevron-shaped	V-shaped long continuous design.
[93,101]	<ul> <li>Improved performance compared to straight grooves, as the flowing chip does not encounter the entire groove length altogether due to the zig-zag nature of its design.</li> <li>Directional dependency persists.</li> </ul>
Micro-dimples/holes/pits	Less prone to derivative cutting due to
[34-36,39,40,43,91,92,97,100]	<ul> <li>this design's short, discontinuous nature.</li> <li>Good CF retention capability, but ingress is challenging due to its closed nature.</li> <li>Adverse conditions are created at the interface in dry machining due to excessive cavity filling and mechanical interlocking.</li> </ul>
Micro-spots/dots/pyramids [35,38,100]	<ul> <li>Converging top (like in pyramids) results in significant wear due to weakening of the tool.</li> <li>Additional deposition of nickel or Stellite on the rake face is needed to develop these patterns.</li> <li>Higher chip curling.</li> <li>Better heat dissipation.</li> </ul>
Dual texture: Micro-grooves in the	Perpendicular micro-grooves in the
sticking region and Micro-dimples in	sticking region and micro-dimples in
the sliding region [91]	the sliding region.
Cutting edge	<ul> <li>Estimation of sticking and sliding region is challenging.</li> <li>Challenges associated with the individual patterns persist.</li> </ul>

#### 2.2.3. Conclusion from the literature

Based on the findings from the literature it can be concluded that textured tools have the potential to promote dry and near-dry machining. However, it is observed that the performance of textured tools is highly dependent on their pattern. Micro-grooves and micro-dimples are the majorly employed texture patterns. Directional dependency and derivative cutting are the prime challenges associated with the grooves, while poor air/CF infiltration leading to adverse tribological conditions are reported for dimples. Researchers have tried to overcome these limitations by altering the pattern design, such as aligning the grooves along the inclination angle, chevron-shaped grooves, and dual textures. However, the problems persist. Micro-spots are a promising pattern design with better chip curling and heat dissipation. These spots are micro-pillars of nickel and stellite protruding from the rake surface. Therefore, it is challenging to determine whether the performance improvement is due to the pattern design or the superior materials. Moreover, depositing different materials on cutting tool inserts will increase the production time and cost. Therefore, it becomes imperative to design a texture pattern that mitigates the existing challenges but incorporates the benefits of the existing patterns. Cutting tool temperature severely restricts the material removal rate of the process due to excessive tool wear. Textured tools are reported to enhance heat dissipation from the tool, but adequate coverage is missing. Several fabrication techniques for developing textured tools are reported in the literature. However, not much analysis has been reported on the fabrication feasibility of the textures. Additionally, the effect of these techniques on the cutting tool's elemental property has not been explored.

### 2.3. Research gaps

Based on the extensive literature survey on textured tool performance, texture pattern, and fabrication techniques, the following research gaps are identified:

- Dependency of texture performance on its pattern:
   A variety of texture patterns are available in the literature, each having its own merits and demerits. The associated drawbacks of each pattern restrict its usage to some instances only.
- 2. Insufficient analysis of fabrication feasibility of the textures: Various techniques are used to develop the texture patterns on the cutting tools, but very little has been discussed about the feasibility of the chosen process alongside its effects on the cutting tool.
- 3. Inadequate study on heat dissipation capability of textured tools:

High cutting tool temperatures are detrimental to its life. Textured tools are expected to control tool temperature. The heat dissipation capability of the existing texture pattern is not explored adequately.

4. Inadequate study on sustainable machining conditions: The ecological damage and occupational health hazards associated with cutting fluids have received much criticism. Sustainable strategies such as dry and near-dry machining are being adopted in this context. However, these strategies are yet to be explored to their full potential with respect to textured tools.

## 2.4. Research objectives

Based on the research gaps, this research work aims to "Explore the potential of a novel texture pattern on the rake face of cutting tools in reducing the tool/chip contact area and enhancing heat dissipation during the machining of a titanium alloy under sustainable dry and near-dry environments."

To achieve this aim, the following research objectives are proposed:

- 1. Design and development of a novel texture pattern on cutting tool inserts:
  - Design: Based on the literature findings, a new texture pattern is proposed.
     This pattern is designed to mitigate derivative cutting and directional dependency and enhance air/cutting fluid penetration into the seizure zone, making it a generic design for every use case.
  - *Development:* Perform fabrication feasibility of the texture pattern on the rake face of cutting tool inserts.
- 2. Performance analysis of developed textures under dry machining conditions:
  - *Experimental:* Evaluation of machining performance based on cutting force, temperature, tool surface morphology, and chip morphology.
  - Theoretical: Evaluation of shear plane angle
- 3. Performance analysis of developed textures under different machining conditions:
  - Evaluation of machining performance under compressed air, minimum quantity lubrication, and wet conditions.
- *4. Numerical modeling of cutting tool temperature:* 
  - Determination of tool temperature under different machining conditions
  - Effect of texture shape and size on its heat dissipation capability.

## 2.5. Research methodology

Methodology refers to the systematic framework and procedure used in research to collect, analyze, and interpret data. It encompasses the principles, strategies, and tools that guide research to ensure the study's validity and reliability [102,103].

An overview of the adopted methodology is presented in Figure 2.6. The first step involves selecting workpiece material and a suitable cutting tool insert, followed by developing the novel texture pattern on the rake of selected inserts. The experimental setup is developed in the next step, followed by running trial runs to determine the machining process parameters. The next and most vital step is evaluating the machining performance of the textured tools under different machining conditions.

#### Selection of Workpiece material and cutting tool insert

- Workpice Titanium Alloy Ti6Al4V (Wrought and Additively manufactured)
- •Insert TCMW 16 T3 04 H13A (Make: Sandvik)

## Fabrication of the proposed texture pattern on insert's rake face

- •Micro-pillar fabrication RµEDM
- Effect of process parameters

#### Development of experimental setup

- •Orthogonal machining Cylindrical tube workpiece
- •Turning Cylindrical rod workpiece (Wrought and Additely manufactured)

#### Selection of process parameters and machining conditions

- •Trial runs at varying parameters to ensure vibration free machining
- •Conditions dry, compressed air, MQL, wet

#### Measurement of machining performance

- Cutting forces
- Chip morphology
- •Chip curl radius
- Rake face morphology
- Tool-chip contact region
- Chip adhesion
- Prediction of shear plane angle (Orthogonal machining)
- Flank face morphology
- •Flank wear width
- Workpiece surface roughness (Turning)
- Tool temperature
- •Indirect approach using embedded thermocouples (orthogonal machining)

#### Numerical modeling of cutting tool temperature

CFD based approach to estimate the cutting tool temperature (using ANSYS Fluent)

#### Post process analysis of the acquired data

Discussions and conclusions

Figure 2.6. Research methodology overview

## CHAPTER 3 DESIGN AND DEVELOPMENT OF THE NOVEL TEXTURE PATTERN

The review of the literature in Chapter 2 highlights the need for a texture pattern that can mitigate the drawbacks of the existing patterns without compromising the associated performance enhancement of the machining operation. This chapter presents the design and development of a novel micro-pillar texture pattern on the rake face of tungsten carbide inserts.

#### 3.1. Design of texture pattern

The basis for the proposed texture pattern was to reduce the dependency of the textures on the chip flow direction, suppress additional micro-cutting at the long edges of the textures, and promote air/cutting fluid penetration close to the cutting edge of the tools. The new texture pattern is schematically represented in Figure 3.1. This new design is an array of circular micro-pillars on the rake face of a cutting tool. The circular discontinuous design imparts an isotropic nature to the texture pattern, making it less directionally dependent. Additionally, this discontinuity would cut short the interaction between the micro-pillars and the flowing chips, making the chips less prone to derivative cutting. The passage between these micro-pillars shall promote capillary suction of the air/cutting fluids in the scarce seizure zone, lubricating and cooling the interface. This texture pattern is fabricated on tungsten carbide inserts of suitable grade (TCMW 16 T3 04 H13A, Make: Sandvik) for machining Ti6Al4V. The dimensions of the texture are determined based on their performance with respect to tool wear and heat dissipation, discussed in detail in the subsequent chapters.

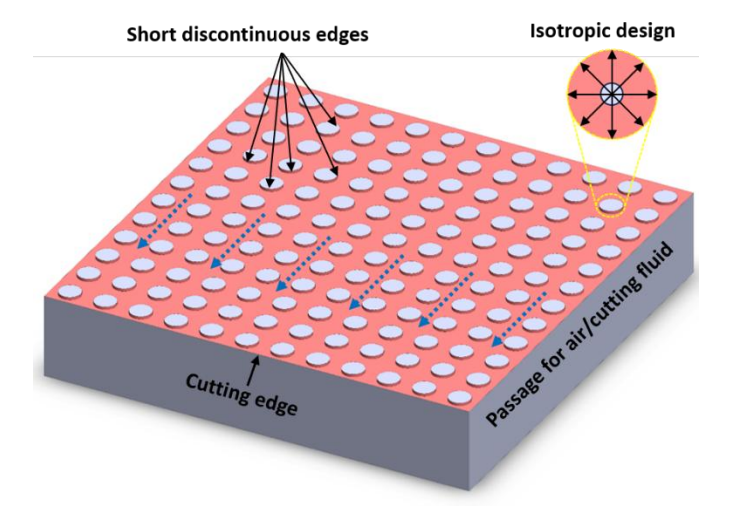


Figure 3.1. Schematic representation of the proposed texture pattern

## 3.2. Development of the texture pattern

Several fabrication methods, like laser ablation, electrical discharge machining, microgrinding, photolithography, focused ion beam, and micro-plasma transferred arc powder deposition, have been explored for texture development on cutting tools. Reverse Micro Electrical Discharge Machining (RµEDM) has been proven to fabricate protruding structures on soft materials like brass and magnesium [104,105]. Owning to the protruding nature of the proposed texture pattern, this method has been explored. The Texture fabrication process is carried out in two-step:

Step I: Fabrication of a planar electrode using a suitable micro-machining process, usually Laser Beam Micro Machining (LB $\mu$ M). This electrode, consisting of an array of desired shape and size micro-holes, acts as the tool in the next step. A schematic illustration is presented in Figure 3.2.

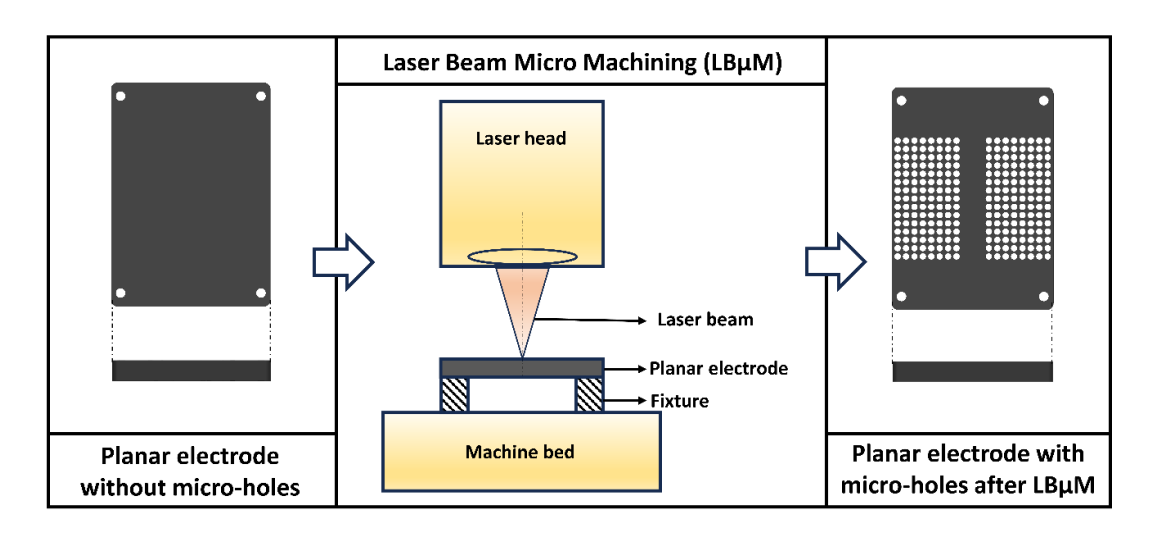


Figure 3.2. Schematic illustration of the fabrication of planar electrode in step I

Step II: Fabrication of an array of micro-pillars on the cutting tool inserts using  $R\mu EDM$ . Here, a negative replica of the micro-holes from step I is generated on the rake face of the inserts due to spark erosion caused by the EDM process. The process is schematically illustrated in Figure 3.3.

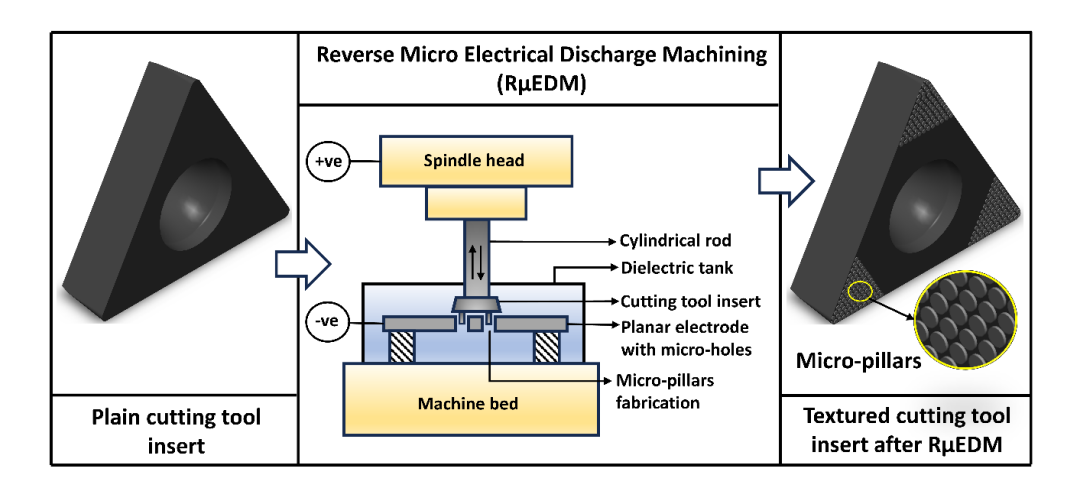


Figure 3.3. Schematic illustration of the fabrication of micro-pillars on cutting tool inserts in step II

All the experiments for texture fabrication are performed on a hybrid micromachining center (Make: Mikrotool, model: DT 110i) integrated with a laser cutting head, as shown in Figure 3.4. The process parameters for LB $\mu$ M and R $\mu$ EDM are listed in Table 3.1 and Table 3.2. The composition of the tool insert used is also presented in table 3.3.

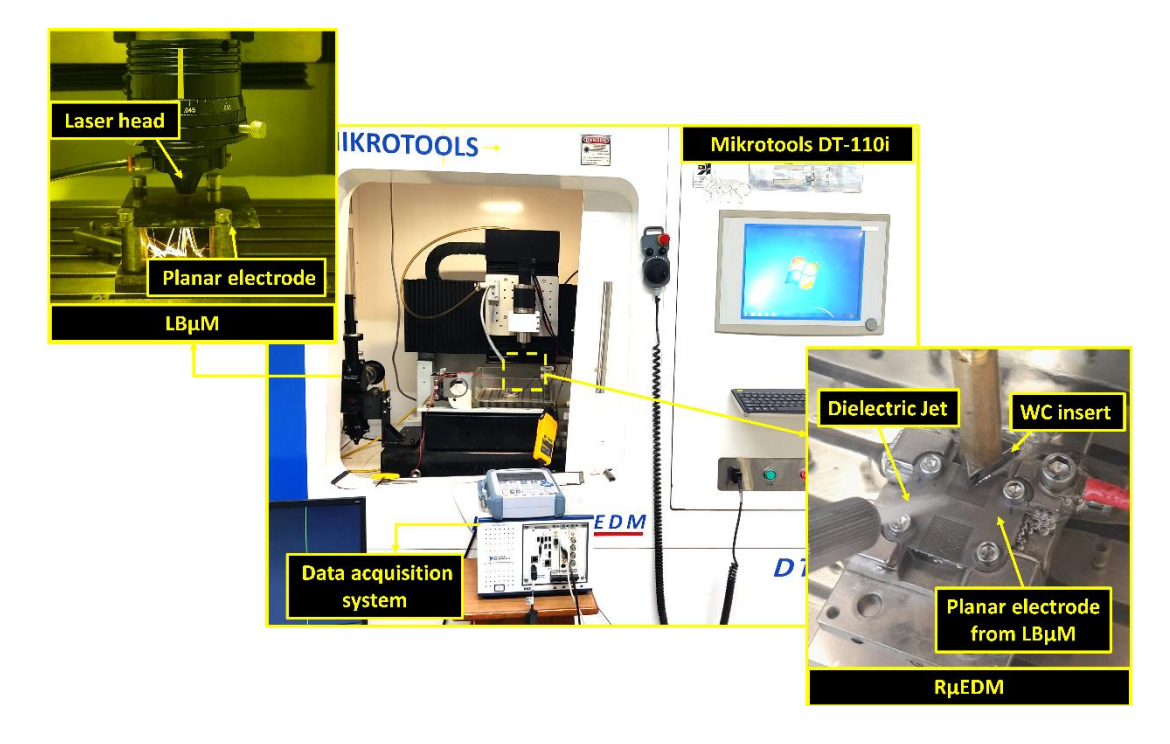


Figure 3.4. Experimental setup for LB  $\mu M$  -  $R\mu EDM$  process

Table 3.1. LBµM parameters

Laser type	Nd-YAG
Average power	150 W
Wavelength	1070 nm
Spot diameter	45 μm
Feed rate	80 mm/min
Stand-off distance	0.2 mm

Table 3.2. RµEDM parameters

Circuit	RC based
Planar electrode (tool plate)	0.2 mm titanium plate
Workpiece	Tungsten carbide (Make: Sandvik)
Feed rate	10 μm/min
Voltage sensor	Yokogawa (model: 701938)
Voltage	90, 100, 110 V
Capacitance	68, 100, 120, 150 nF

Table 3.3. Composition of cutting tool insert

Constituents	WC	Со	VC+Cr <sub>3</sub> C <sub>2</sub>
Wt%	88.4-90	9.5-10.5	0.5-1.1

Preliminary tests are performed at different voltage-capacitance combinations to determine the fabrication feasibility based on the Material Removal Rate (MRR) and surface finish obtained from the R $\mu$ EDM process. Discharge voltage data is captured during the R $\mu$ EDM process using a voltage probe to gain insight into the material removal process during texture fabrication.

## 3.2.1. Preliminary fabrication tests

The non-isoenergetic nature of the pulses in an RC-based  $\mu EDM$  process makes it challenging to estimate the MRR and surface finish. Therefore, it is imperative to acquire live discharge data to gain insight into the material removal process. During the fabrication of the micro-pillars, discharge voltage was captured and analyzed to study the effect of input voltage and capacitance on the texture fabrication process. Machining was performed at three different input voltages, 90 V, 100 V, and 110 V, to decide on a suitable input voltage. The capacitance was kept constant at 100 nF during

this trial. The discharge voltages recorded for these three input voltages are displayed in Figure 3.5. An excessive short circuit is observed in 90 V and 100 V (Figure 3.5 (a, b)), indicating that these input voltages are unsuitable for machining an array of micropillars. Accumulation of debris fills the narrow inter-electrode gap between the tool plate and the workpiece, causing the potential difference to drop to zero, resulting in a short circuit. On increasing the voltage to 110 V, continuous charging and discharging of the capacitor is observed, which results in constant spark generation and material removal (Figure 3.5 (c, d)).

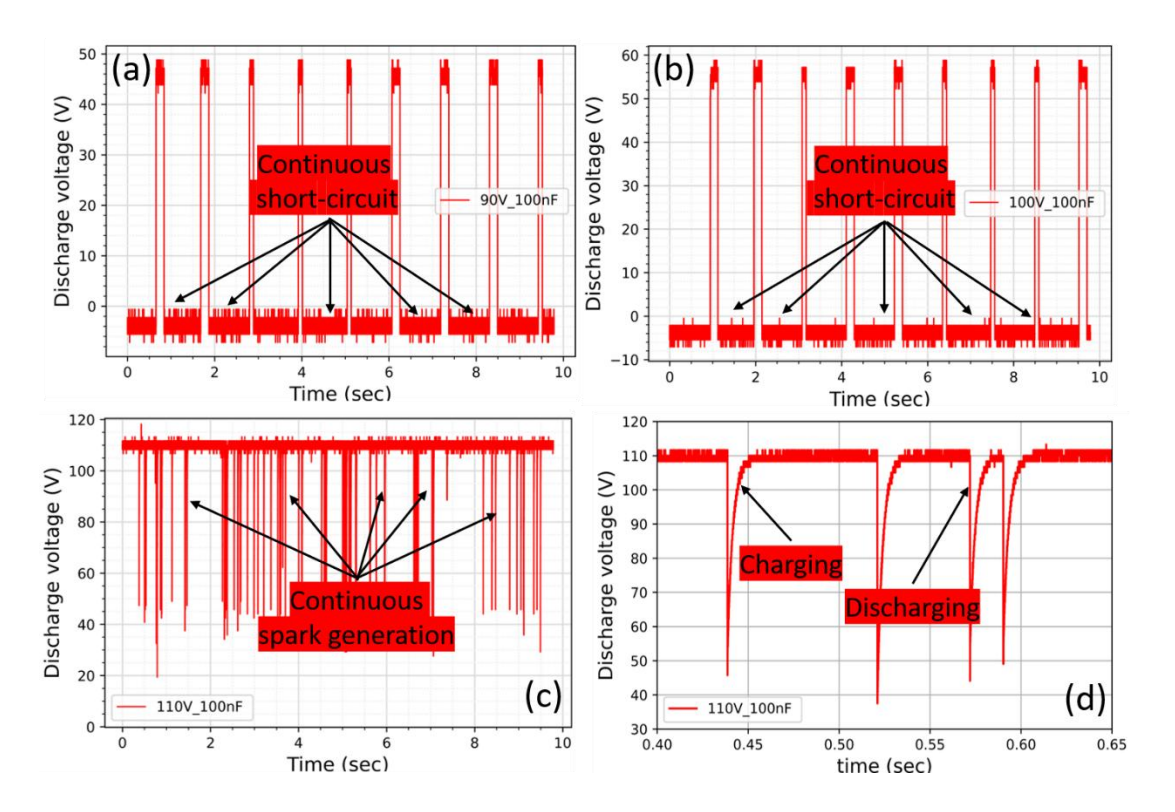


Figure 3.5. Measured discharge voltage at 100 nF: (a) 90 V; (b) 100 V; (c) 110 V; (d) Magnified view of capacitor charging and discharging at 110 V

To determine the inter-electrode distance, discharge gaps were measured for four different input voltages ranging from 90 V to 120 V. The results are compiled in Figure 3.6.

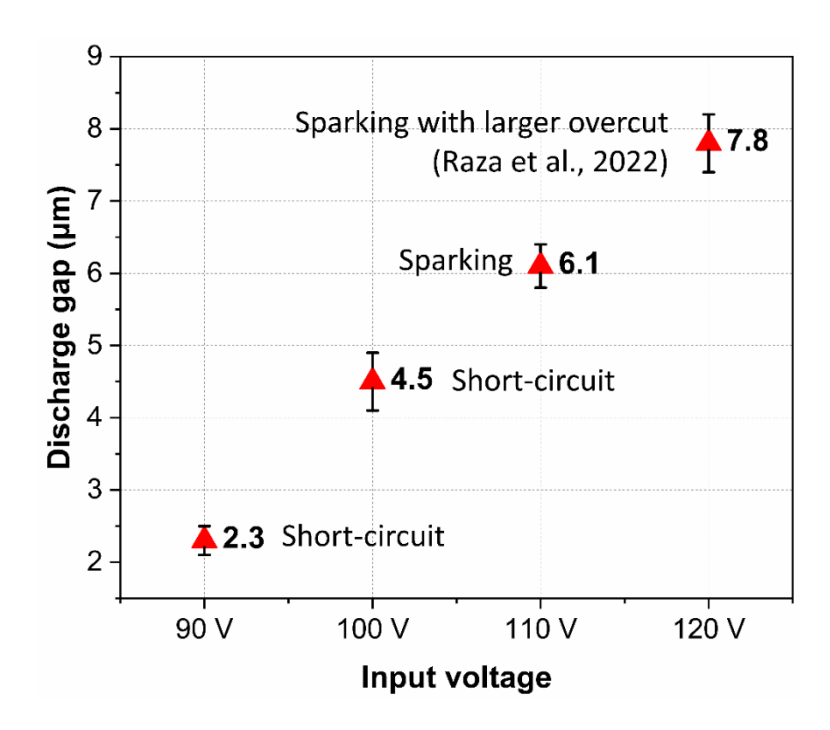


Figure 3.6. Average discharge gap measured at different input voltages

The excessive short-circuiting observed in 90 V and 100 V indicates that an average discharge gap of 2.3  $\mu$ m and 4.5  $\mu$ m is highly narrow for the dielectric to access the region and flush the debris. A discharge gap of 6.1  $\mu$ m corresponding to the continuous spark generation at 110 V indicates that a gap above this shall overcome the problem of debris accumulation and short-circuiting. However, it does not imply that higher voltage is always beneficial. It has been observed that a higher voltage generates a wider discharge gap, but it also promotes overcut and inaccurate profile dimensions [106]. Therefore, an input voltage of 110 V is fixed for this study as a trade-off between short-circuiting and overcut.

To determine a suitable capacitance value for the fabrication of arrayed micro-pillars, four sets of capacitors (68 nF, 100 nF, 120 nF, and 150 nF) are explored at the previously determined input voltage of 110 V. The discharge voltages recorded during machining and the final machined surfaces are depicted in Figure 3.7 and Figure 3.8. The spark frequency can be observed as a differentiating parameter amongst these capacitor values from Figure 3.7. Frequent sparking is witnessed at the lowest capacitance (Figure 3.7 (a)), while the least is observed at the highest (Figure 3.7 (d)).

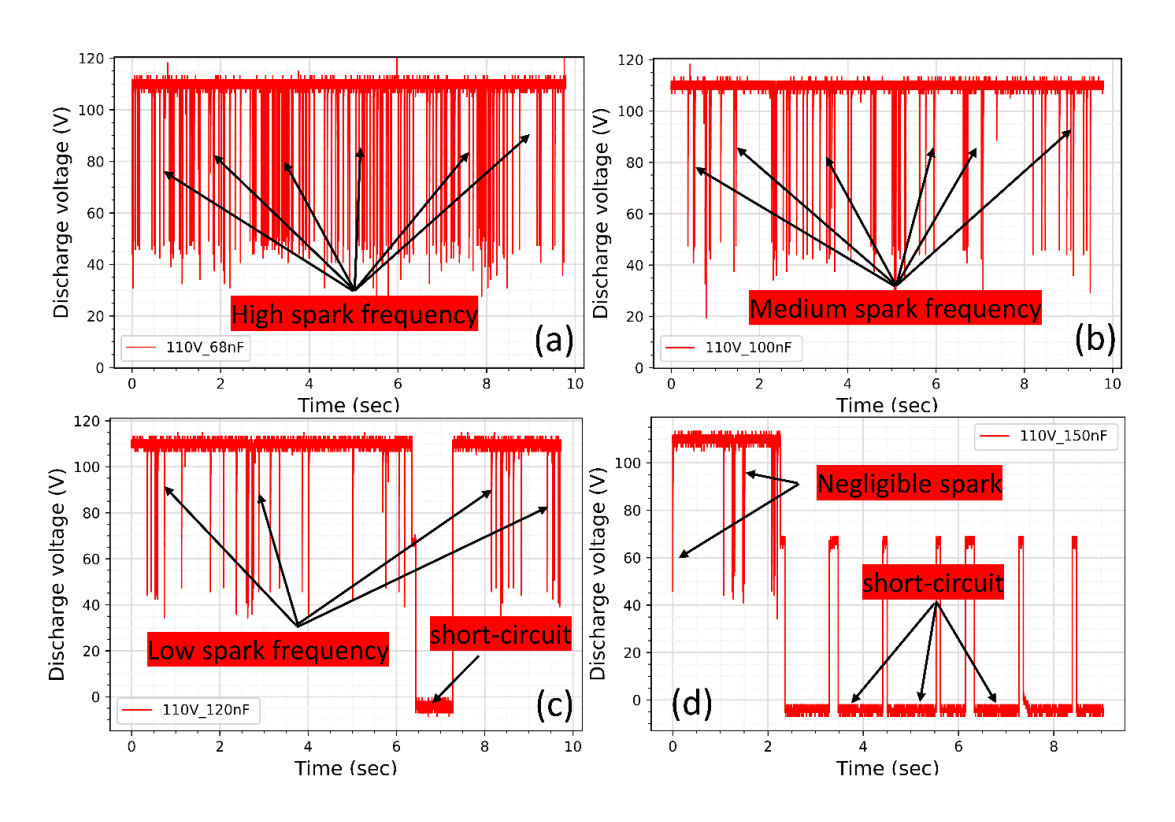


Figure 3.7. Measured discharge voltage at 110 V: (a) 68 nF; (b) 100 nF; (c) 120 nF; (d) 150 nF

At low capacitance (68 nF), due to low input energy, the amount of material removed per spark is less, as evident from the fine craters on the machined surface (Figure 3.7 (a)). This helps maintain a uniform inter-electrode gap close to the discharge gap, thus enabling continuous spark generation at 68 nF. As the capacitance value increases, the material removed per spark also escalates, resulting in a more significant interelectrode gap. Thus, no spark is generated until the required discharge gap is regained, resulting in a time gap between two successive sparks, refer to Figure 3.6 (b, c, d). Small short-circuit phases are recorded at 120 nF capacitance, while at 150 nF, negligible machining is noticed due to excessive short-circuiting (Figure 3.6 (c, d). Due to the high energy per spark at this capacitance value, large debris is formed, which clogs the inter-electrode gap, resulting in a short circuit. This non-evacuation of the large debris leads to its re-solidification, as evident from Figure 3.7 (c). The machined surface at 100 nF capacitance indicates uniform material removal and flushing debris, as visible in Figure 3.7 (b). Based on these observations, a combination of 110 V and 100 nF is used in this study to fabricate arrayed micro-pillars on tungsten carbide tool inserts.

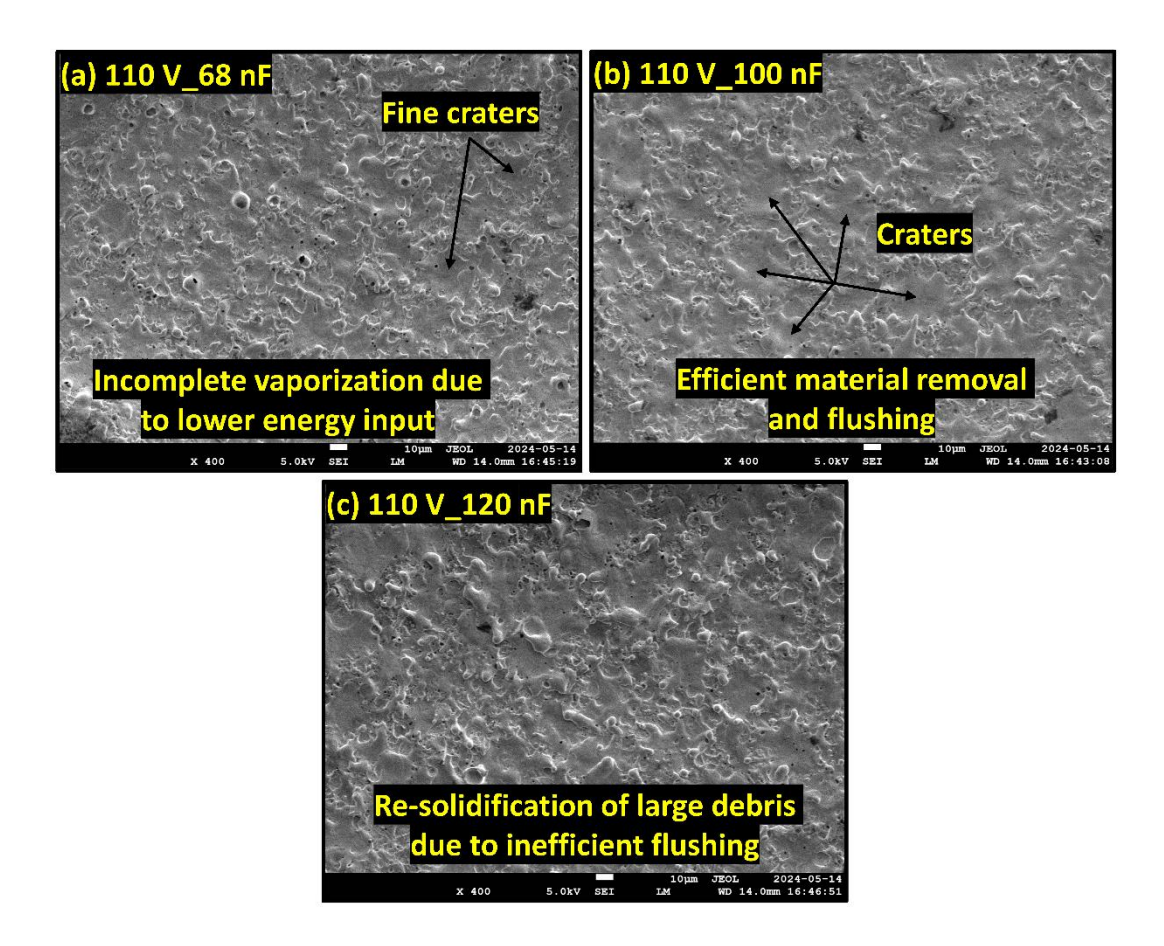


Figure 3.8. RµEDM machined surface at 110 V: (a) 68 nF; (b) 100 nF; (c) 120 nF

#### 3.2.2. Textured tools

The preliminary tests revealed 110 V and 100 nF as the most suitable voltage-capacitance combination for texture fabrication on tungsten carbide inserts. Figure 3.9 depicts the fabricated textured tool and a plain tool for comparison. The dimensioning parameters of the micro-pillars are shown in Figure 3.9 (d). The diameter (d), pitch (p), and depth (D) of the fabricated texture arrays were measured using a digital microscope (Make: Olympus GX53 and DSX510). The average diameter of the micro-pillars is 304  $\mu$ m, and the average pitch is 97  $\mu$ m. Varying depths of micro-pillars ranging between 8  $\mu$ m to 80  $\mu$ m were developed, as shown in Figure 3.10, to check for a suitable texture depth.

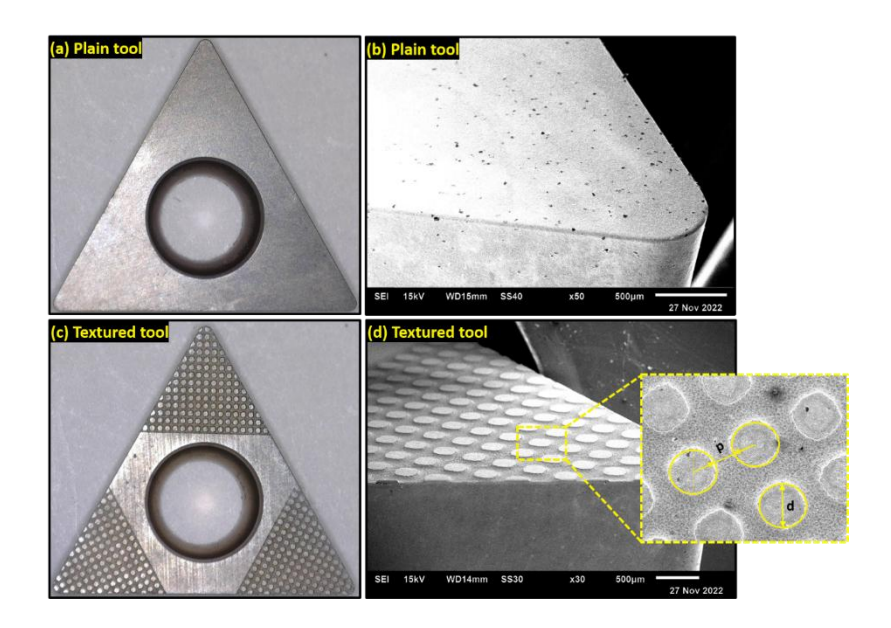


Figure 3.9. (a, b) Plain tool; (c, d) Textured tool with dimensioning parameters

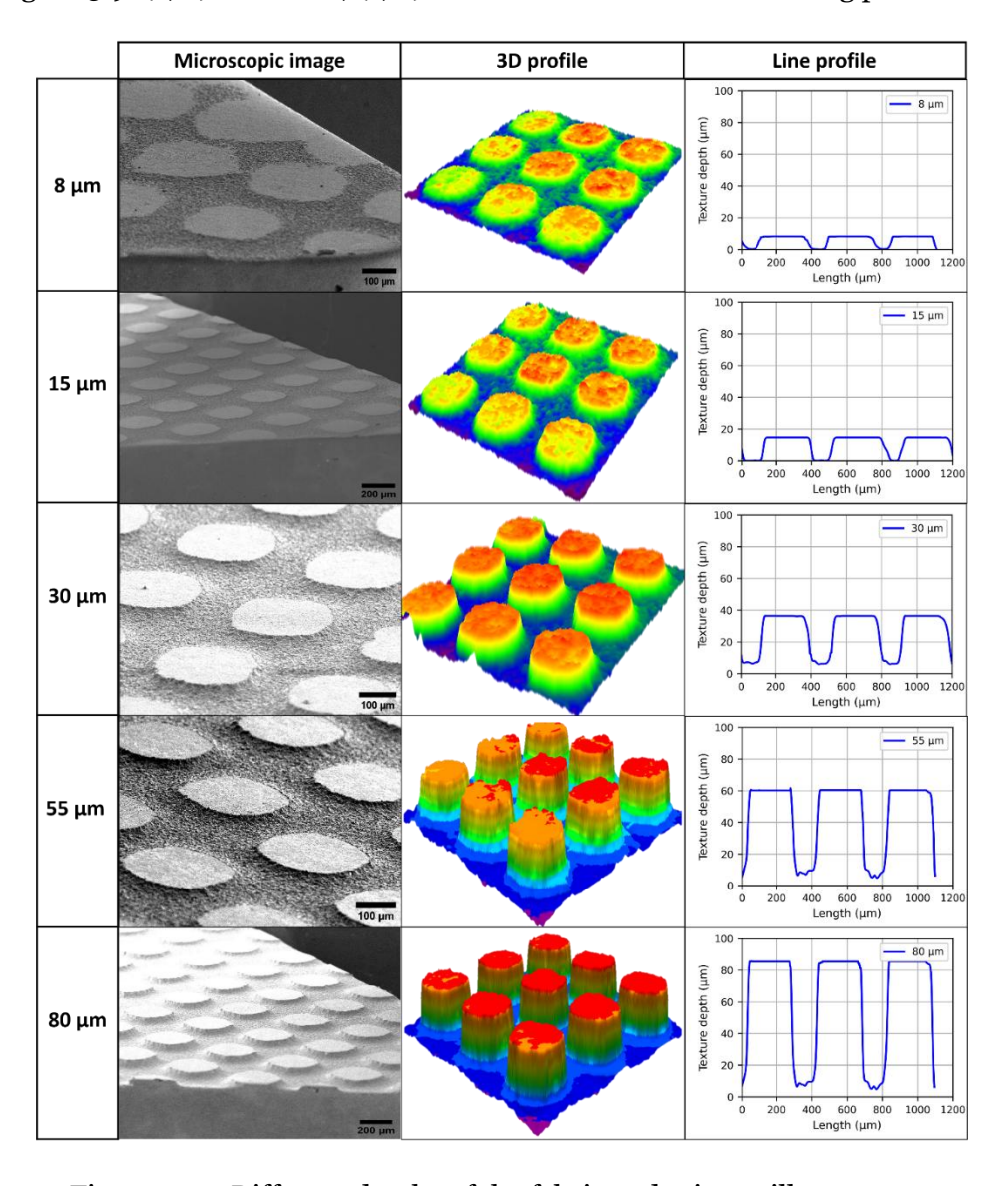


Figure 3.10. Different depths of the fabricated micro-pillar textures

#### 3.3. Chapter conclusions

The design and development of a novel texture pattern on the rake face of cutting tool inserts are discussed in this chapter. The limitations of the existing texture patterns discussed in the previous chapter form the basis for the proposed pattern design. The arrayed circular micro-pillars are a potential candidate to reduce the directional dependency and derivative cutting, alongside promoting air/cutting fluid penetration into the seizure and enhancing heat dissipation through the increased surface area of the rake surface. The key findings are:

- The reverse micro electrical discharge machining was highly capable of developing micro-pillar arrays on the rake face of tungsten carbide inserts.
- An input voltage of 110 V and capacitance of 100 nF for the RµEDM were the most feasible combination for the arrayed micro-pillar fabrication process, based on spark frequency, discharge gap, and machined surface morphology.

# CHAPTER 4 ORTHOGONAL MACHINING OF Ti6Al4V USING TEXTURED TOOL UNDER DRY CONDITION

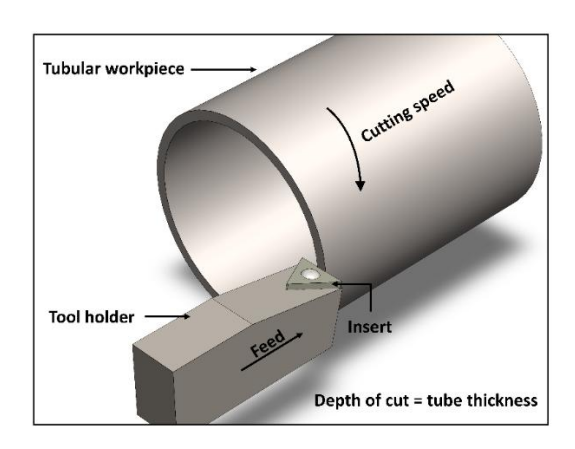
The successful fabrication of the proposed texture pattern calls for its performance evaluation during the machining operation. This chapter presents a thorough analysis of the performance of the micro-pillar textured tools during orthogonal machining of Ti6Al4V under dry condition. The effect of texture depth variation is also explored. Successful implementation of dry machining using these textured tools shall promote sustainability in machining. The objective of this chapter is to comprehensively understand the micro-pillars' interaction with the workpiece material under a dry environment to determine the mechanism behind the performance of the textured tools.

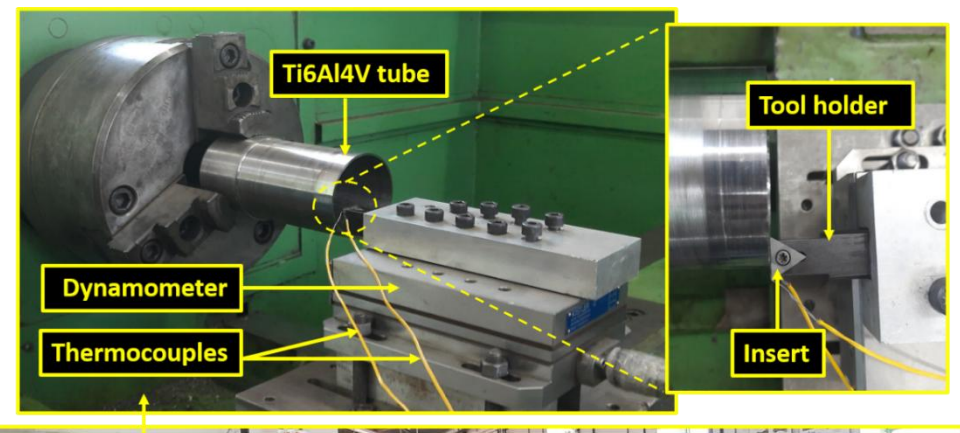
## 4.1. Experimental plan

This section outlines the adopted plan for the study. It includes details of the machining process and criteria for the selection of process parameters, followed by measurement and characterization of the various output responses.

## 4.1.1. Orthogonal machining

Orthogonal machining was chosen because of its low complexity, making it easier to model and gain fundamental insight into the process. Orthogonal machining is performed on a cylindrical tube of Ti6Al4V under dry condition using a semi-automatic lathe (Make: HMT NH 22). Here, the depth of cut is equal to the tube thickness, i.e., 2 mm, and the feed motion of the tool results in the length reduction of the tube, demonstrated schematically in Figure 4.1 (a) and the actual machining setup is presented in Figure 4.2 (b).







**(b)** 

Figure 4.1. Orthogonal machining setup: (a) schematic view; (b) actual setup

## 4.1.2. Selection of process parameters

This study is performed with an aim to increase the material removal rate of titanium alloys. The general cutting speed for titanium alloy ranges from 60 to 120 m/min [107–109]. Since turning operation is also planned as a later part of this work, several trials were performed to determine a suitable combination of cutting speed, feed, and depth of cut to obtain a vibration-free high material removal rate for both turning and orthogonal operation. The trial process parameters and the machine behavior during the turning operation are listed in Table 4.1.

Table 4.1. Trial process parameters and machine behavior during turning operation

<b>Cutting speed</b>	Feed (mm/rev)	Depth of cut	Machine
(m/min)		(mm)	behavior
60	0.1	0.25	Pass
60	0.2	0.25	Pass
60	0.3	0.25	Vibration
60	0.2	0.5	Pass
60	0.3	0.5	vibration
60	0.3	1	Machine jammed
90	0.1	0.25	Pass
90	0.2	0.25	Pass
90	0.3	0.25	Pass
90	0.2	0.5	Pass
90	0.3	0.5	Pass
90	0.3	1	Machine jammed
120	0.1	0.25	Pass
120	0.2	0.25	Pass
120	0.3	0.25	Pass
120	0.2	0.5	Vibration
120	0.3	0.5	Vibration
120	0.3	1	Machine jammed
150	0.1	0.25	Vibration
150	0.2	0.25	Vibration
150	0.3	0.25	Vibration
150	0.2	0.5	Vibration
150	0.3	0.5	Machine jammed
150	0.3	1	Machine jammed
100	0.2	0.5	Pass
100	0.3	0.5	Pass
100	0.3	1	Machine jammed
110	0.2	0.5	Pass
110	0.3	0.5	Pass
110	0.3	1	Machine jammed

Similarly, trial runs were conducted to finalize the process parameters for the orthogonal machining process, listed in Table 4.2. Here, the depth of cut is fixed to 2

mm (tube thickness), while the remaining two parameters are kept close to the turning process parameters. The final process parameters are listed in Table 4.3.

Table 4.2. Trial process parameters and machine behavior during orthogonal machining

Cutting speed	l Feed (mm/rev)	Machine behavior
(m/min)		
110	0.3	Vibration
110	0.2	Pass
110	0.1	Pass

Table 4.3. Final parameters for orthogonal machining

Variable	Attribute	
Workpiece	Ti6Al4V (tube)	
Tool insert	TCMW 16 T3 04 H13A (Make: Sandvik)	
	Plain tool.	
	Textured tool of different texture	
	depths.	
Cutting speed	110 m/min	
Length of cut	500 mm	
Feed	0.2 mm/rev	
Depth of cut	2 mm (tube thickness)	
Rake angle	O°	
Machining condition	Dry	

#### 4.1.3. Measurement and characterization of output responses

Numerous output responses were systematically recorded and analyzed to evaluate the influence of textured tools on cutting performance. This section discusses the adopted measurement and characterization techniques.

## (a) Cutting force

To measure the forces generated during the machining operation, the cutting tool holder is mounted on a multi-component piezoelectric dynamometer (Make: Kistler - 9257B) in combination with a charge amplifier (Make: Kistler - 5070) and data acquisition system (Make: 2855 A4), represented schematically in Figure 4.2. The measured raw data is analyzed using the Dynoware software to perform a partial Fast

Fourier Transform analysis, which gives an understanding of the natural frequencies of the machine and the cutting process. Then, a low-pass filter is applied to eliminate the noise from the acquired force signals, see Figure 4.3.

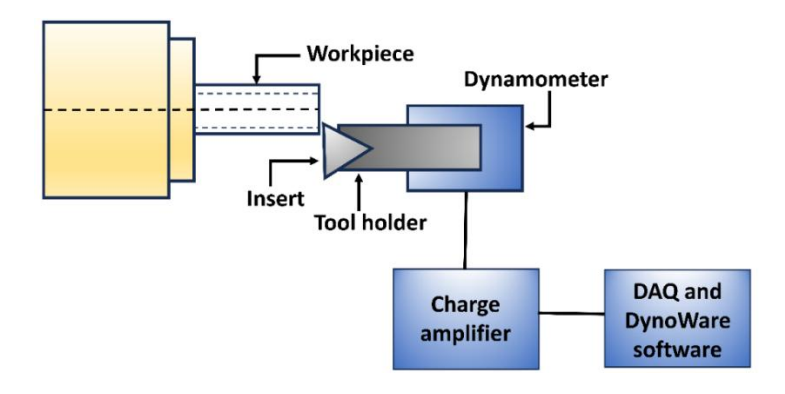


Figure 4.2. Schematic representation of force measurement setup

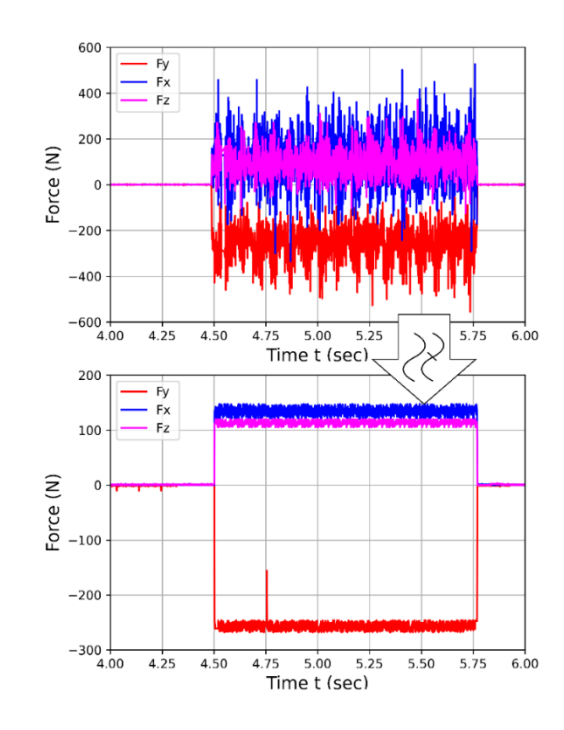


Figure 4.3. Data processing of the acquired force signal using a low-pass filter

#### (b) Chip morphology

The chips produced during the machining operation are collected and observed to comment on the extent of their entanglement, curvature, and continuity. The chips produced by the textured tool are expected to witness tighter curling. Therefore, the curl radius is measured for the chips produced by textured tools and compared with plain tools. This is achieved by observing the chip rings at multiple locations under a Scanning Electron Microscope (SEM) (Make: JEOL - JSM 6610LV), as shown in Figure

4.4, and compiling the average chip curl radius. Examining the tool-chip contact area shall further enrich the understanding of chip curling.

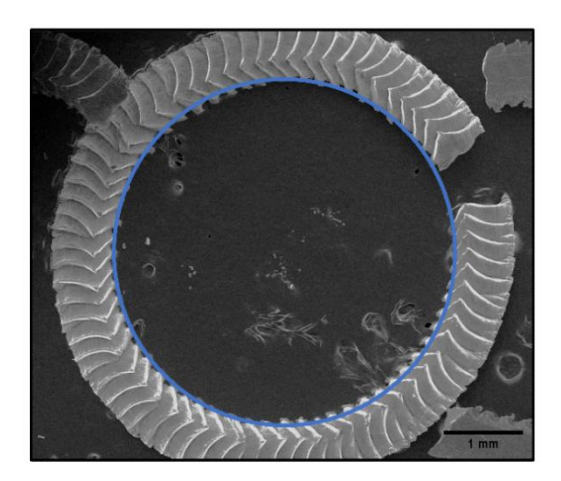


Figure 4.4. Microscopic image of chip segment used to measure its curl radius

#### (c) Rake face investigation

To investigate the frictional condition at the tool-chip interface, the rake surface of the used tools is observed under SEM. The obtained micrographs are marked and measured using image J to determine the sticking contact length after orthogonal machining, as illustrated in Figure 4.5.

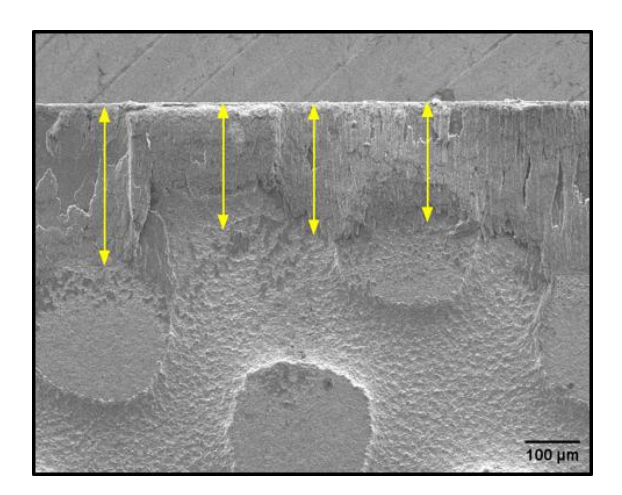


Figure 4.5. Measurement of tool-chip contact length on the rake face

## (d) Flank face investigation

The seizure at the tertiary shear zone is much more detrimental than at the secondary shear zone as the adhered work material is sheared along the flank face at the cutting velocity, contrary to the rake surface, where the adhered chip is sheared at chip velocity. Therefore, examining the flank face is necessary as the tertiary shear zone can become a significant heat source at considerable flank wear. The tools used are

observed under SEM to understand the flank face morphology and measure the average flank wear width, as shown in Figure 4.6

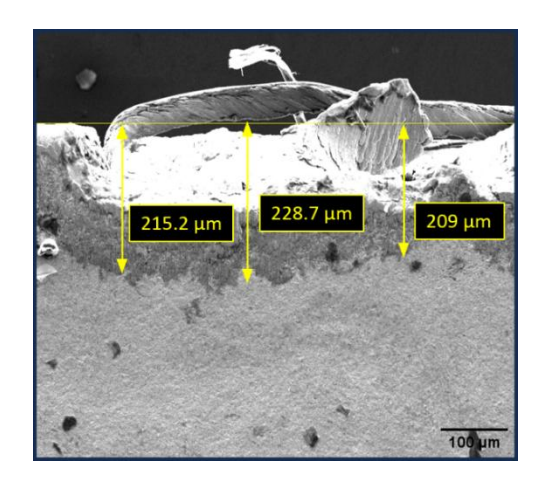


Figure 4.6. Measurement of flank wear width

## (e) Cutting tool temperature

The high tool temperature generated during the machining operation severely restricts its material removal rate. Therefore, the knowledge of the temperature generated during the process is vital. This section outlines the technique adopted to obtain the cutting tool's temperature.

Measuring temperature and its distribution around the tool's cutting edge is quite challenging due to the continuously moving chips in this region and the nature of contact at the interface [110]. Therefore, an indirect technique is adopted to determine the temperature of the cutting edge during orthogonal machining. Three K-type thermocouples are placed at a distant location of 0.8 mm below the rake face and at a successive distance of 1.5 mm away from the cutting edge, for which micro EDM is employed to drill holes on the back side of the insert, labeled as A, B, and C in Figure 4.7. Preliminary tests are performed on plain and texture tools to establish a relationship between the cutting-edge temperature and the temperature measured by these thermocouples. In these tests, external heat input is applied at the cutting edge, and the corresponding temperatures are measured at the edge and the other three thermocouples, A, B, and C. The setup for which is shown in Figure 4.8. During the actual machining process, temperature shall be measured at one or more of these locations, A, B, and C, and based on the correlation developed from the preliminary tests, the cutting-edge temperature can be estimated.

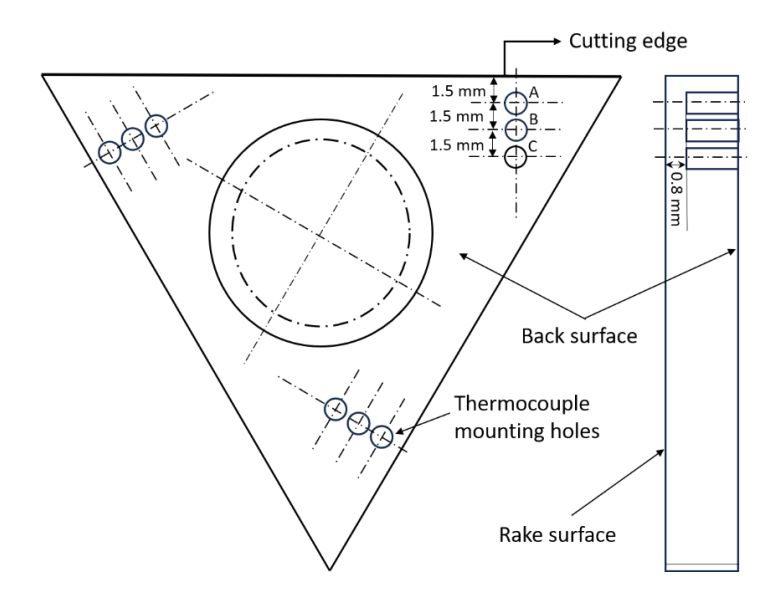


Figure 4.7. Schematic illustrations of thermocouple mounting holes on tool insert

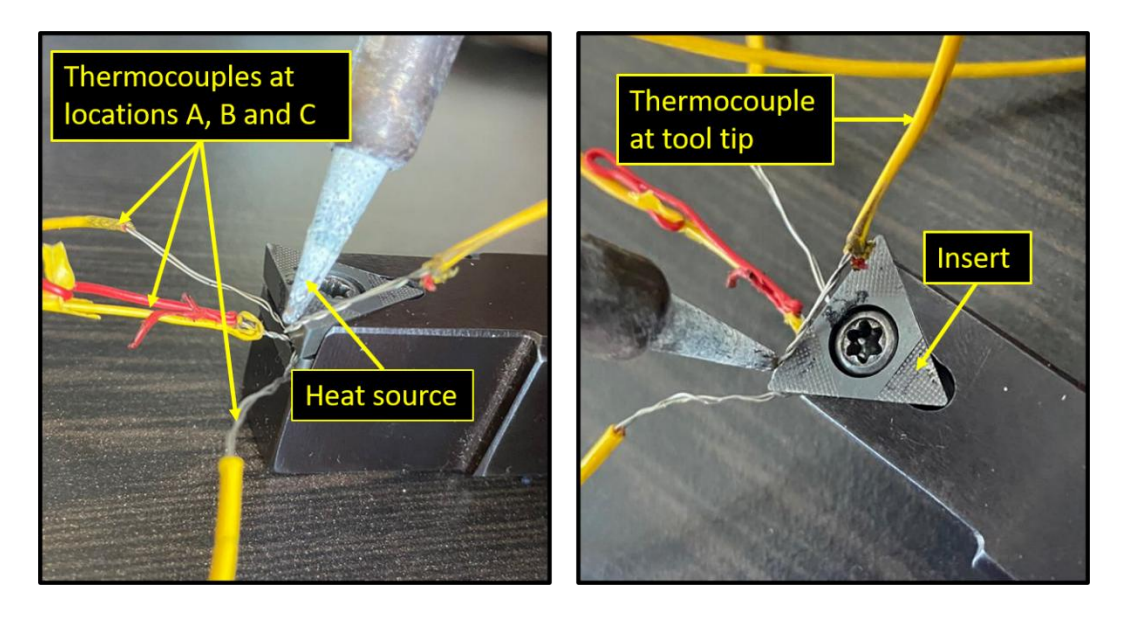


Figure 4.8. Thermocouple arrangement in preliminary temperature test for correlating cutting edge temperature to the temperature of thermocouples at locations A, B, and C

## 4.2. Results and discussion

A condition of seizure is prevalent in metal-cutting operations. Seizure implies that the contact is almost complete over a significant part of the chip tool contact on the rake face. Thus, additional shearing in a very thin zone around this contact becomes necessary to maintain the continuous flow of chips. The continuous shearing in this seizure zone is the primary heat source for the tool [6]. The tool tends to soften at elevated temperatures, losing its strength and rigidity and cutting its life short. The cutting edge loses its sharpness, leading to considerable flank wear. This heat

generation also severely restricts the material removal rate, especially for high melting point materials like Ti6Al4V. This section presents the results obtained from the orthogonal machining of Ti6Al4V using the textured tools having different micro-pillar depths ranging between 8  $\mu$ m and 80  $\mu$ m.

### 4.2.1. Rake surface morphology

This section provides a detailed examination of the rake surface obtained after the cutting operation. Figure 4.19 shows the morphology of the rake surface after the machining operation. Severe adhesion followed by sliding marks is evident in the plain tool; see Figure 4.9 (a). The capability of the textured tools to mitigate tool-chip contact area is observed in Figure 4.9 (b-d). The depth of the micro-pillars for these tools are 8, 15, and 30 µm. The mechanism responsible for this phenomenon is the disruption in the chip flow momentum created due to the discontinuous contact at the tool-chip interface. The gap between the micro-pillars breaks the continuous contact at the interface and promotes tighter curling of the chips, as illustrated schematically in Figure 4.10. The interconnectivity of these gaps acts as micro-channels for air to penetrate underneath the chips up to the cutting edge. The penetrating air reacts with the underside of the freshly generated chips and reduces its chemical activeness, thus decreasing its adhering tendency [6]. Thus, the combined effect of higher chip curling and air infiltration reduces contact length. No sliding marks are observed in texture tools. But on a further increase of the texture depth (55, 80 µm), work-material accumulation is observed in the gaps between the micropillars. This indicates that the chip material entering the gaps between the micro-pillars cannot come out of the gaps and gets severely stuck due to the more considerable depth of the pillars, thus obstructing the continuous flow of chips. It is also observed that this accumulation is not evenly distributed over the entire width of the cut; see Figure 4.9 (e-f). This nonuniform accumulation can lead to unpredictable behavior of the tool.

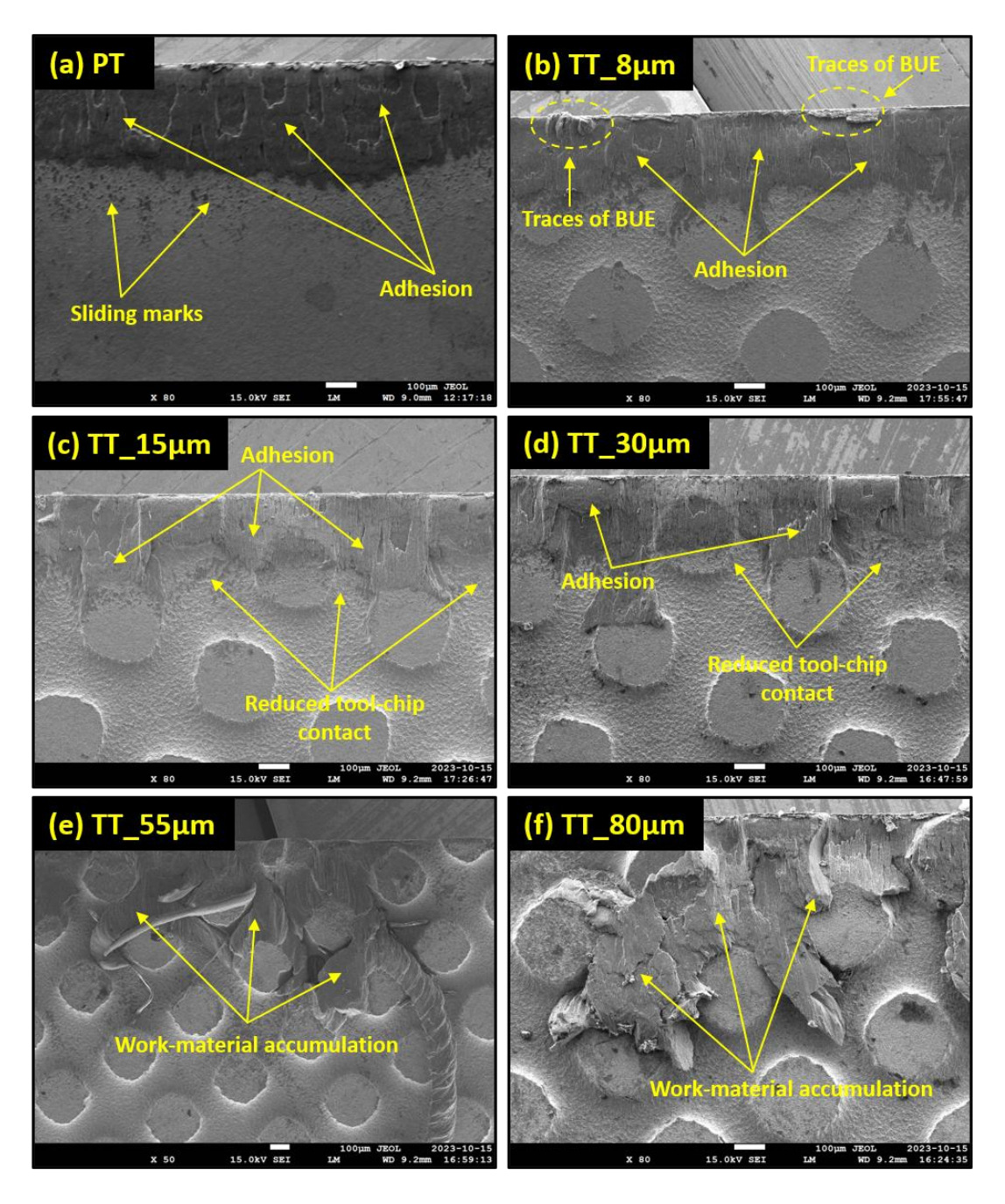


Figure 4.9. Rake surface morphology under the dry condition: (a) Plain tool (PT); (b-f) Textured tool (TT) of 8, 15, 30, 55, and 80  $\mu$ m micro-pillar depth

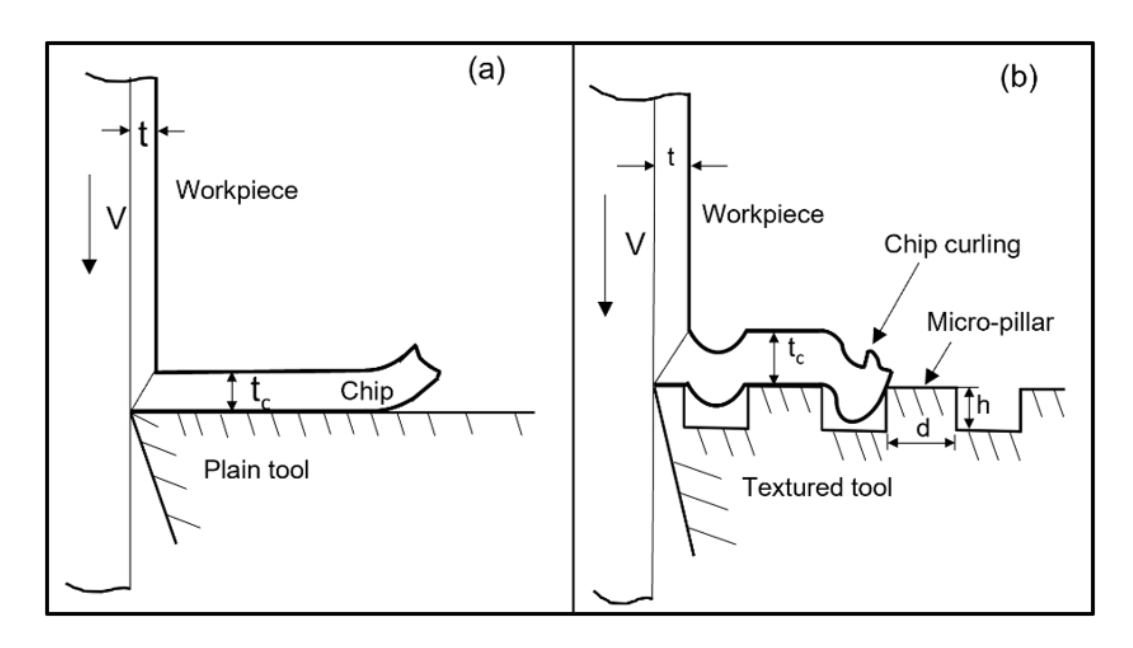


Figure 4.10. Schematic illustration of chip curling: (a) Plain tool; (b) Textured tool

### (a) Tool-chip contact length

Based on the method shown in Figure 4.5, the tool chip contact length is measured. Figure 4.11 presents the average tool chip contact length for plain tools and textured tools of varying micro-pillar depths. The textured tool with 15 µm depth performed the best, followed by 30 µm and 8 µm. In contrast, the 55 and 80 µm depth tools exhibited more extensive contact than the plain tool. The contact length in these two tools is not uniform, but the average values are more significant than that of the plain tool. The variation of the contact length with the depth of textures establishes a strong relation between these two parameters. It indicates that the depth of the texture should be such that the flowing chip does not get stuck into the gaps between the textures. This will lead to poor performance of the tools, even worse than plain tools. In the 8 µm textured tool, the depth may be too shallow to cause enough disruption in the chip flow momentum, whereas, in the 30 µm tool, the depth falls on the higher side, indicating the onset of work-material accumulation between the gaps. Therefore, a depth above 8 μm and below 30 μm appears to be a suitable choice of depth (15 μm). The tendency of Ti6Al<sub>4</sub>V to readily react with WC and its low thermal conductivity leads to higher adhesion of the freshly generated chips onto the rake face [23]. In addition to this, sizeable work-material accumulation in 55 and 80 µm tools will result in severe tool wear. Higher tool wear has been reported in tools exhibiting larger contact areas [107].

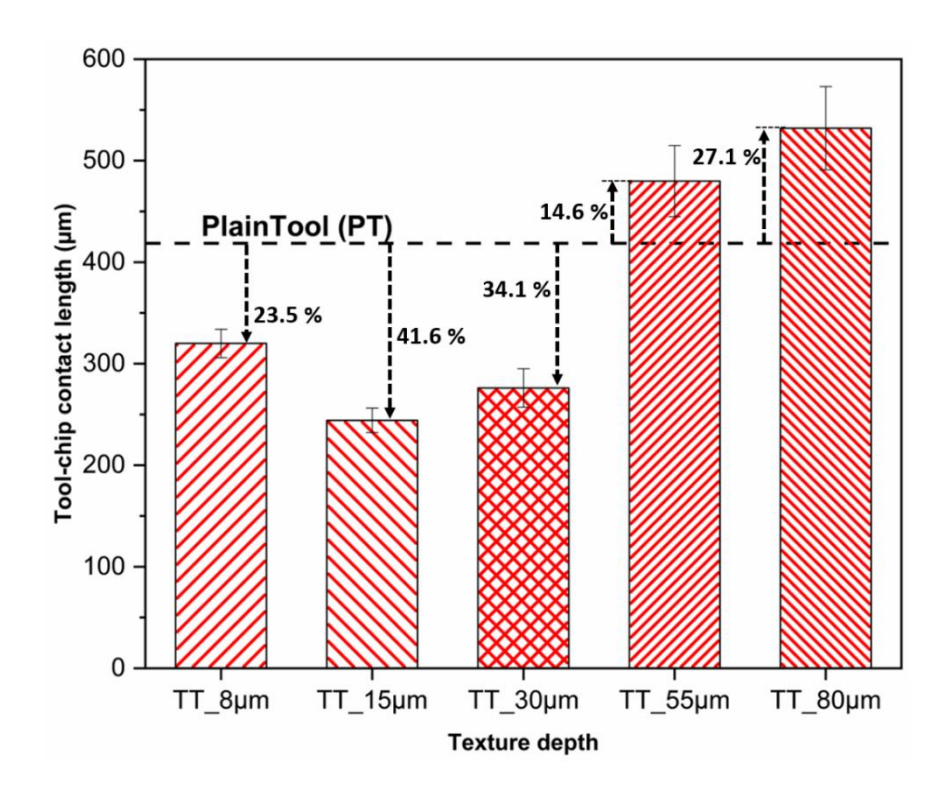


Figure 4.11. Average tool-chip contact length for plain tool and textured tools of different texture depth

# 4.2.2. Chip morphology

A detailed discussion on the chips formed during the orthogonal machining of Ti6Al4V using the plain tool and textured tools of varying depths is provided in this section. An up-curling motion is exhibited by all the chips, with different degrees of entanglement, curvature, and continuity, Figure 4.12. Chips produced using plain tools have shown undesirable traits of high entanglement and continuity with low curvature (Figure 4.12 (a)). Continuous chips quickly entangle the machined surface, leading to a subpar finish and interrupted cutting [35,111]. Moreover, handling and disposal are always challenging for long-entangled chips [112]. Chips produced using 8, 15, and 30 µm textured tools have shown tighter curling of the chips compared to PT (Figure 4.12 (b, c, d)). The chip deviates from its regular straight-line motion as it enters the gaps between the micro-pillars. This ability of the chip to enter the gaps tends to bend the chips and result in higher curling of the chips. Furthermore, the contact with the succeeding micro-pillars will exert an additional bending moment on the chip underside, see Figure 4.10. Chip lengths are observed to be shorter for 15 and 30 µm TTs. This is possible because the chip material is fractured under the resultant bending stress from contact at multiple points [112].



Figure 4.12. Chips obtained during machining operation using plain and textured tools

Chips produced from 55 and  $80~\mu m$  TTs are highly entangled and distorted (Figure 4.12 (e, f)). This distortion is due to the high resistance to the flow of chips entrapped in the gaps of considerable depths between the micro-pillars. The trapped work material must undergo larger shearing to move out of the gaps. Overall, tighter curling of the chips results in shorter contact length on the rake face, resulting in reduced adhesion and temperature rise of the tool.

To quantify the curvature of chips collected from the machining operation, the radius of chips is marked and measured at multiple locations, as depicted in Figure 4.4, and the average chip curl radius is summarized in Figure 4.13. The 15 µm textured tool has

shown the maximum reduction in curl radius, followed by 30  $\mu$ m and 8  $\mu$ m TT. The chip morphology and curl radius suggest that a texture depth above 8  $\mu$ m and below 30  $\mu$ m suits this texture pattern.

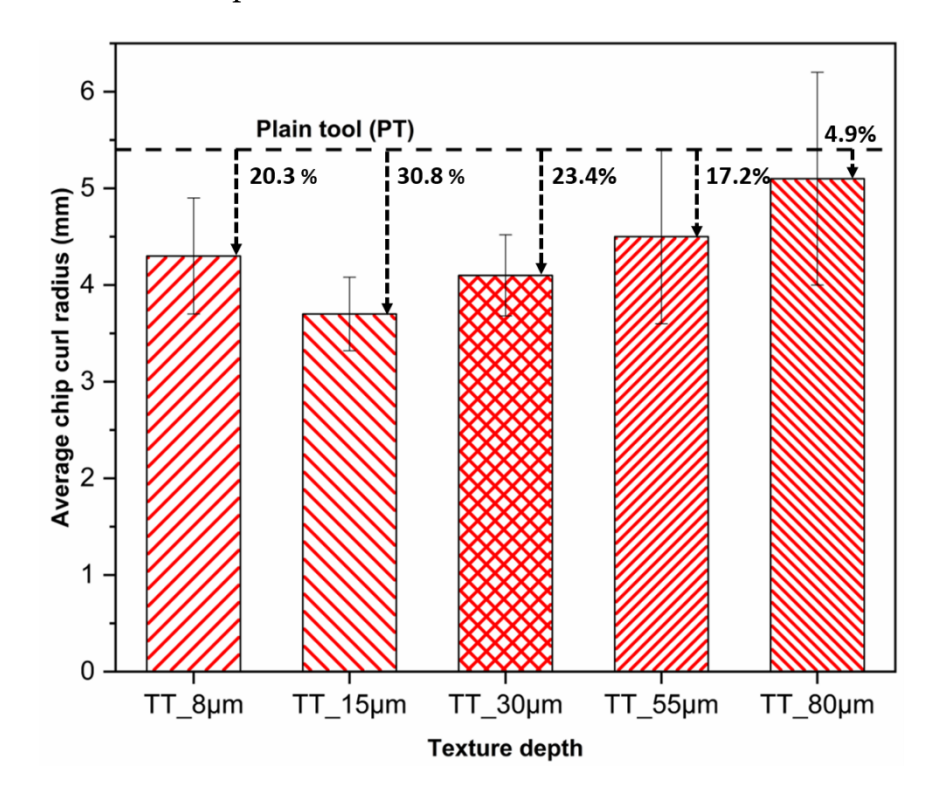


Figure 4.13. Average chip curl radius for plain tool and textured tool of different depths

### 4.2.3. Flank surface morphology

While machining with a sharp cutting-edge tool having a large clearance angle, the tool only briefly contacts the work material in the tertiary shear zone. A contact of around 0.2 mm is established for a tool with a  $6^{\circ}$  clearance angle [113]. But with continuous cutting, a seizure condition develops on the flank face, followed by tool wear. Unlike the rake face, where shearing of the adhered chip occurs at chip velocity, the adhered work material is sheared at cutting velocity. It makes the tertiary shear zone a significant contributor to heat influx to the tool. Therefore, it becomes vital to examine the flank face morphology and wear. Figure 4.14 indicates the flank face morphology of plain and various textured tools post-machining. The plain tool shows a significant amount of work-material adhesion because the cutting edge loses its sharpness quickly at elevated temperatures. Micro-particles are also visible at the cutting edge (Figure 4.14 (a)). The texture tool with 8  $\mu$ m depth shows a trend similar to the plain tool but with a lower width of contact, see Figure 4.14 (b).

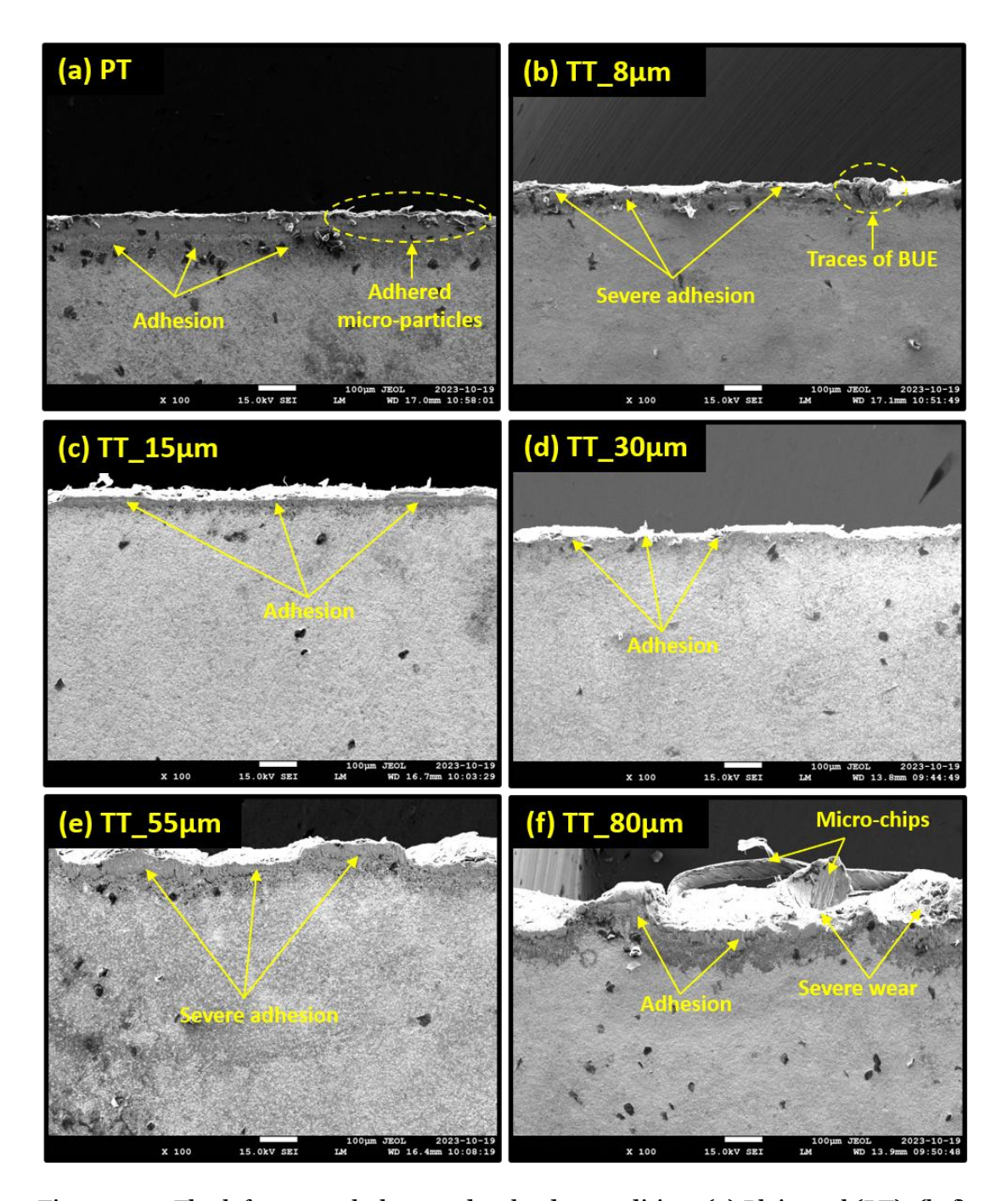


Figure 4.14. Flank face morphology under the dry condition: (a) Plain tool (PT); (b-f) Textured tool (TT) of 8, 15, 30, 55, and 80  $\mu$ m micro-pillar depth

This suggests that the 8  $\mu m$  TT only partially enhances cutting performance because the shallow depth may get buried, causing the textured tool to act like a plain tool. Textured tools with 15 and 30  $\mu m$  depth have shown a substantial reduction in contact; see Figure 4.14 (c, d). Air penetration up to the cutting edge helps retain its sharpness for an extended period. Whereas TT with 55 and 80  $\mu m$  have exhibited severe wear (Figure 4.14 (e, f)). The work-material accumulation on the rake face restricts the free flow of the chip, raising the temperature of the region. This adversely affects the cutting

edge in retaining its sharpness, which promotes rubbing of the work material on the flank face.

Figure 4.6 represents the method followed to measure the average flank wear width. The results are summarized in Figure 4.15. The allowable width of flank wear is 0.3 mm, as recommended by ISO 3685:1993. Textured tool with 15  $\mu$ m depth showed the least flank wear width, whereas 80  $\mu$ m depth showed the maximum flank wear. The heat generated in the machining region due to the accumulation of work material, along with the high compressive stress, weakened the edge, resulting in a very high wear. The 8 and 30  $\mu$ m TTs performed better than the plain tool but less than the 15  $\mu$ m Tool. This suggests that a depth of 8  $\mu$ m is insufficient for the TT to perform at its full capability, whereas a depth of 30  $\mu$ m proves to be on the higher side, marking the onset of increased flank wear.

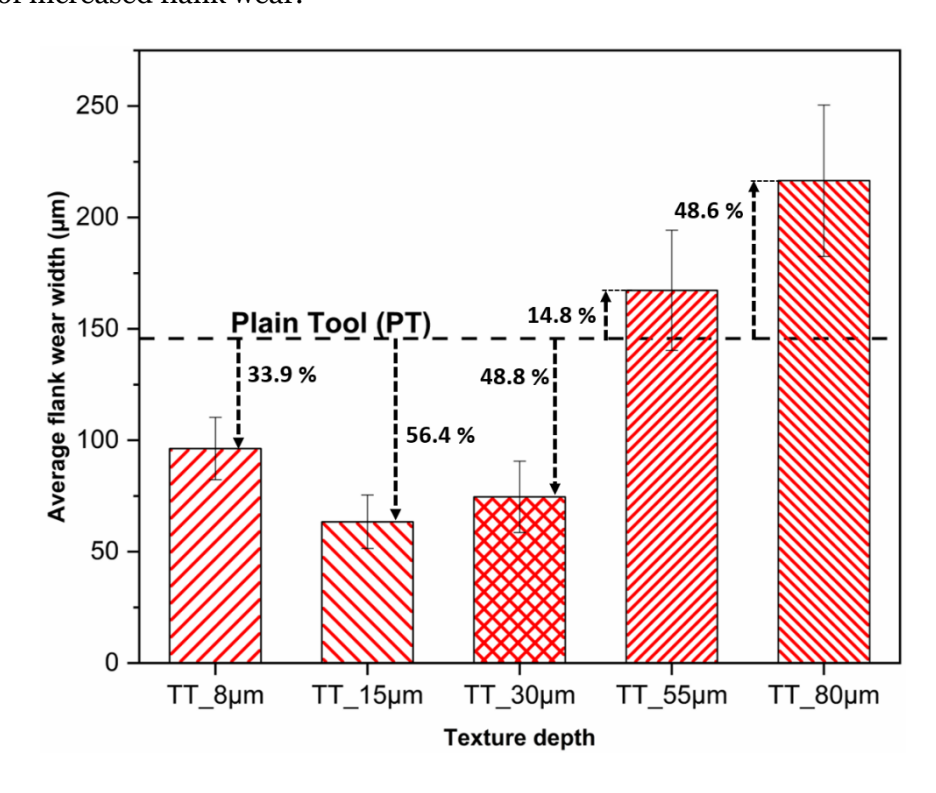


Figure 4.15. Average flank wear width for plain tool and textured tool of different depths

### 4.2.4. Force analysis

The forces applied to the tool play a pivotal role in the machining process. The thrust force, in particular, offers valuable information about the frictional state at the junction of the tool and chip underside. It serves as a direct indicator of the resistance to chip flow, especially for a o° rake angle. Additionally, the cutting force provides a quantification of the material shearing during the cutting process. Initially, a force

analysis is conducted to assess the directional independence of the developed cutting tools. Subsequently, the impact of texture depth on force variation is examined and compared with that of a plain tool. The force measurement setup and signal processing have been depicted in Figures 4.1, 4.2, and 4.3.

# (a) Directional independence of the developed texture pattern

Considering the limitation of the existing texture pattern discussed in Chapter 2, the directional dependency of the developed texture pattern has been examined in this study.

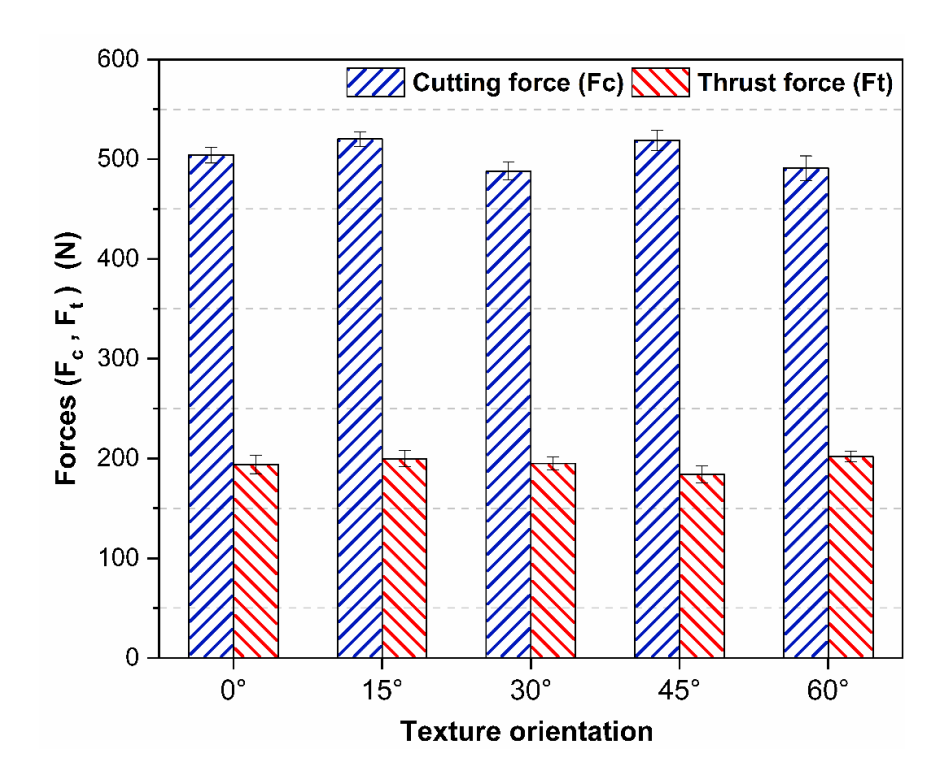


Figure 4.16. Average force variation against different texture orientation

Textures at five different orientations (o°, 15°, 30°, 45°, and 60°) with respect to the cutting edge were fabricated and tested at a specific chip flow direction (perpendicular to the cutting edge). Based on the average cutting force variation for the different texture orientations depicted in Figure 4.16, the developed texture pattern can be rightly labeled as directional independent. The change in forces is found to be within 5% on comparing the cutting and thrust force for each orientation against the o° orientation. Due to the design's isotropic nature, the chip flow direction and the texture orientation are now independent. This feature of the texture pattern will enable its widespread applicability in the metal-cutting industry and generalize the concept of tool texturing.

### (b) Effect of texture depth on machining forces

Figure 4.17 depicts the variation in cutting and thrust force for each depth of the textured tool and is compared with a plain tool.

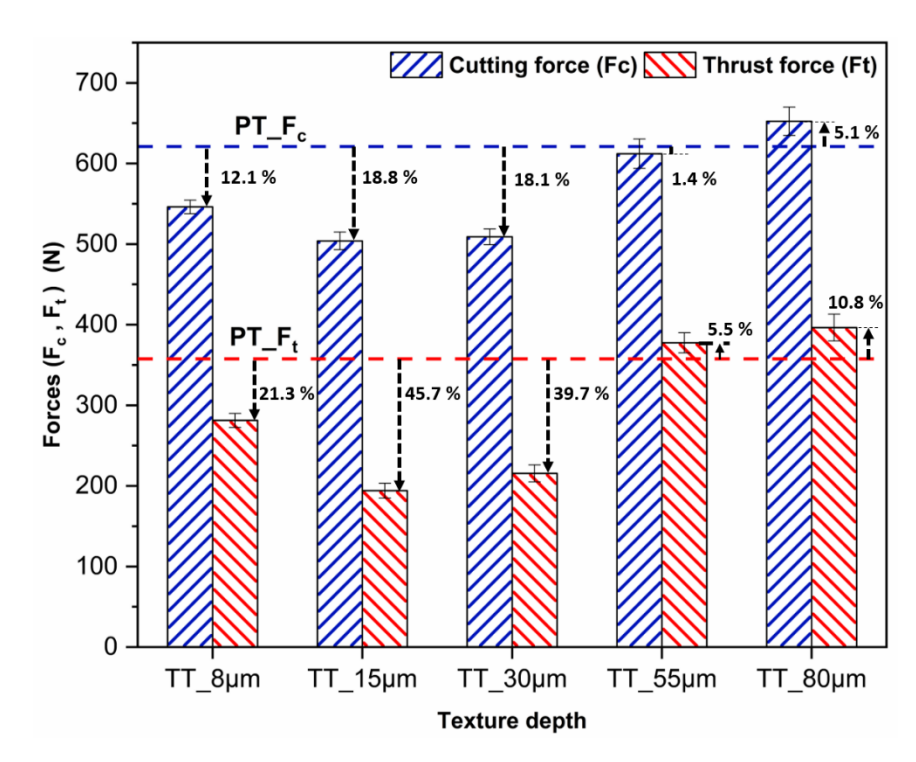


Figure 4.17. Average measured forces for plain tool and textured tool of different depths

A significant reduction in feed force can be observed for 8, 15, and 30 µm textured tools as compared to plain tool. As the feed force is the measure of resistance to the chip flow for a o<sup>o</sup> rake tool, it strongly depends on the tool-chip contact length. Therefore, a reduced contact ensures a lower feed force, with the maximum reduction observed at 15 µm TT. Feed forces for 55 µm and 80 µm TTs exceed the plain tool due to more considerable contact on the rake face (Figure 4.11). However, the percentage rise is not as significant as the contact length. Due to the non-uniform accumulation of the work material into the gaps between the micro-pillars, the contact length for these two depths of the TTs is inconsistent, with some regions having high contact while others having low contact. Therefore, the percentage rise in average feed force is not as significant as the contact length. Although tool texturing has no direct impact on the shearing of the workpiece, indirectly, it improves the machining condition at the primary shear zone by altering the shear plane angle. Based on the minimum energy theory, reducing contact length at the rake face will increase the shear plane angle [114], which in turn ensures easier shearing of the work material [6]. This is reflected in the measured cutting forces for 8, 15, and 30 µm TTs. Additionally, a decrease in the

flank wear helped maintain the sharpness of the cutting edge to prevent the undesirable rubbing action, and the reduction in temperature rise at the tool tip also ensured better performance of the TTs.

### 4.2.5. Tool temperature

A significant part of the energy spent in machining is converted into heat. This section discusses the rise of the temperature of the tool tip during the cutting operation. It is difficult to measure the temperature of the tool tip directly because of the fast-moving chips and the constant intimate contact between the tool surface and chip. Therefore, K-type thermocouples are placed at distant locations A, B, and C from the cutting edge on the rake face (see Figure 4.7) to measure the temperature rise during the machining operation. Further, to correlate the temperatures of these three thermocouples to the temperature of the tool tip, preliminary tests are performed for the plain tool and textured tools by using an external heat source at the tool tip, and the corresponding temperature is measured at the tool tip, and the other three thermocouples A, B, and C as shown in Figure 4.8. The temperature results obtained from the preliminary tests are plotted in Figure 4.18.

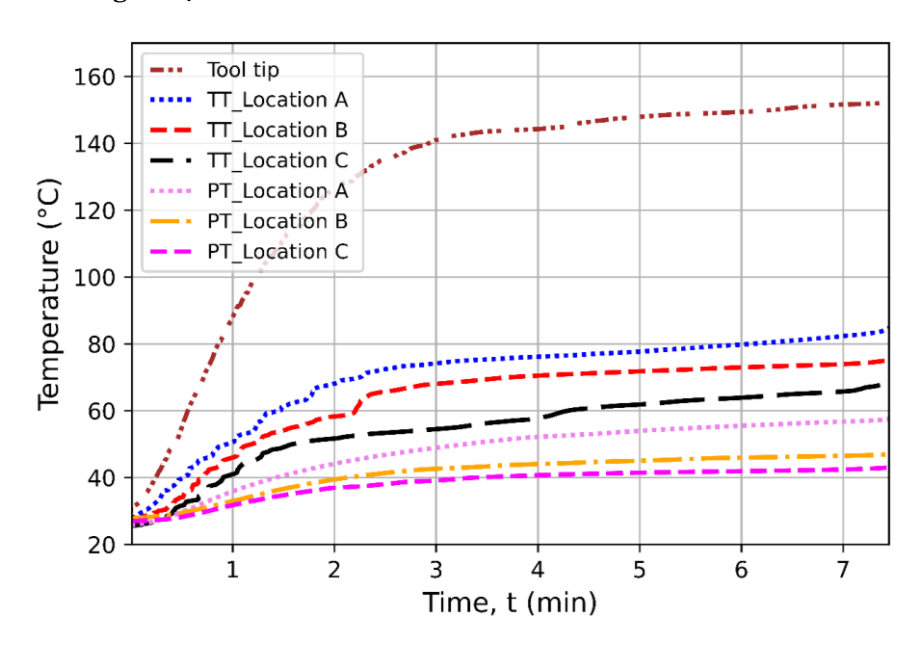


Figure 4.18. Measured temperature at the tool tip and location A, B, and C for plain tool and textured tool from preliminary test

Rake surface temperature at locations A, B, and C is seen to increase with tool tip temperature for plain as well as textured tools. Additionally, all the temperature curves almost converged to a stable value at the same time. It can be observed that for the same tool tip temperature, textured tools produced higher rake surface temperature at all three locations compared to plain tools. Moreover, a larger temperature gradient is

also witnessed between two successive locations for textured tools. This illustrates the effectiveness of the micro-pillars on the rake face of the textured tool to rapidly carry away heat from the tool tip. Thus, promoting heat dissipation from the seizure zone during actual machining. The increased surface area of the rake face due to the presence of micro-pillars enables better heat exchange between the tool surface and the surroundings. To further understand the relation between the rake surface temperature and tool tip temperature, these temperatures were plotted against each other, as shown in Figure 4.19.

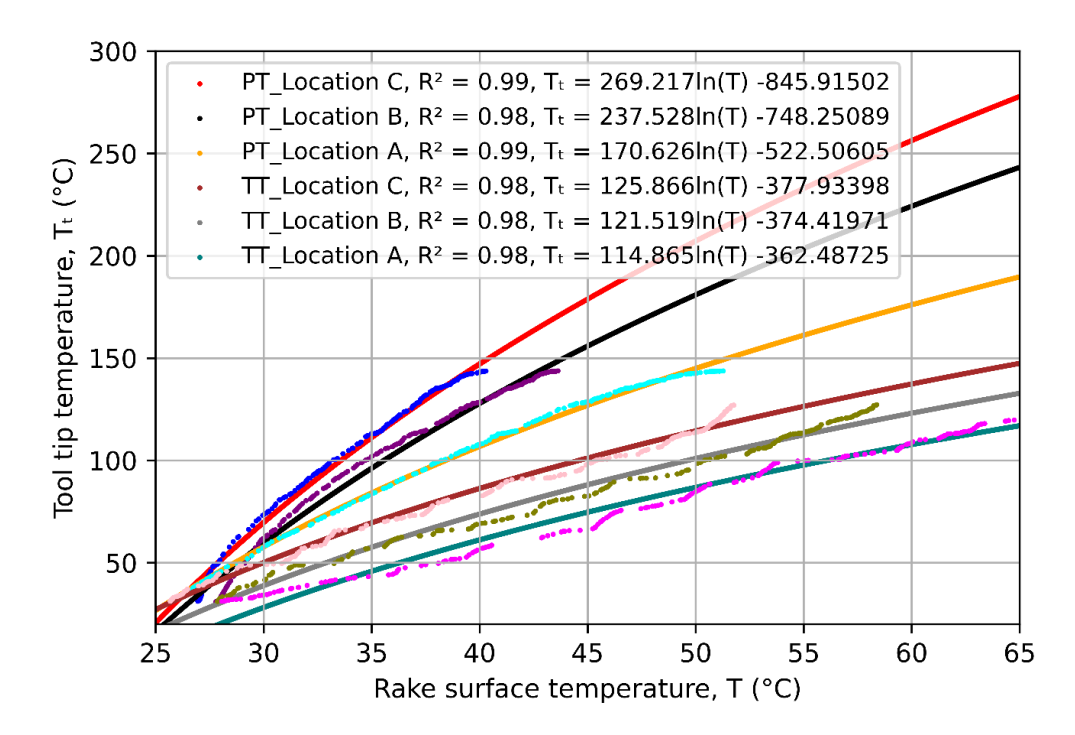


Figure 4.19. Correlation between measured tool tip temperature and rake surface temperature at locations A, B, and C

A logarithmic relation fits best between the tool tip and rake surface temperatures with a very good correlation value (R<sup>2</sup>). This observation is in good agreement with an earlier reported study [98]. The logarithmic relation established from this preliminary test is now utilized to estimate the tool tip temperature during the actual operation by measuring the temperature of the rake surface at either of the locations A, B, or C.

Figure 4.20 depicts the rake surface temperature measured at location B during the machining operation for the plain and textured tools of 15  $\mu$ m micro-pillars. It can be observed that the rake surface temperature initially increased rapidly with time for both tools and then it converged to a stable value for the textured tool, whereas it maintained its increasing trend for the plain tool. This is due to faster heat dissipation from the machining area around the tool tip in the textured tool compared to the plain tool.

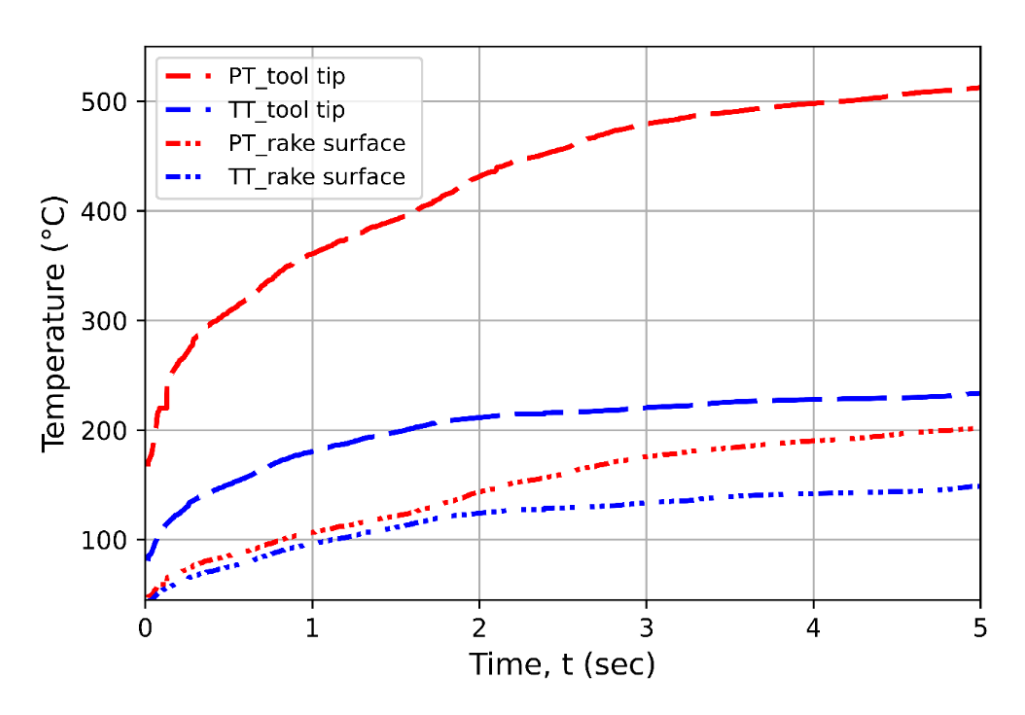


Figure 4.20. Measured rake surface temperature and estimated tool tip temperature during the actual machining operation for plain and textured tool

Based on the logarithmic fit obtained from the preliminary test (see Figure 4.19), the tool tip temperatures are estimated for the plain tool and the textured tool, Figure 4.20. The tip of the plain tool attained a temperature of around 512.3 °C during the first five seconds of machining, whereas the corresponding temperature for the textured tool was 233.5 °C. Two major factors contribute to this drastic reduction in temperature. First, the reduction in contact length obtained because of tighter curling of chips restricts the area of seizure on the rake face, which mitigates the shearing of the chips in the secondary shear zone, leading to reduced heat generation in this area. Second, the gaps present underneath the flowing chip, due to the fabrication of the micropillars, provide a passage for the surrounding air much closer to the cutting tool tip, which facilitates a continuous heat rejection from the machining area to the surroundings. A lower temperature around the cutting edge will help the tool maintain its sharpness for a longer duration, thus the flank wear can be delayed significantly.

Figure 4.21 reveals the effect of texture depths on the rake surface temperature during the machining operation. The accumulation of work-material in between the micropillars (see Figure 4.9) obstructs the penetration of surrounding air up to the cutting edge, slowing down the heat dissipation.

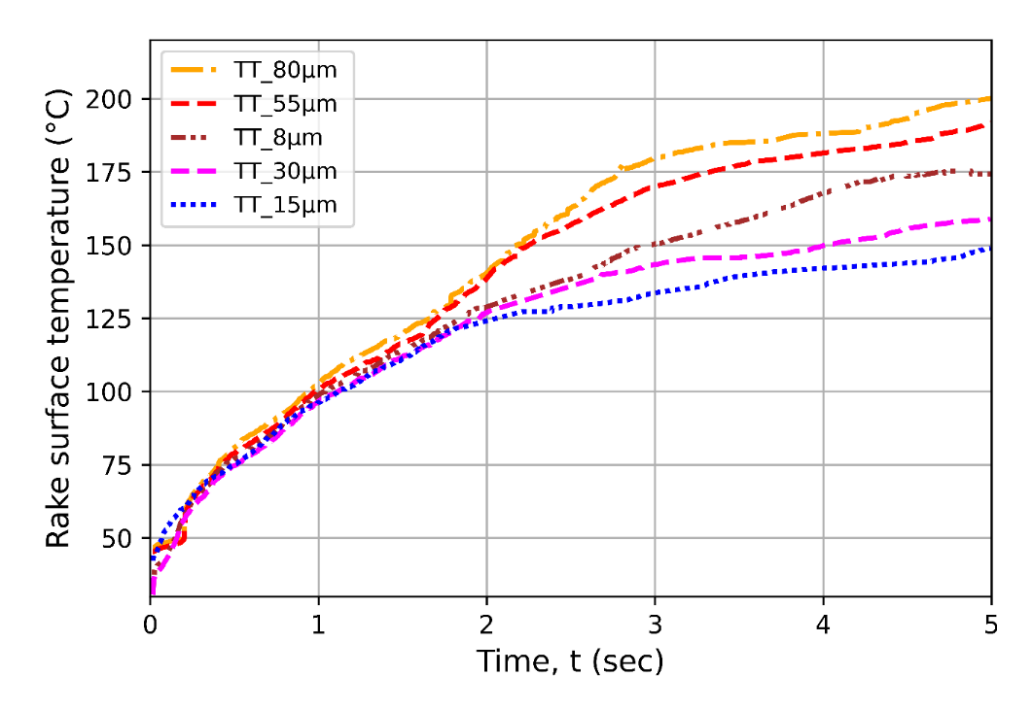


Figure 4.21. Measured rake surface temperature variation with texture depth

And the low thermal conductivity of the accumulated titanium further retards the heat dissipation process in the case of textured tools with 55  $\mu m$  and 80  $\mu m$  micro-pillars. Thus, both these tools have witnessed a higher temperature compared to the other textured tools. Tool with 15  $\mu m$  micro-pillars showed the least temperature rise, followed by 30  $\mu m$  and then 8  $\mu m$ . The depth of the micro-pillars should be sufficient to disrupt the momentum of the flowing chip and cause it to curl higher. This does not seem to be the case in 8  $\mu m$  textures, the micro-pillar depth may be too shallow to promote chip curling and to provide a passage for the surrounding air. This observation is in good agreement with the tool-chip contact length (see Figure 4.11). Whereas a depth of 30  $\mu m$  indicates the onset of work-material accumulation in between the micro-pillars due to the inability of the chips to curl out from the deep grooves created between the micro-pillars. The accumulated material obstructs the heat dissipation from the tool tip and hence the temperature rise. This leads to the conclusion that a textured tool should have micro-pillars above 8  $\mu m$  and below 30  $\mu m$  to restrict the temperature rise to a lower value.

### 4.3. Theoretical estimation of shear plane angle

Theoretical estimation of shear plane angle is made based on tool-chip contact length obtained during orthogonal machining. Like Merchant's minimum energy theory, Rowe and spick [114] proposed a theory stating that the primary shear plane shall attain an inclination such that the rate of work done will be maximum or minimum (Eq. 4.1). However, unlike the constant frictional coefficient assumption made by

Merchant, this theory incorporates the interfacial sticking tool-chip contact length into the shear plane angle estimation. Therefore, Rowe and spick theory is adopted in this work to estimate the shear plane angle based on the experimentally obtained tool-chip contact length.

$$\frac{d}{d\phi}(total\ rate\ of\ work\ done) = 0$$
 Eq. 4.1

The total rate of work done is the summation of the energy expended on the primary and the secondary shear plane [114].

$$\frac{d}{d\phi} \left( \sum primary \, shear + Secondary \, shear \right) = 0$$
 Eq. 4.2

A 2D schematic representation of the orthogonal cutting process, along with its corresponding hodograph during chip formation, is represented in Figure 4.22.

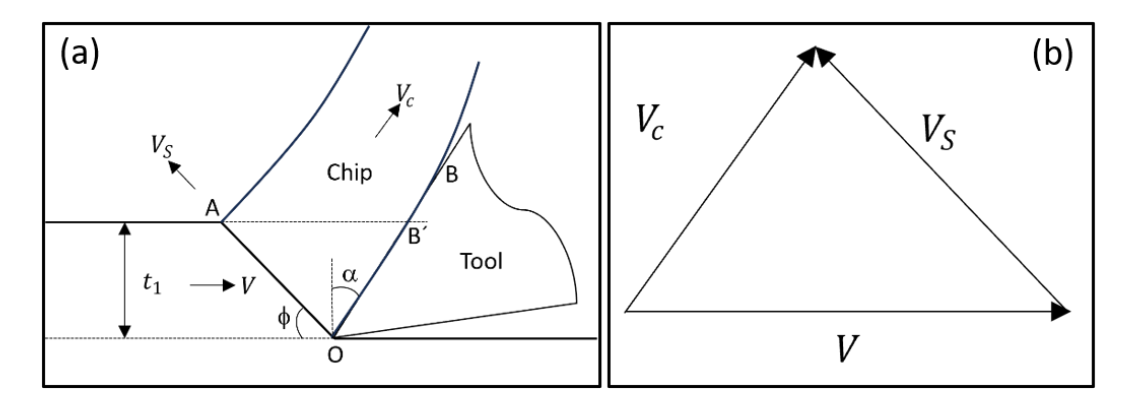


Figure 4.22. (a) 2D representation of an orthogonal cutting process (width b = constant); (b) Corresponding hodograph

Further expressing the primary and secondary shear in terms of force and its corresponding velocity.

$$\frac{d}{d\phi} \left( (F_{OA} \cdot V_S) + (F_{OB} \cdot V_C) \right) = 0$$
 Eq. 4.3

Where  $F_{OA}$  and  $F_{OB}$  are the forces while  $V_S$  and  $V_C$  are the chip velocities along the primary and secondary shear plane. With reference to Figure 4.22, Eq. 4.3 can be further expressed as,

$$\frac{d}{d\phi} ((K \cdot OA \cdot b \cdot V_s) + (\beta K \cdot OB \cdot b \cdot V_c)) = 0$$
 Eq. 4.4

Where K is the shear yield strength of the material, OA is the length of the primary shear zone, OB is the sticking length between the chip underside and the tool rake face, and b is the constant width of the chip, Figure 4.22 (a). A parameter  $\beta$  is introduced to model the friction condition at the chip and tool interference on the rake face, ranging from 0 to 1.  $\beta$  is the ratio of shear stress at the seizure zone to the yield strength of the chip.

$$\beta = \begin{cases} 0, & perfect sliding \\ 1, & complete sticking \end{cases}$$

Referring to the hodograph in Figure 4.22 (b),  $V_S$  and  $V_C$  can be expressed in terms of cutting velocity (V), rake angle ( $\alpha$ ), and shear plane angle ( $\phi$ ). To represent the chip and tool contact length (OB) in terms of feed, the parameter  $\xi$  is introduced such that,

$$OB = \xi OB'$$

Here, OB´ is the projected length on the rake face and  $\xi$  accounts for the chip tool sticking length factor. Feed is equal to the uncut chip thickness ( $t_1$ ). Referring to Figure 4.22 (a),

$$OB = \xi \frac{t_1}{\cos \alpha}$$
 Eq. 4.5

Eq. 4.4 can be re-written as,

$$\frac{d}{d\phi} \left( \left( K \cdot \frac{t_1}{\sin \phi} \cdot b \cdot \frac{v \cdot \cos \alpha}{\cos(\phi - \alpha)} \right) + \left( \beta K \cdot \frac{\xi t_1}{\cos \alpha} \cdot b \cdot \frac{v \cdot \sin \phi}{\cos(\phi - \alpha)} \right) \right) = 0$$
 Eq. 4.6

This can be differentiated to produce the simplified condition as

$$\cos \alpha \cos(2\phi - \alpha) - \beta \xi \sin^2 \phi = 0$$
 Eq. 4.7

The shear plane angle  $(\phi)$  can be estimated for the selected values of  $\beta$ ,  $\xi$  and  $\alpha$  by plotting the following two families of curves as a function of  $\phi$ .

$$P = \beta \sin^2 \phi$$

$$Q = \frac{1}{\xi} \cos \alpha \cos(2\phi - \alpha)$$

In the present study,  $\alpha = 0$  and considering only the sticking region ( $\beta = 1$ ), the shear plane angle is estimated by the intersection of these two curves, P and Q, as shown in Figure 4.23. The sticking region length is taken from Figure 4.11 and is substituted in Equation 4.5 to calculate the value  $\xi$ . The plain tool resulted in the minimum shear plane angle, while the texture tool (15 µm) with the least contact length ( $\xi = 1.22$ ) resulted in the maximum  $\varphi$ . It is well established that an increase in the shear plane angle produces thinner chips and reduces the shear plane area along with the forces [6]. All these factors contribute to improved machining.

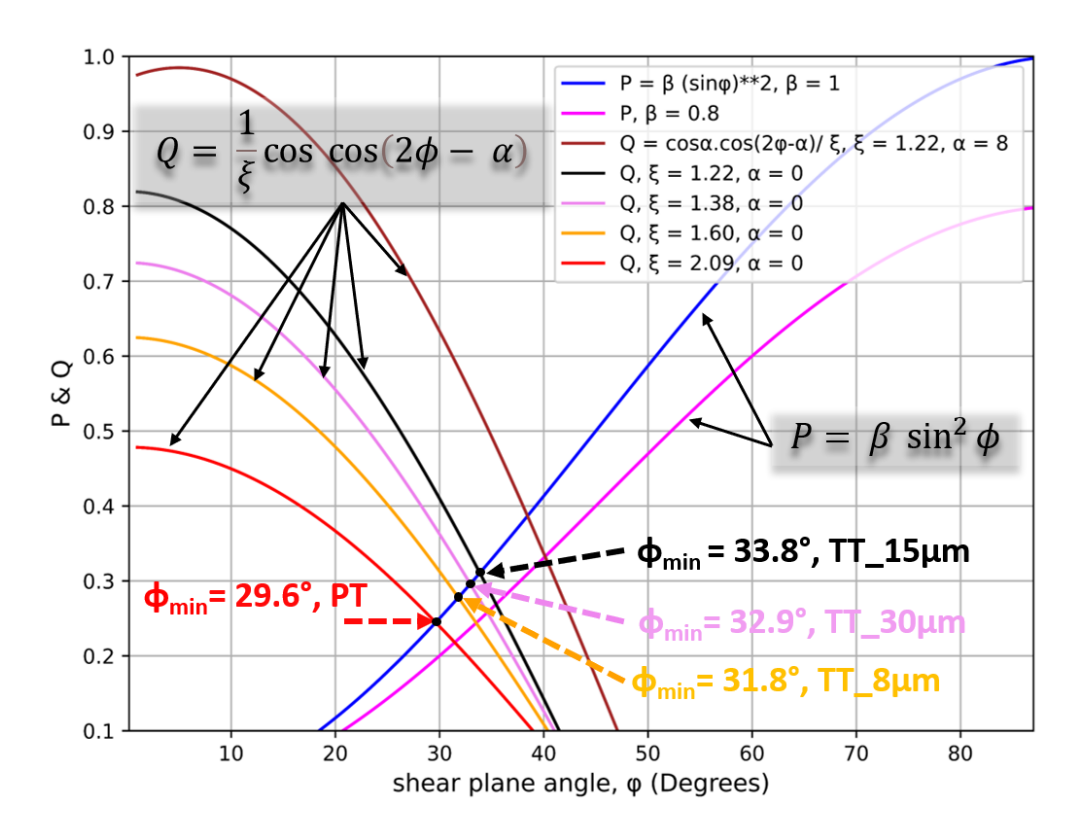


Figure 4.23. Shear plane angle from the intersection of P and Q

To better understand the effect of tool-chip contact length on the rate of work done, the total work done rate is plotted against the shear plane angle for plain and textured tools, as shown in Figure 4.24. Curve A represents the rate of primary shear work for a o° rake angle. The minimum work is always obtained at  $\phi = 45^{\circ}$ . Curve B indicates the increasing trend of work rate in secondary shear with the shear plane angle. The remaining curves of Figure 4.24 represent the summation of curves A and B for plain tool and various textured tools. The minima for all these curves are attained at a higher rate of work and a lower value of  $\phi$ . This demonstrates the importance of secondary shear work and contact length on the cutting performance of the tools. Due to extended tool-chip contact in plain tools, the value of  $\phi$  for minimum work is less than that of textured tools and at an increased work rate. At a low shear plane angle, the area of the

shear plane becomes more significant due to thicker chips, and thus, the cutting force rises. This approach to calculating the work done rate emphasizes the importance of the rake face contact area in metal cutting mechanics. It explains how the contact area affects the thrust and main cutting forces.

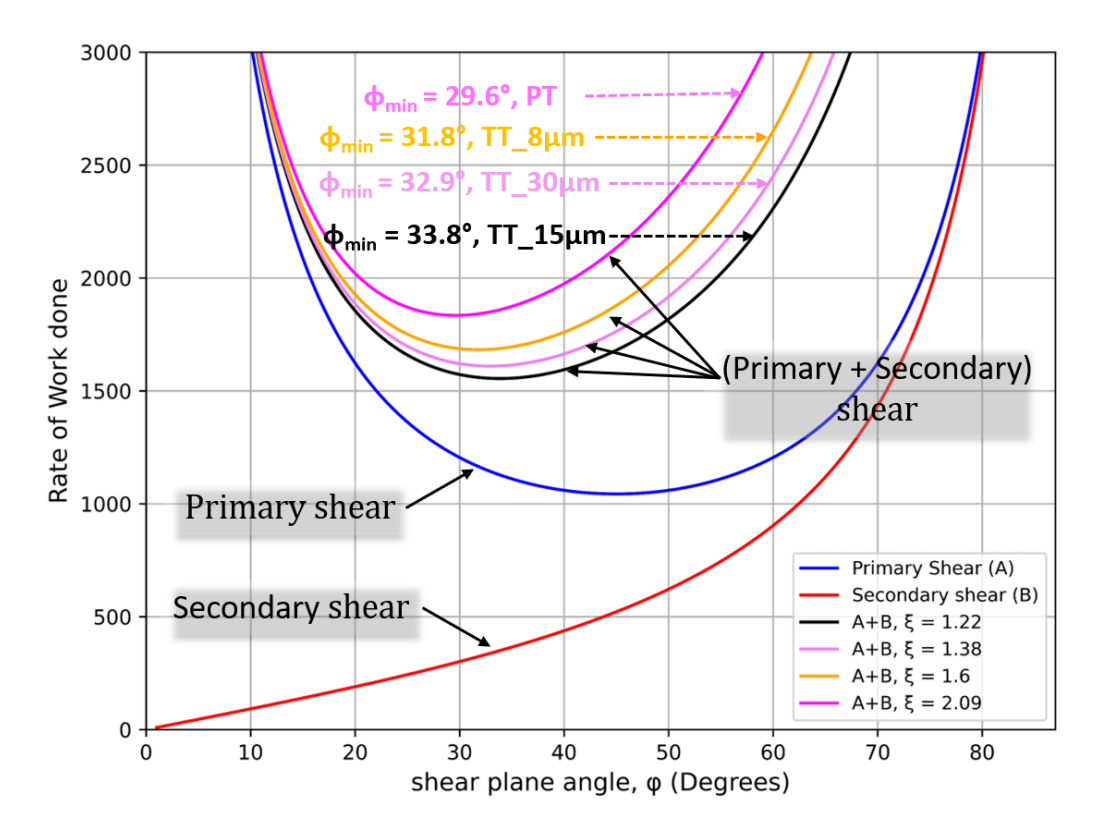


Figure 4.24. Rate of work done vs shear plane angle for plain tool and textured tools of different depths

# 4.4. Chapter conclusions

Orthogonal machining of Ti6Al4V is conducted using micro-pillar textures of depths ranging from 8 to 80  $\mu$ m, with results compared to a plain tool. The novelty of the study can be perceived as the establishment of a link between texture depths and cutting performance under dry condition, covering aspects such as tool-chip contact length, forces, cutting temperature, chip morphology, and tool wear. Valuable insights into the chip curling mechanism are obtained, and a theoretical model based on minimum energy theory highlights the impact of contact length on cutting performance. Key findings include:

• Textured tools reduce sticking contact, with optimal performance at 8 to 30  $\mu$ m texture depths. Depths beyond 55  $\mu$ m were less effective as compared to plain tools. Improved results are attributed to disrupted chip momentum and reduced

- chemical activity beneath the chip. High-depth textures result in subpar performance due to excessive work material accumulation.
- Shorter, untangled, and highly curled chips are produced for 15 and 30  $\mu$ m micropillars. Suitable depths of these textures lead to considerable disturbance in the chip momentum, and bending moment is exerted on the chip at multiple locations.
- The cutting edge could maintain its sharpness for extended periods in case of low micro-pillar depths (8 to 30 μm) compared to high depths (55, 80 μm). This conclusion is evident from the measured flank wear widths. Reduced contact mitigates the heat influx to the tool, which helps retain the sharp edges. Sharp edges ensure proper cutting and less rubbing between the tool and work material.
- A considerable improvement in the measured feed forces is observed in low texture depths. This indicates improved frictional conditions at the junction of the chip underside and the tool surface since feed force is the direct measure of resistance to chip flow. Force analysis also reveals that the micro-pillar textures are independent of the chip flow direction.
- A significant reduction of about 54% in tool tip temperature is observed in the 15
   µm textured tool compared to a plain tool. The measured rake surface temperature
   reveals that high-depth textures are not very effective in lowering the temperature
   due to work-material accumulation between the micro-pillars.
- Theoretical estimation of shear plane angle based on total energy expended in the machining operation reveals the significance of contact length on the shear plane.
   A lower contact length implies a higher minimum shear angle and a lower total work rate.

This chapter concludes that micro-pillared textured tools enhance the machinability of titanium alloys in dry conditions. A low texture depth (8-15  $\mu$ m) is key, as it reduces tool-chip contact and promotes chip curling, improving overall tool performance.

# **CHAPTER 5**

# TURNING OF TI6Al4V USING TEXTURED TOOL UNDER DIFFERENT MACHINING CONDITIONS

The performance of the micro-pillar textured tools during dry orthogonal machining of Ti6Al4V is presented in Chapter 4. This chapter evaluates the performance of these cutting tool inserts under different machining conditions during the turning of Ti6Al4V. Minimum Quantity Lubrication (MQL) and compressed air environments are used to perform the turning operation. The dry and wet conditions are also used for comparison. The performance of the cutting tools is evaluated in terms of tool surface morphology, cutting forces, chip morphology, and workpiece surface roughness.

# 5.1. Experimental plan

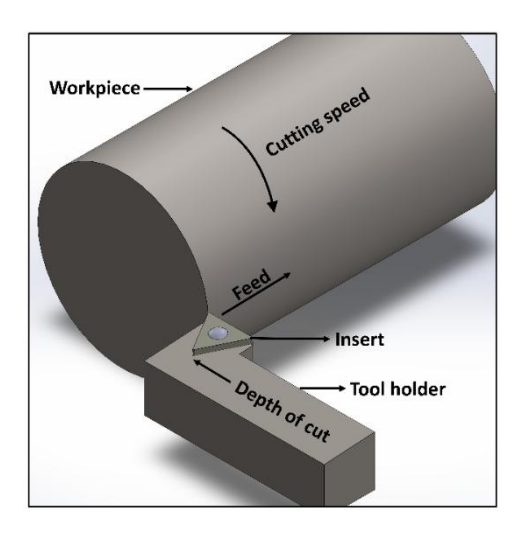
This section outlines the adopted plan for performing the experiments. The machining process, process parameter selection, and output response evaluations are mentioned in this section.

# 5.1.1. Turning operation

Turning operation is performed on a cylindrical rod of Ti6Al4V using a CNC lathe (Make: FANUC Series *oi* Mate-TC). The performance of textured tools is investigated under compressed air and MQL conditions and is compared with dry and wet conditions, details of which are listed in Table 5.1. Figure 5.1 (a) and (b) present the schematic and the actual turning setup.

Table 5.1. Details of machining conditions

Conditions	Attributes
Dry	Air at atmospheric and 1.125 bars pressure
Compressed air	Pressurized air at 5 bars; Nozzle dia: 2 mm
MQL	Synthetic oil; pressurized air at 5 bars; Nozzle dia: 2 mm; Flow
	rate: 10 ml/hr
Wet	Emulsion; synthetic oil in water; Nozzle dia: 8 mm



(a)



\_\_\_\_

Figure 5.1. Turning process setup: (a) Schematic illustration; (b) Machine tool and setup

**(b)** 

# 5.1.2. Selection of process parameters

The basis for the selection of the process parameters is discussed in section 4.1.2 of chapter 4. Several combinations of cutting speed, feed, and depth of cut were tried to obtain vibration-free machining at high MRR (Table 4.1). the final process parameters are summarized in Table 5.2.

Table 5.2. Final parameters for turning operation

Variable	Attributes
Workpiece	Ti6Al4V (rod)
Tool insert	TCMW 16 T3 04 H13A (Make: Sandvik)
	Plain tool
	Textured tool
Cutting edge angle	90°
Rake angle	O°
Cutting speed	110 m/min
Feed	o.3 mm/rev
Depth of cut	0.5 mm
Length of cut	300 mm

#### 5.1.3. Measurement and characterization of output responses

To analyze the machinability of Ti6Al4V using textured tools, several output responses were evaluated. The morphology of the crater and flank surfaces of the tool was closely examined using a Scanning Electron Microscope (SEM, Make: Joel 6610LV) to assess the tool wear. Sticking regions on the rake and flank surfaces were identified, measured, and compared with those on plain tools across all machining conditions. The cutting forces and surface roughness of the machined surface were measured for each experimental setup. The chip morphology was investigated to get insight into the chip curling mechanism.

### 5.2. Results and discussion

Titanium alloys, in general, are complex to machine due to the generation of high temperatures in the seizure region. Seizure implies an intimate contact between the chip and the tool's rake face. The continuous shearing of the chip, which becomes necessary to maintain its constant flow, is the primary source of heat input to the tool. The cutting tool tends to soften at such raised temperatures, losing strength and rigidity. As the cutting edge loses its sharpness, the surface finish of the final part is affected.

### 5.2.1. Rake surface morphology

To understand the machinability of Ti6Al<sub>4</sub>V and the performance of the cutting tools used, it is crucial to study the chip flow over the tool rake surface. Over a major portion of the tool-chip interface, the contact is so nearly complete that the condition of seizure

arises at the interface. Due to this, additional shearing is witnessed in a thin section of the chip adjacent to the interface to maintain relative movement between the chip and rake surface. This continuous shearing in the secondary shear zone is the main source of heat transferred to the tool [6]. This section examines the tool-chip contact phenomenon for textured and plain tools using SEM. The images obtained from SEM were analyzed using Image J software to calculate the sticking contact area at the interface.

Figure 5.2 shows the rake surface morphology of textured tools (TT) and plain tools (PT) post-turning operation under dry, compressed air, MQL, and wet machining environments. A significant improvement is shown by the textured tools in lowering the sticking region at the chip/tool interface, along and perpendicular to the feed direction, irrespective of the cutting condition. The reduction in the feed direction could be achieved because of the novel texture pattern, which disrupts the momentum of the chip as the chip encounters the gap between two successive micro-pillars on the rake surface. This gap breaks the constant contact between the chip and the tool and encourages larger curling of the chips, thus, restricting the tool-chip contact. Another significant contributor to the improved performance of the textured tools is the interconnectivity of these gaps which promotes deeper penetration of the air/cutting fluids underneath the chips. This helps reduce the adhering of the freshly generated chip underside to the rake surface by mitigating its chemical activeness, as the cutting fluids react with the chip underside and form a protective layer [6]. Typically, for a plain tool, CF penetrates the tool-chip contact region through capillary suction. The penetration of CFs into the network of capillaries can be divided into three phases [115]: (i) entry of the CF into the capillary due to pressure gradient; (ii) evaporation of the CF due to the excessive heat in the region; (iii) spreading of the CF vapour into the capillary and formation of a thin vapour film at the interface. This process has been schematically represented in Figure 5.3. For proper cooling and lubrication at the interface, the total time to complete these three phases should be smaller than the capillary life. However, the intimate contact at the interface makes it very challenging for CF penetration. The gaps between the micro-pillars of the textured tool act as permanent capillaries aiding in the regular suction of CF into the seizure zone, as illustrated schematically in Figure 5.4. Thus, the combined effect of disturbed chip movement and deeper cutting fluid penetration has resulted in the reduced sticking region. Depending on the type of cutting fluid used, the intensity of this reduction will vary.

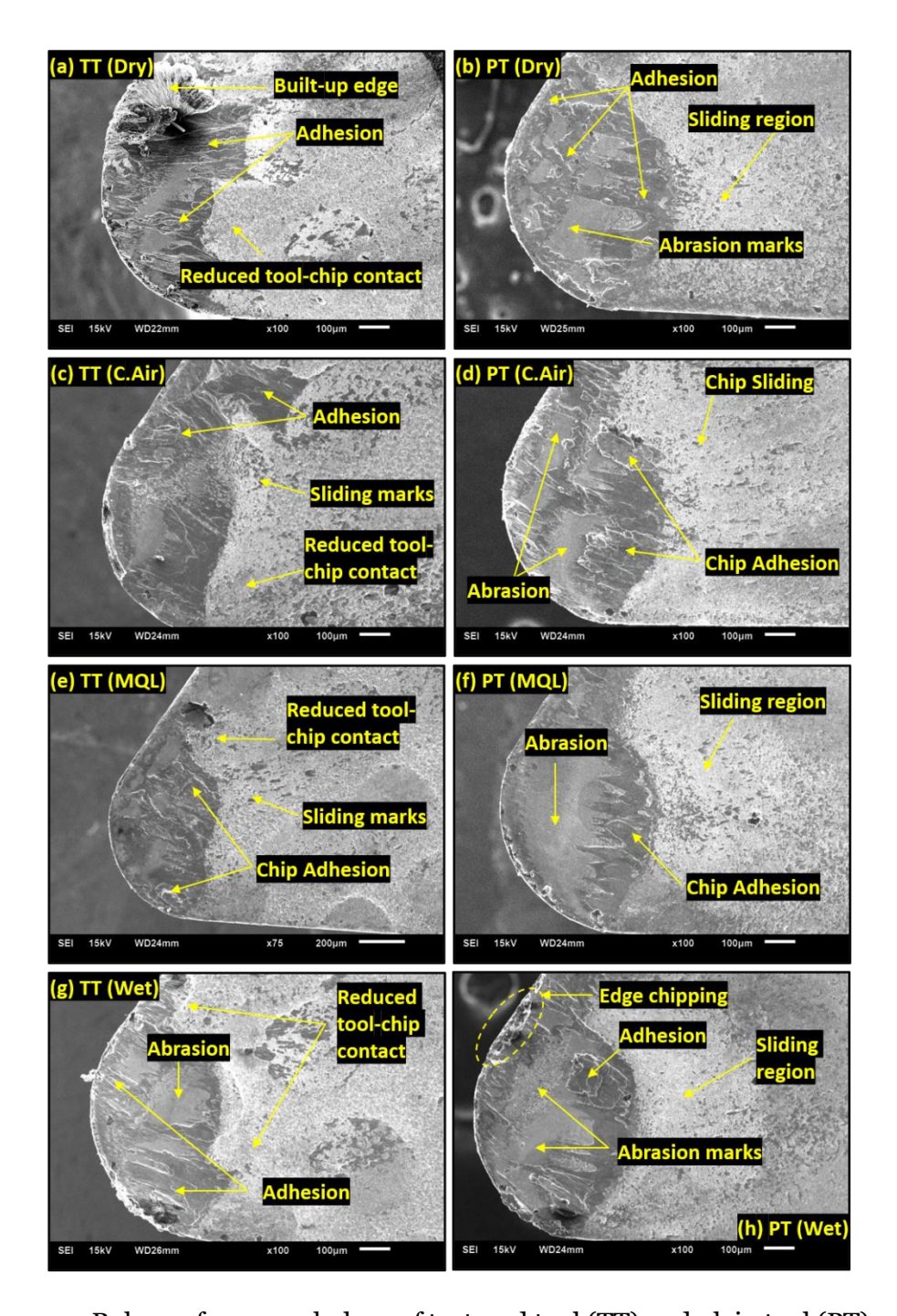


Figure 5.2. Rake surface morphology of textured tool (TT) and plain tool (PT) under dry, compressed air, MQL, and wet condition

Textured tool under dry turning has resulted in a BUE formation, and adhesion is observed, although the extent of adhesion is minimized due to reduced sticking area, as shown in Figure 5.2 (a). Plain tools under dry environments have shown severe adhesion, as observed in Figure 5.2 (b). It was due to the high temperature (as high as 900 °C) at the chip/tool interface, which could not be dissipated, unlike in TT. Similar observations of BUE and severe adhesion are made during the machining of titanium alloys [27]. Furthermore, the trapped micro-particles between the chip and tool under

the adverse condition of high temperature and pressure have led to abrasion on the rake face. These abrasion marks are less severe in texture tools as the micro-particles would have escaped through the passage provided in the form of gaps between the micro-pillars, which aligns with prior observation [109].

Similar rake face morphology is observed for textured tool under Compressed air and MQL environment, as shown in Figures 5.2 (c) and (e). Adhesion is found to be slightly lower for MQL as the layer of CF particles formed at the interface helps reduce heat and friction in the region. Traces of sliding marks are visible under both these conditions, unlike dry or wet conditions. This is because the pressurized air jet continuously tries to uplift the chip from the rake surface, leaving sliding marks on a small region. A similar observation of increased friction due to pressurized air has been witnessed earlier [27]. Figures 5.2 (d) and (f) show plain tools under Compressed air and MQL conditions. These tools have witnessed more adhesion and abrasion than the corresponding TT. The added benefit of CF along with pressurized air in the case of MQL has resulted in less severe adhesion in PT in contrast to the Compressed air environment, although the abrasion problem persists. The extent of adhesion is found to be much less in the wet condition for TT, as shown in Figure 5.2 (g). The CF dissipates the heat and lubricates the interface more effectively in TT due to the ease of access provided by the micro-channels up to the cutting edge. The inability of the CF to penetrate up to the cutting edge in a plain tool can induce thermal stresses in the tool due to uneven cooling [27], which could be the possible reason for edge chipping witnessed in Figure 5.2 (h). Significant abrasion marks are witnessed on the plain tools due to the sliding of the eroded micro-particle from the tool. The significant sliding regions observed in all the plain tools are almost negligible in the case of textured tools.

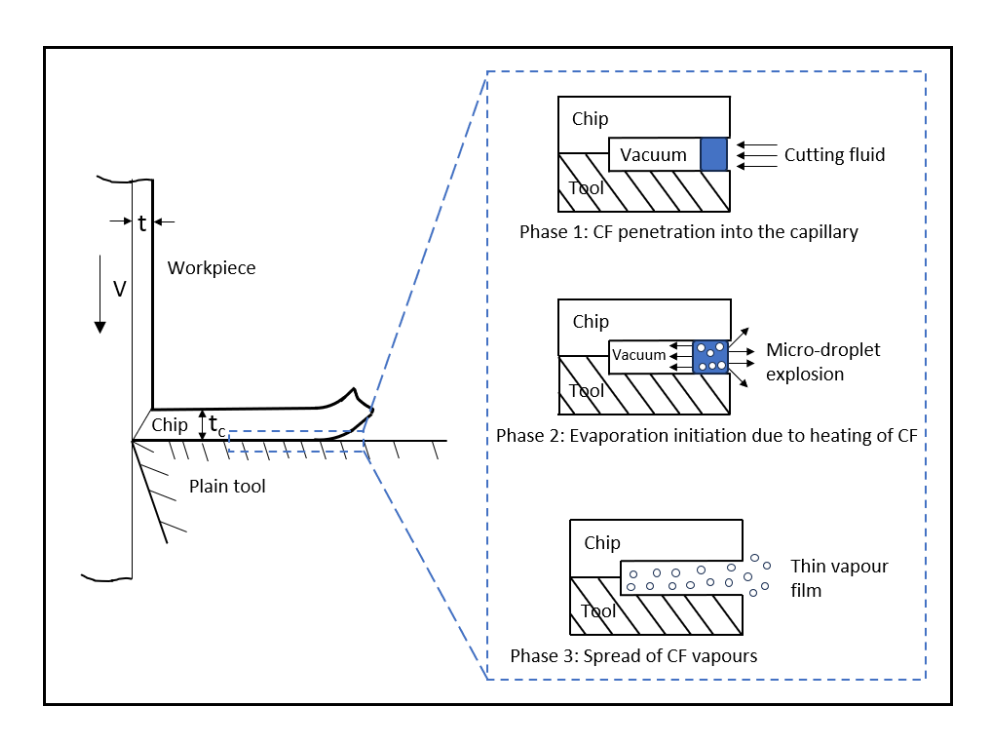


Figure 5.3. Schematic illustration of cutting fluid penetration for plain tools into the tool-chip interface [adopted from [115]]

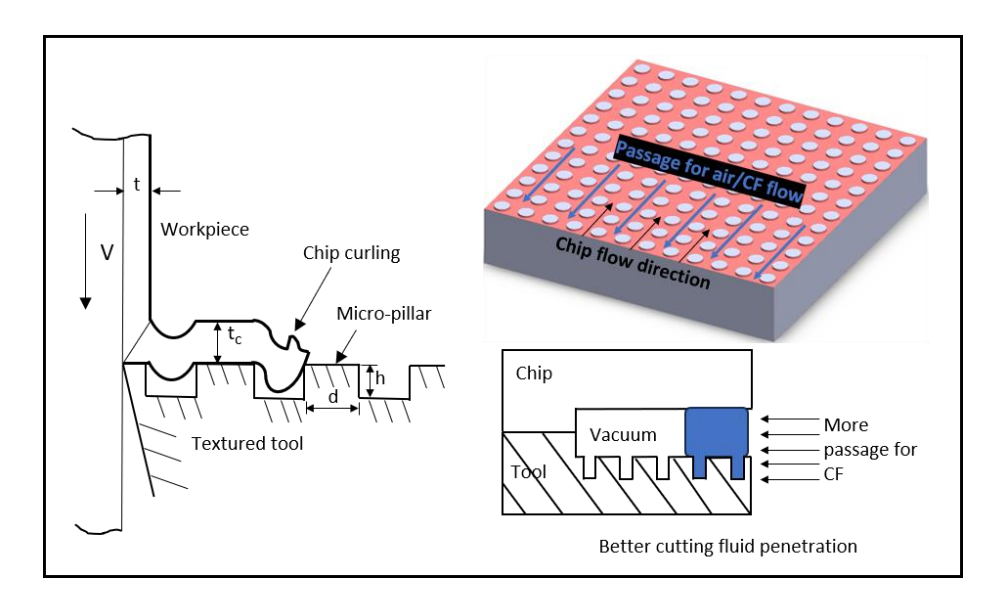
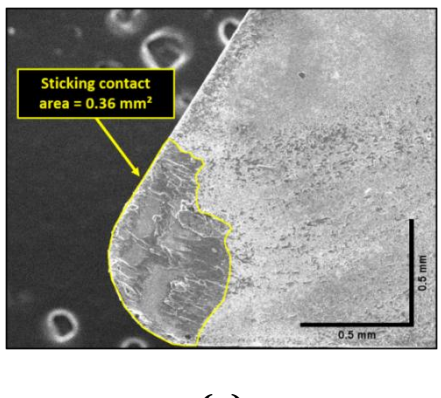


Figure 5.4. Schematic illustration of Cutting fluid penetration for textured tools into the tool-chip interface

## (a) Tool-chip contact area

Estimation of the chip/tool contact area is an important parameter to recognize the influence of textured tools on tool wear. Figure 5.5 (a) shows the chip/tool sticking region for a plain tool, marked and quantified using Image J software. A similar approach was used to estimate the area of all the tools, which are plotted in Figure 5.5 (b).



(a)

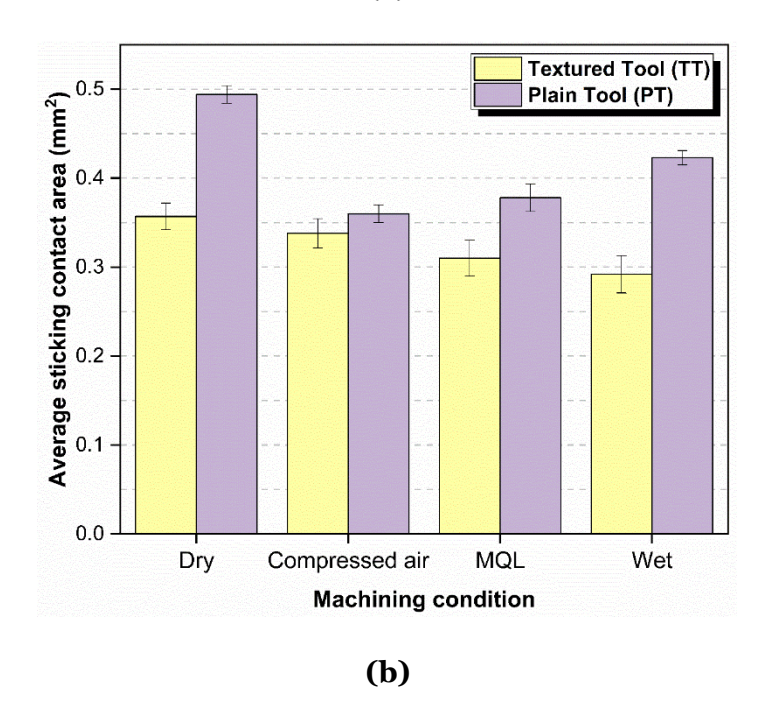


Figure 5.5. (a) Measurement of tool-chip sticking area; (b) Average sticking contact area under different machining conditions

The maximum contact area is observed in plain tool under dry condition. The low thermal conductivity of Ti6Al4V and its tendency to react readily with WC leads to high adhesion of the freshly generated chip underside onto the rake surface [23]. Higher tool wear has been reported due to larger contact areas in the case of non-textured tools [107]. On the contrary, the textured tool has shown a significant reduction in the contact area due to the passage provided on the rake face, even under dry condition. Another possible region specific to this case can be the formation of BUE, which restricted the subsequent chips from adhering to the rake face. The plain tool under Compressed air and MQL conditions have shown almost similar contact areas. This is because the pressurized air jet used in both cases, directed in the opposite direction to the chip movement, restricts the free flow of the chip over the rake surface by lifting it from its usual flow path. But even for such low contact areas, textured tools have been

able to reduce the contact area further to some extent. The MQL condition performed slightly better due to the presence of CF and the air jet. Under both conditions, the TT performed better than PT because of enhanced penetration of air/CF underneath the chip. Textured tool in the wet environment has shown the most promising results, indicating that the CF could effectively utilize the benefits provided by the textured rake face. However, the plain tools continue to struggle with the problem of adhesion and poor heat dissipation.

### 5.2.2. Chip morphology

Chip morphology examination can provide a clearer insight into the sticking condition at the tool-chip interface. Chip curling is the process of shaping the produced chip to the desired form. Curling can be either natural or forced. If the chip curls without meeting any obstruction, it is termed natural curling. Differential stress intensity in the chip, thermal strain due to temperature gradient at the tool/chip interface, and compressive stress-induced plastic bending are the major factors contributing to natural chip curling. However, in the actual machining operation, the chips have the tendency to encounter obstruction at multiple locations, such as the workpiece surface, the flank face of the tool, and the grooves of the specially designed tools. These obstructions exert an additional bending moment on the chip, encouraging it to curl further [116,117].

This section provides a discussion on the chips formed during the turning of Ti6Al4V using the Textured (TT) and Plain Tool (PT) under Dry, Compressed air, MQL, and Wet machining environments, Figure 5.6. As can be observed, all the chips have undergone up-curling movement, with varying degrees of curvature. Chips formed by textured tools are more tightly curled than the chips formed by plain tools. This is because the TTs have a restricted contact area with the chip, and when the chip encounters the grooves between the micro-pillars, it will deviate from its straight-line motion and tend to enter the grooves. This tendency of the chip to enter the grooves will bend them and result in tighter curling of the chips. When the chips make contact with the succeeding micro-pillar, the contact will exert an additional bending moment onto the chip underside, assisting it in curl further curling, refer to Figure 4.10. Higher curling of the chips in texture tools helps in reducing the heat input to the cutting tools by restricting its contact area with the rake face of the tool. Thus, making a positive impact on the surface quality and tool life. The regular chips formed using the plain tool cover a larger area of the rake face and obstruct cutting fluid penetration. Both result in a higher heat input to the tool, giving a shorter tool life. Chip entanglement with the workpiece produces a subpar surface finish and frequent stopping of the machine [35].

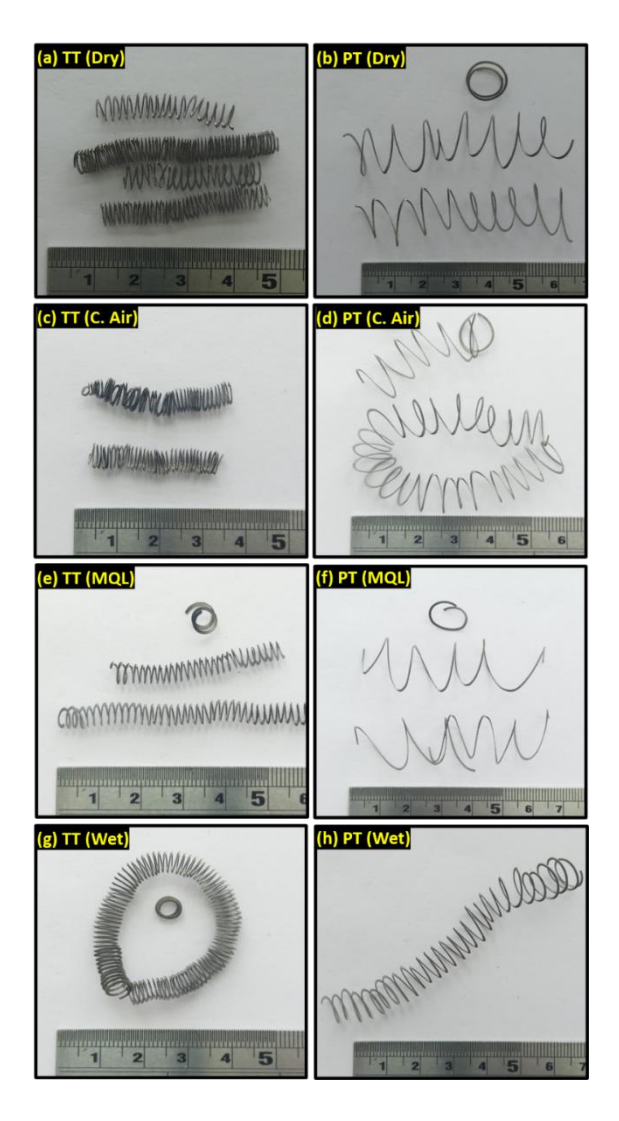


Figure 5.6. Chip form obtained under various machining conditions for textured tool (TT) and plain tool (PT)

In order to quantify the chip curling, the radius of the chip rings was measured at multiple locations, and the average chip curl radius is plotted in Figure 5.7. Textured tools have shown a substantial amount of chip curling, as indicated by the low values of chip radius. An increasing trend can be observed in textured tools, with the least radius in dry condition and a slightly higher radius in wet condition. A higher thermal gradient in conjunction with the bending moment promotes higher curling of TT/Dry. The enhanced CF penetration in MQL and wet conditions will quench the chip material, which alters the flow stress of the material and reduces the thermal gradient within the chip body, resulting in lower curling. Whereas, due to uncertainty in CF/ air penetration in PT, no such direct correlation can be observed for plain tools, as here

the chips undergo natural curling after making a relatively larger contact with the flat rake face.

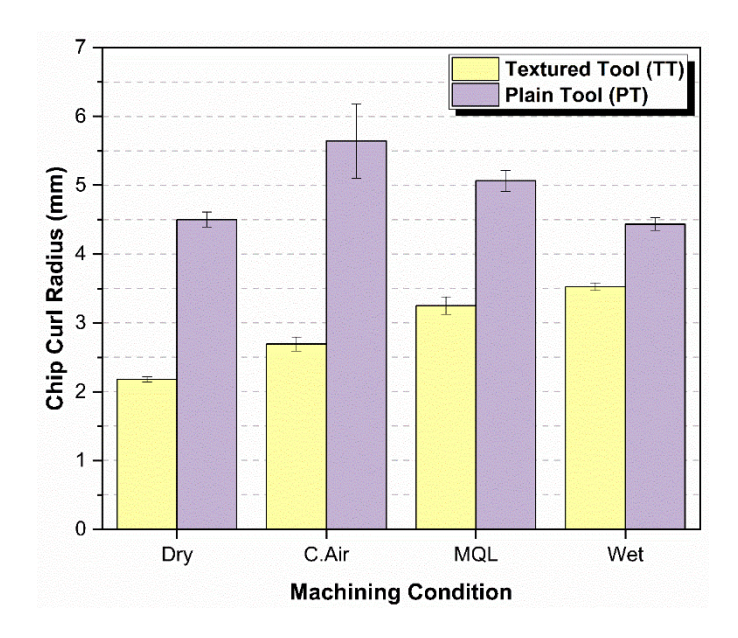
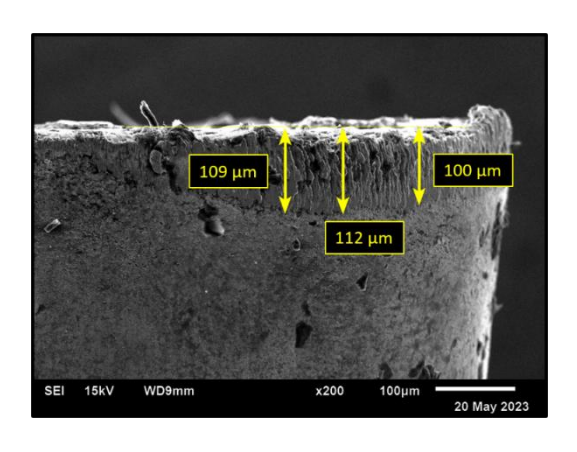


Figure 5.7. Chip curl radius under various machining conditions plain and textured tools.

# 5.2.3. Flank face morphology

The tool-work material contact length is usually too short to produce unfavorable temperatures in the tertiary shear zone while machining with a sharp cutting edge and a large clearance angle. With a clearance angle of 6°, the work material encounters the tool's clearance face in the order of 0.2 mm below the cutting edge [113]. But continuous cutting with the tool leads to wear in this region, resulting in a seizure condition on the flank surface, like that of the rake surface. Here, the seizure is much more detrimental, as the adhered work material is sheared along the flank surface at the cutting velocity, contrary to the rake surface, where the adhered chip is sheared at the chip velocity. Therefore, examining the flank wear becomes necessary as the tertiary shear zone can become a major heat source at large flank wear. The tools used are observed under SEM to understand the flank face morphology and measure the flank wear width. The wear width is measured at three different locations, as indicated in Figure 5.8 (a), and then the average flank wear width is plotted for all machining conditions in Figure 5.8 (b). The textured tool under dry condition has witnessed the maximum flank wear, possibly because of the large BUE formation. The heat generated in the BUE region, along with the high compressive stress, weakened the cutting edge, resulting in larger flank wear in contrast to the plain tool under dry condition. Textured tools performed better than plain tools in all the remaining conditions, with the least

wear in wet condition, followed by MQL and then the compressed air environment. The penetration of the CF up to the cutting edge helps maintain the sharpness of the cutting edge by better heat dissipation and thus prevents wear on the flank face for a longer period. The wear value in the case of MQL and wet conditions for plain tools are almost equal, indicating the inefficiency of the flood cooling approach to provide sufficient cooling to the cutting zone.



(a)

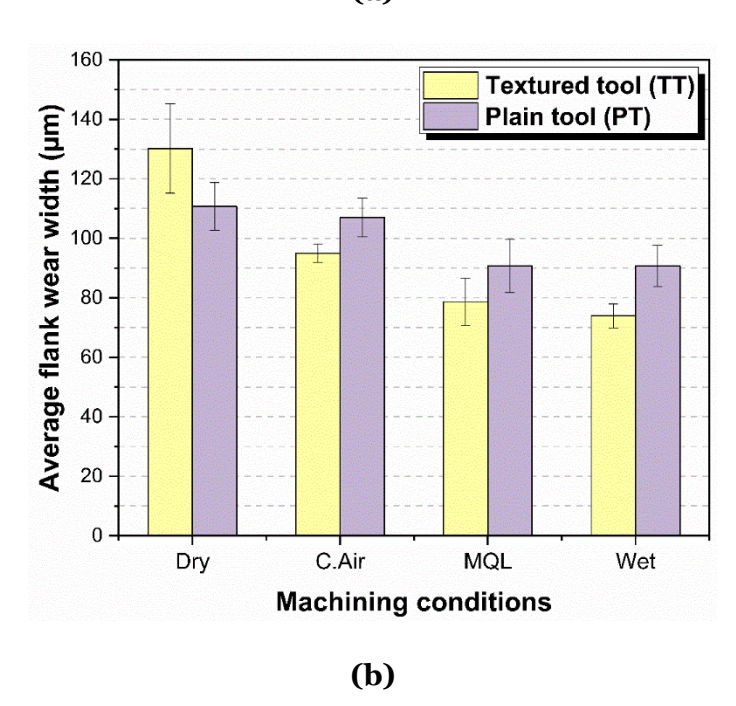


Figure 5.8. (a) Measurement of flank wear width; (b) Average width of flank wear under different machining conditions for TT and PT

Figure 5.9 shows the worn flank faces of all the tools under various machining conditions. All the tools have shown a similar trend in flank wear with varying degrees of adhesion, abrasion, BUE formation, and edge chipping. The BUE formation under TT/Dry condition has restricted the tool-work contact along the width of cut. However, the flank wear width is found to be maximum in these conditions. Under PT/ Dry

condition, no BUE is formed, but severe adhesion of work material can be found, succeeded by abrasion marks because the cutting edge is not able to retain its sharpness at elevated temperatures, which promotes rubbing of the work material onto the flank face. In TT/Compressed air condition, adhesion is witnessed but in patches, which indicates mild rubbing of the work material against the clearance face, whereas, in PT/Compressed air condition, adhesion persists similar to dry condition. Under MQL condition, micro-particles are found to adhere to the flank face. The thin layer of CF penetrating up to the cutting edge helps lower the temperature and hence the adhesion under TT/MQL condition, whereas it is not so evident in PT/MQL condition. Since in MQL, the CF is available in less quantity, chances are the high-temperature accumulation (low thermal conductivity of Titanium alloys) might decompose the CF and react with the highly reactive Ti6Al4V, which will promote adhesion. Under TT/Wet condition, the least adhesion is observed due to the availability of CF in large quantities up to the cutting edge. However, substantial abrasion marks are visible.

In PT/Wet condition, the extent of adhesion is lower than dry, compressed air, and MQL, but not as low as TT/Wet. And the reason for this is insufficient cooling and lubrication in the cutting zone. The non-uniform cooling due to restricted CF penetration has also resulted in minor BUE formation and edge chipping.

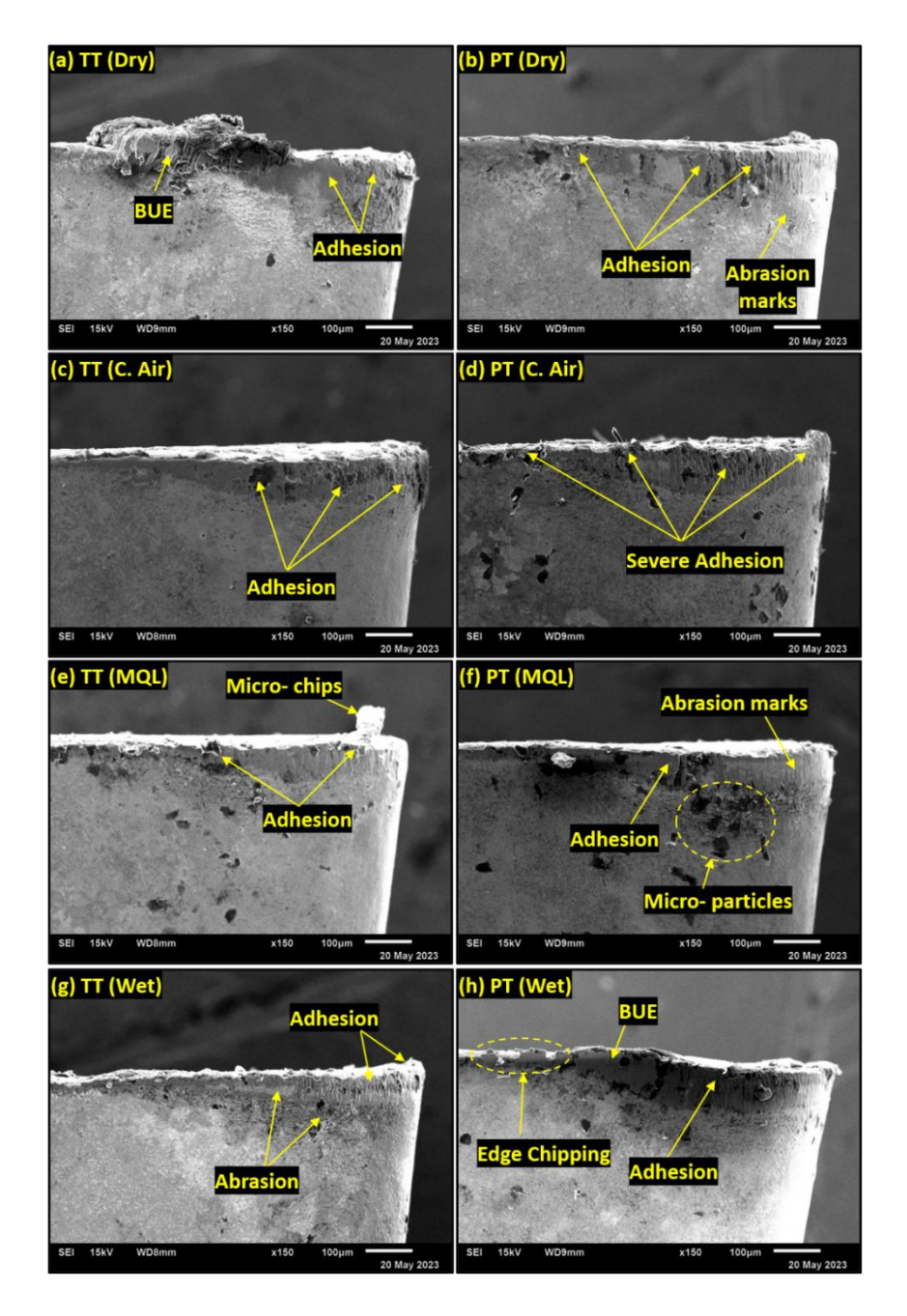


Figure 5.9. Flank surface morphology of textured tool (TT) and plain tool (PT) under dry, compressed air, MQL and wet conditions

## 5.2.4. Force analysis

The force acting on the cutting tool is a vital feature of the machining operation. The knowledge of the feed force is needed to study the effect of textured tools on the frictional condition at the tool-chip interface. For a o° rake tool, the feed force directly measures the aversion to chip flow on the rake surface. The radial component of the force tends to push the tool away from the workpiece. A larger radial force indicates chattering and deteriorated surface finish. The cutting force is related to the actual shearing of the workpiece during the machining operation. The forces generated

during the turning operation are measured using a multi-component piezoelectric dynamometer (Make: Kistler, 9129 AA) in combination with a charge amplifier (Make: Kistler, 5070) and Data Acquisition System (Make: Kistler, 2855 A4). The measured raw data is analyzed using the DynoWare software (Type: 2825A 03), and a low-pass filter is applied to eliminate the noise from the acquired force signals, see Figure 4.3.

The difference in forces between textured and plain tools is believed to be governed by two major but opposing mechanisms. First, the reduced chip/ tool contact area restricts the seizure zone to a smaller area (Figure 5.5), reducing the additional shearing of the chips in the secondary shear zone. This mechanism is directly reflected in measured feed forces, refer to Figure 5.10. Second is the CF penetration beneath the chip and up to the cutting edge. Although this phenomenon is expected to reduce friction at the chip/tool interface, it also alters the flow stress of the work material due to quenching by the CF jet. As observed from Figure 5.10, the cutting forces for MQL and Wet conditions are relatively higher than dry condition, irrespective of the tool type, indicating an increase in flow stress of the material due to quenching by CF application. A similar observation of an increase in cutting forces is reported using a grooved tool under MQL condition [118]. As discussed in the earlier section, textured tools can restrict the tool-chip sticking area, a similar conclusion can be drawn from the measured feed forces, see Figure 5.10.

In general, the forces in the radial direction are the least, but here, they are of considerable magnitude mainly because of the low elastic modulus of Ti6Al4V, which is usually half of the Steel [23]. The low elastic modulus causes high workpiece material deflection, thus inducing chatter during the operation leading to a low surface finish of the final surface. It must be considered that although the forces associated with machining Titanium and its alloys are lower than those of Steel, the tool life is short due to high temperatures and unfavorable temperature distribution on the rake surface. Therefore, it can be argued that even though the textured tools increase the compressive stress on the rake face by reducing the contact area, they control the temperature generation in the chip flow zone by controlling the sticking area and enhance heat dissipation in this region due to effective CF/air penetration.

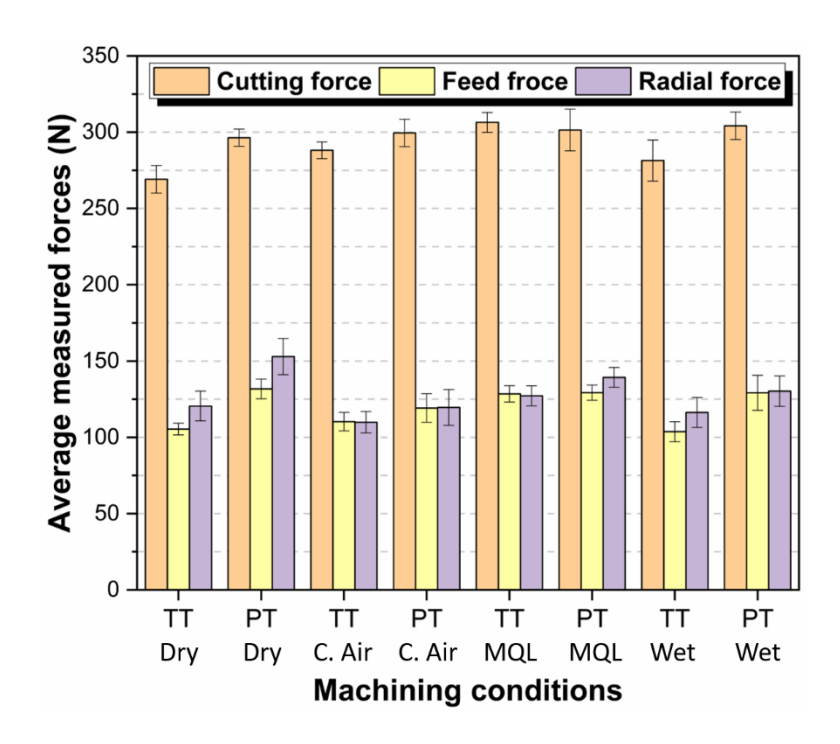


Figure 5.10. Measured forces under all the machining environments for textured tool (TT) and plain tool (PT)

### 5.2.5. Surface roughness analysis

The work material surface quality in a turning operation depends on the process parameters, cutting tool material and geometry, workpiece material, cutting environment, etc. The machining process parameters like cutting speed, feed, and depth of cut are found to contribute significantly to the surface finish of the product [119,120]. Generally, the average surface roughness (Ra) value is used to quantify the surface finish of the components. A contact-type 2D surface roughness measuring device (Make: Mitutoyo SJ-210) is used to measure the Ra value after each cutting experiment. Before every Experiment, a finishing cut is performed on the workpiece to maintain a Ra around 1 µm. It is to be noted that a textured tool was used to perform these finishing cuts, indicating these tools are capable of achieving this level of surface finish. However, the Ra values presented in Figure 5.11 are on the rougher side for both tool types. The major reason for this high surface roughness is the high feed and depth of cut, added with the low elastic modulus of Titanium alloys, which contributed to a larger deflection of the workpiece material. Therefore, instead of maximizing the process parameters to enhance productivity, they should be optimized to make a tradeoff between productivity and surface finish. Texture tools have been reported to improve the surface quality of the products due to a reduction in contact length and its micro-reservoir effects. It is also observed that when drilling titanium alloys with textured tools, there are fewer defects and burrs in the resulting holes [121]. Dry machining condition has resulted in the highest surface roughness for both types of tools. However, it is lower for TT as compared to PT. Similarly, TT has performed better under all the other machining conditions than PT. This observation can be correlated with the radial forces (Figure 5.10), which are also found to be lower in the case of TTs. It can be observed the percentage reduction in surface roughness is lower for wet machining compared to dry machining. This can be explained by the two opposing mechanisms associated with textured tools. First, the reduced contact area restricts the secondary shearing of the chip, which contributes to a better surface finish. Second, the enhanced cutting fluid penetration underneath the chip increases the flow stress of the material due to quenching in wet machining, which will have adverse effects on the surface finish. Whereas in dry machining, thermal softening is the dominant factor, contributing to a good finish. The ability of the TTs to mitigate tool wear is responsible for the overall improved surface finish.

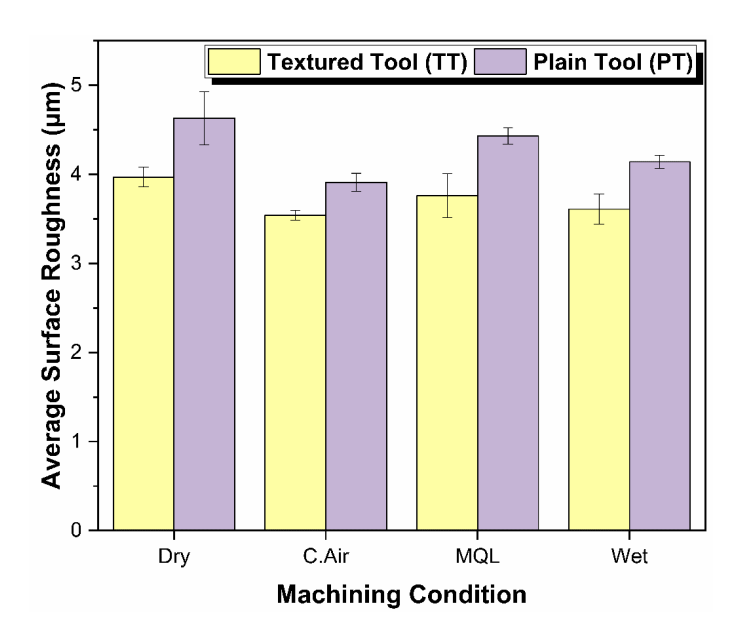


Figure 5.11. Average roughness (Ra) of the machined surface under different conditions

# 5.3. Machinability of additively manufactured titanium alloy

With the advent of additive manufacturing in recent decades, its ability to produce near-net-shaped components is being widely explored [122]. Production of components close to their final shape and size has reduced the dependency of titanium alloy components on machining. However, machining is still necessary as a post-processing operation to incorporate immediate design adjustments, dimension alterations, and surface quality enhancement of the Additively Manufactured (AM) components [123]. In additive manufacturing, successive deposition of new layers onto

the preceding ones is used to build the final component. These components are often exposed to undesirable phase transformation and thermal stress due to cyclic heating and cooling after each deposition layer [124]. Additionally, substantial residual stress emerges owing to a thermal gradient as high as 50 × 103 K/cm [125,126]. Due to a higher temperature gradient along the scan direction, residual stresses usually peak along that direction, thus inducing anisotropic stress distribution in the component [127]. Significant disparities exist in the mechanical properties and microstructures of the Conventionally Manufactured (CM) and AM components [128]. CM Ti6Al4V typically comprises an alpha (α) phase dispersed in a beta (β) matrix, existing in lamellar, equiaxed, or bimodal microstructural forms. The microstructure variations are controlled by diffusion-based nucleation and growth during the transformation from  $\beta$  phase to  $\alpha$  phase [129]. However, due to the inherent high cooling rates in the additive manufacturing process, martensitic alpha ( $\alpha'$ ) transformation is dominant in as-built components [130]. Due to the presence of partial or complete  $\alpha$  and finer  $\alpha$ laths, additively manufactured products generally have higher strength and hardness but poor ductility compared to conventional components [131,132]. Another significant difference between the CM and AM components is their surface roughness. The additively manufactured components are always seen to have poor surface finish. The powder that partially melts and adheres to the component being built contributes significantly to the inferior surface finish. The poor surface finish adversely affects the fatigue life of these components [133]. The surface irregularities can be considered as micro-notches with a depth equal to the surface roughness value, contributing to the poor fatigue life of the AM components [134].

Post-process machining of additive manufacturing components is imperative to achieve the necessary final finish and dimensional accuracy by utilizing appropriate machining operations. The machinability of AM Ti6Al4V is notably affected by variations in its mechanical properties. Sartori et al. [135] studied the contribution of the material properties on crater wear during the turning of AM Ti6Al4V printed using various additive manufacturing processes. The results were compared with a wrought titanium alloy of the same grade under cryogenic and dry environments. The study revealed maximum crater wear in the AM component under dry and cryogenic conditions. This was attributed to the component's low thermal conductivity and high hardness. Reduced cutting temperature due to the application of LN<sub>2</sub> eliminated diffusion wear. Abrasion and flank wear are also reported to be minimal in cryogenic cooling [136]. Bordin et al. [137] performed a comparative study on wrought and AM Ti6Al4V machinability. AM alloys witnessed higher tool wear and poor surface finish compared to wrought. Craters were observed only in the case of the additively

manufactured component owning to its higher hardness. Bordin et al. [138] also investigated the contribution of cryogenic cooling on AM components during turning operation and revealed a substantial reduction of tool wear and improved chip breakability. Polishetty et al. [139] studied cutting forces and surface roughness of wrought and AM Ti6Al4V. Higher cutting forces due to higher strength and better surface finish due to higher hardness and poor ductility were observed in the AM component. Li et al. [140] reported the depth of cut as the most critical parameter. AM titanium alloy witnessed lower resultant cutting force at a lower depth of cut, whereas at a higher cutting depth, the wrought part experienced more downward force. The surface roughness of both these components was found to be in the same range after machining. Raval et al. [132] reported vibration over a wide range of frequencies while machining AM Ti6Al4V, which led to abrupt chipping of the tool edge. The martensitic microstructure is believed to be the primary cause of this outcome. The literature available thus far clearly indicates that the machinability of AM Ti6Al4V is quite different and challenging compared to conventionally developed Ti alloys. Therefore, it becomes imperative to explore various options to improve the machinability of titanium alloys developed using AM. The micro-pillar textured tools are studied in relation to the machining of Ti6Al4V fabricated using selective laser melting (SLM).

The turning experiment setup and the process parameters are presented in Figure 5.1 and Table 5.2, respectively. Sandvik-made TCMW 16 T3 08H13A turning tool inserts are used in this study. Figure 5.12 and Table 5.3 demonstrate the difference in microstructure and mechanical properties exhibited by SLM Ti6Al4V compared to its wrought counterpart.

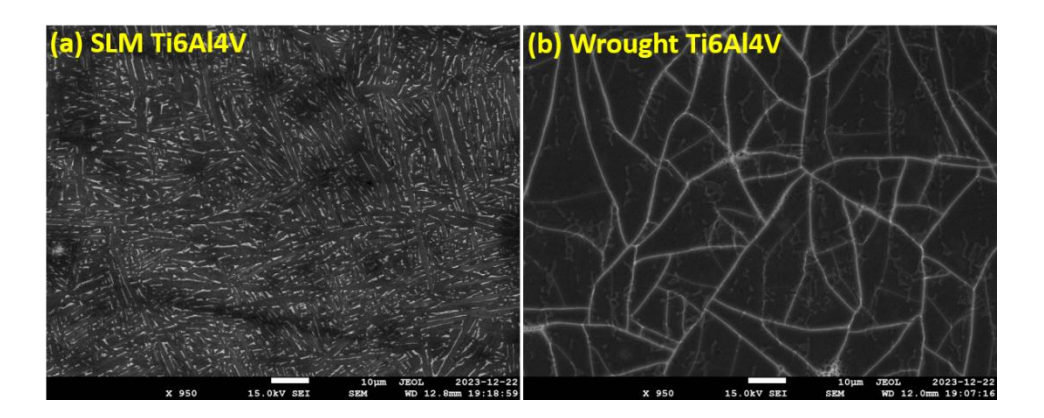


Figure 5.12. Microstructure (a) SLM Ti6Al4V; (b) Wrought Ti6Al4V

Table 5.3. Properties of SLM and wrought Ti6Al4V

Properties	SLM Ti6Al4V	Wrought Ti6Al4V
Tensile strength (MPa)	1110 ± 13	895
Yield strength (MPa)	996 ± 10	825
Hardness (HV)	399 ± 4	340
Elongation at fracture (%)	7 ± 4	10
Modulus of Elasticity	112 ± 1	110

#### 5.3.1. Tool-chip contact area and force analysis

Figure 5.13 presents the sticking tool-chip contact area over the rake face of plain and textured tools. The textured tool under dry condition has shown a 16.1 % reduction in contact area compared to the plain tool. This can be attributed to the reduced chemical activeness of the freshly generated chips and the higher curling of the chips. The atmospheric air infiltrating the passage between textures reacts with the chip underside and forms a protective layer, which reduces the sticking tendency of the chip on the rake face. Moreover, the disturbance in chip flow momentum induced by the gaps between the micro-pillars induces higher chip curling, which restricts the tool-chip contact area, refer to Figure 4.10.

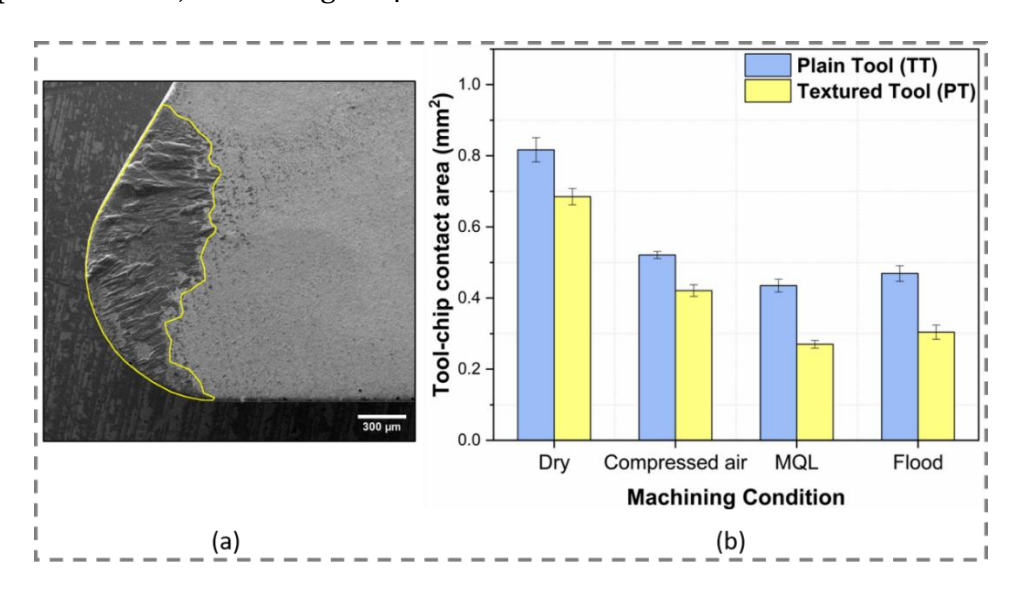


Figure 5.13. (a) Measurement of tool-chip sticking area; (b) Average sticking contact area under different machining conditions

The contact area for plain tool under compressed air and MQL condition is significantly lowered by 36.2 % and 46.7 % respectively, compared to PT/Dry condition. The pressurized air jet directed toward the incoming chips tends to uplift them, breaking continuous contact with the rake face. Under the compressed air and

MQL conditions the textured tools have exhibited lower contact area than their counterparts. This is mainly because of the greater CF/air penetration. Similar improvement is observed under wet condition. Amongst all the conditions, MQL has demonstrated the best results. This is because the pressurized air jet uplifts and unsettles the chips, and the accompanying CF helps control the sticking region's temperature.

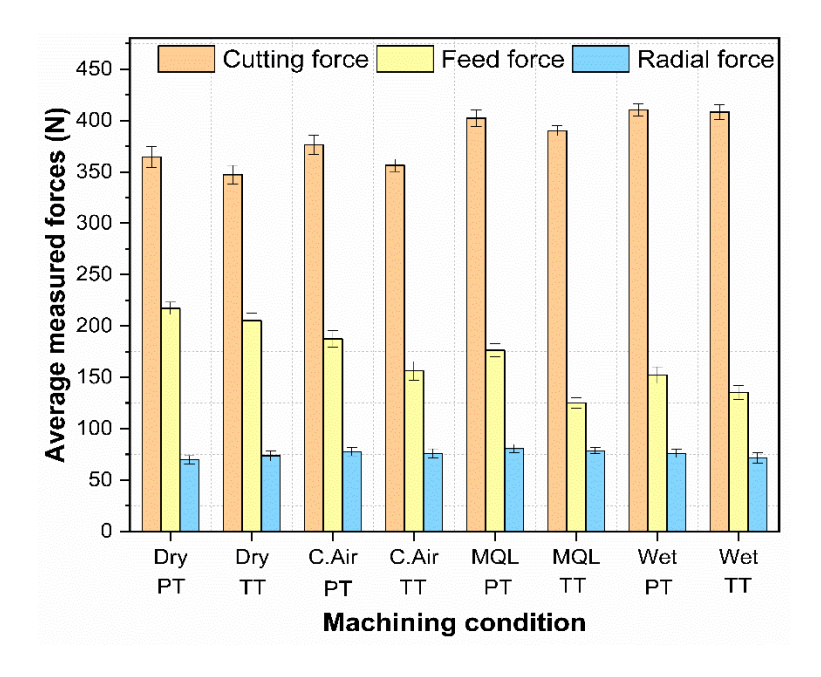


Figure 5.14. Average measured forces for plain and texture tools under different machining conditions.

The average measured machining forces are presented in Figure 5.14. Two crucial but contradicting mechanisms govern the measured forces in textured tools. First, the reduced contact area and adhesion on the rake face of the textured tool mitigate the seizure effect, irrespective of the machining condition. This improves the frictional condition at the interface and is reflected in the measured feed forces, Figure 5.14. Amongst all the tools and conditions, TT/MQL witnessed the least feed force, which amounted to a reduction of 28.9 % compared to PT/MQL. The second mechanism is dependent on the machining condition. The penetration of the CFs underneath the sticking region is expected to cool and lubricate the area, but at the same, it alters the flow stress of the material due to quenching by the CF. It can be observed in Figure 5.14 that the cutting forces in MQL and wet conditions are relatively higher than those in dry and compressed air conditions, as here, the material has undergone quenching, which has resulted in an increase in the flow stress of the material. The radial forces are almost constant for plain and textured tools in all machining conditions. This indicates that a slight variation in chattering is observed.

# 5.4. Chapter conclusions

Turning of Ti6Al4V using a micro-pillar texture pattern under dry, compressed air, MQL, and wet conditions has been presented in this chapter. The tool-chip contact area, flank wear width, and surface roughness improved significantly for textured tools compared to plain tools, as shown in Table 5.4. It is due to the disturbed momentum of the chip and deeper penetration of the cutting fluids (air/liquid) underneath the freshly generated chip, restricting its adhesion to the rake face.

Table 5.4. Machining performance comparison: % reduction in TT compared to PT

Evaluation	Dry	C. Air	MQL	Wet
parameter				
Tool-chip contact area	27.7	6.1	17.9	30.9
Flank wear	-	11.2	13.2	18.4
Surface roughness	14.2	9.4	15.1	12.8

The performance of the textured tool under dry, compressed air, and MQL conditions is compared with its performance under wet condition, shown in Table 5.5. Results of TT under MQL are comparable to those under wet conditions, suggesting it is a viable sustainable alternative to excessive cutting fluid use.

Table 5.5. Machining performance of TT: % difference compared to wet condition

<b>Evaluation parameter</b>	Dry	C. Air	MQL
Tool-chip contact area	22.2	15.7	6.16
Flank wear	76	28.4	6.4
Surface roughness	9.9	-	4.1

Textured tools are also capable of improving the machinability of additively manufactured components, as illustrated by the reduced tool-chip contact area and measured feed forces compared to a plain tool.

# CHAPTER 6 NUMERICAL MODELING OF TOOL TEMPERATURE

The superior performance of the proposed micro-pillar textured tool over plain tools is well established in chapter 4 and chapter 5. This chapter presents a Computational Fluid Dynamics (CFD) based numerical analysis of the heat dissipation capabilities of the micro-pillar array developed on the rake face of tungsten carbide inserts. The effect of micro-pillar shape and size on the tool temperature is also studied in detail through this numerical analysis.

## 6.1. Background

Estimating temperature and its distribution around the tool's cutting edge is quite challenging due to the continuously moving chips in this region and the nature of contact at the interface [110]. Cutting temperature can be experimentally measured by direct conduction techniques using tool-work thermocouples or embedded thermocouples, indirect radiation technique using infrared thermography or pyrometer, and metallographic techniques. In a tool-work thermocouple, the tool-chip interface acts as a hot junction, while the tool or the workpiece acts as a cold junction. The measured temperature is the mean of the entire interface; hence, the locally generated high temperatures cannot be captured [141,142]. An embedded thermocouple is used to measure the temperature of a fixed point or multiple fixed points below the rake surface of the tool [98]. Several holes must be drilled into the inserts to station the thermocouples, which alters the tool strength and heat flow. Drilling holes into the hard tool inserts is also very challenging. The temperatures measured below the rake surface are used to estimate the temperature of the cutting zone using the inverse heat conduction method [143]. Accurate calibration, slow response, and noise are the major problems associated with thermocouple techniques [110]. Due to its non-contact nature, radiation-based methods do not require predrilled holes, eliminating the impact on tool strength and heat flow. It also has a faster response compared to thermocouples. However, the significant challenges reported in radiation-based methods are chip obstruction and surface emissivity determination. The obscured view created by cutting fluid restricts this method only to dry machining. In the metallographic technique, temperature estimation is based on the microstructure and microhardness of the cutting tool, analyzed after machining. For an accurate estimate, the tool material should undergo observable microstructural and hardness changes with temperature, in the range of 600 to 1000 °C. Therefore, this method is restricted mainly to HSS; however, iron-bonded cemented carbides have

been reported to experience such metallographic changes with temperature [144]. Based on the complexity of the machining process and the challenges associated with each measuring technique, no consensus is established between the results from different measuring techniques [110]. Several studies have reported using Computational Fluid Dynamics (CFD) to investigate the heat transfer, cutting fluid flow, and mechanical deformation of the cutting tools during machining [145–147]. The flow of high-pressure coolants via internal cooling channels on the cutting tool inserts was investigated using CFD simulations for turning Inconel 718. The study reveals that heat transfer from the tool was significantly enhanced [148]. Another work used CFD to explore the effect of internal cooling channel profiles on heat dissipation through the cutting tools. To replicate the heat generated during the turning operation, a constant heat flux was applied at the tip of the tool [147]. However, this study did not consider the tool/chip contact area as the source of heat in the tool.

#### 6.2. Simulation procedure and boundary conditions

ANSYS Fluent has been used to perform the CFD simulations. The CAD model of the tools is prepared using SOLIDWORKS and imported into the ANSYS workbench. To avoid the high computational time, only the part of the insert involved in machining is modeled and analyzed. A control volume is defined on the tool's rake face for fluid flow, see Figure 6.1. Since the cutting fluid/air cannot penetrate the tool-chip contact area [6], the control volume is defined from the end of the contact region. The entry and exit boundary conditions are pressure inlet and pressure outlet. A pressure inlet is chosen to replicate the pressurized fluid flow from an external source at the entry. The standard K-E model is used to model the turbulent flow of the fluid. The fluid and the solid interface have been defined as a coupled system for better heat transfer. A uniform heat flux is applied over the experimentally obtained tool/chip contact area (Chapter 5, section 5.2.1), such that the simulated tool temperature matches the experimentally measured temperature at a distant location. This approach leads to the determination of total heat entering the cutting tool and, hence, the tool tip temperature under the various machining conditions. A similar approach of using a uniform heat flux has been adopted earlier [147,149]. The properties of the WC insert and the fluids used in the simulation are listed in Table 6.1.

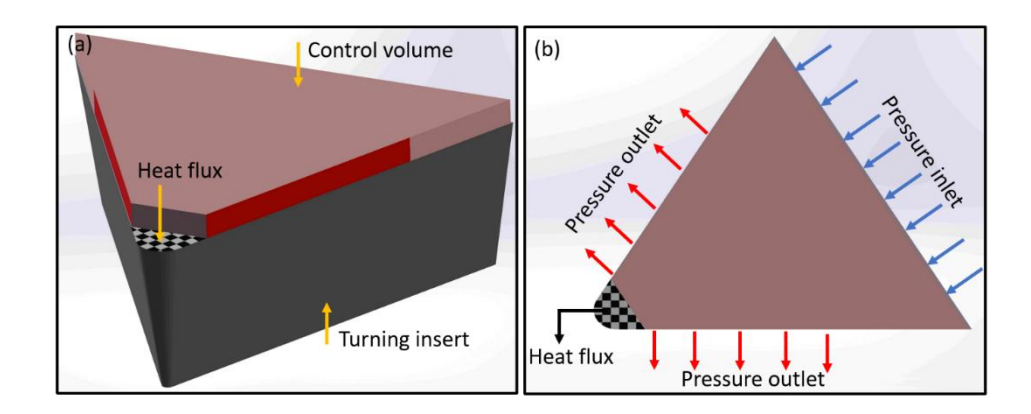


Figure 6.1. (a) Isometric view of the CFD model indicating the fluid control volume, turning insert, and the input heat flux; (b) Top view of the model illustrating fluid inlet and outlet

Table 6.1: Material properties in CFD analysis

Material	Density (kg/m³)	Specific heat (J/kg-K)	Viscosity (kg/m-s)	Thermal conductivity (W/m-K)
Tungsten carbide	15770	180	-	39
Water	998.2	4182	1.003e-03	0.6
Air	1.225	1006.43	1.7894e-05	0.0242

#### 6.3. Governing equations

In the current problem statement, the input heat shall be transferred into the tool body through conduction. This heat shall then be dissipated by the fluid flowing over the rake face through convective heat transfer. The conduction heat energy equation is represented in Eq. 6.1. Here,  $\rho_t$  denotes the density of the tool insert, C is the heat capacity, and K is the thermal conductivity of the insert.

$$\frac{\partial^2 T}{\partial x^2} + \frac{\partial^2 T}{\partial y^2} + \frac{\partial^2 T}{\partial z^2} = \frac{\rho_t C}{k} \frac{\partial T}{\partial t}$$
 Eq. 6.1

The heat conducted into the tool body is dissipated from the rake surface via convention to the fluid flowing over the surface. This governing equation is given by Eq. 6.2.

$$\dot{Q} = hA(T - T_f)$$
 Eq. 6.2

Here, Q is the heat transferred per unit time, h is the heat transfer coefficient, A is the surface area of the insert over which the fluid flows, T is the surface temperature of the insert, and  $T_f$  is the fluid temperature. The surface area term in Eq. 6.2 highlights the advantage of increasing the surface area to accelerate the heat dissipation from the hot body. The development of micro-pillars on the rake face is intended to exploit this feature of the heat transfer process. In CFD, the mass, momentum, and energy conservation approach is used to simulate the problem. The continuity equation gives the mass conservation equation as Eq. 6.3.

$$\frac{\partial u}{\partial x} + \frac{\partial v}{\partial y} + \frac{\partial w}{\partial z} = 0$$
 Eq. 6.3

Where u, v, w are the fluid velocity in the x, y, and z directions. The Navier-stokes equation gives the momentum conservation equation as Eq. 6.4a, 6.4b, and 6.4c. Its conservation equation includes the pressure, viscous, and body forces.

$$\rho\left(\frac{\partial u}{\partial t} + u\frac{\partial u}{\partial x} + v\frac{\partial u}{\partial y} + w\frac{\partial u}{\partial z}\right) = -\frac{\partial P}{\partial x} + \mu\left(\frac{\partial^2 u}{\partial x^2} + \frac{\partial^2 u}{\partial y^2} + \frac{\partial^2 u}{\partial z^2}\right) + F_x \quad \text{Eq. 6.4a}$$

$$\rho\left(\frac{\partial v}{\partial t} + u\frac{\partial v}{\partial x} + v\frac{\partial v}{\partial y} + w\frac{\partial v}{\partial z}\right) = -\frac{\partial P}{\partial y} + \mu\left(\frac{\partial^2 v}{\partial x^2} + \frac{\partial^2 v}{\partial y^2} + \frac{\partial^2 v}{\partial z^2}\right) + F_y \quad \text{Eq. 6.4b}$$

$$\rho\left(\frac{\partial w}{\partial t} + u\frac{\partial w}{\partial x} + v\frac{\partial w}{\partial y} + w\frac{\partial w}{\partial z}\right)$$

$$= -\frac{\partial P}{\partial z} + \mu\left(\frac{\partial^2 w}{\partial x^2} + \frac{\partial^2 w}{\partial y^2} + \frac{\partial^2 z}{\partial z^2}\right) + F_z$$
Eq. 6.4c

Where  $\rho$  is the fluid density,  $\mu$  is the fluid viscosity, and  $F_X$ ,  $F_Y$ , and  $F_Z$  are the forces acting on the fluid in x, y, and z directions. Energy conservation is based on the first law of thermodynamics, according to which the net energy in a control volume is equal to the energy entering the control volume minus the heat going out. Eq. 6.5 expresses the energy conservation equation. Here, Cp is the fluid's specific heat, and  $\lambda$  is the thermal conductivity of the fluid.

$$\rho C_P \left( u \frac{\partial T}{\partial x} + v \frac{\partial T}{\partial y} + w \frac{\partial T}{\partial z} \right) = \lambda \left( \frac{\partial^2 T}{\partial x^2} + \frac{\partial^2 T}{\partial y^2} + \frac{\partial^2 T}{\partial z^2} \right)$$
 Eq. 6.5

#### 6.4. Results and discussion

#### 6.4.1. Temperature measurement at a distant location

Turning experiments were conducted on a Ti6Al4V rod using the fabricated micropillar tool inserts and plain tool inserts (Chapter 5, Section 5.1). K-type thermocouples integrated with a data acquisition system were used to measure the cutting tool temperature at a distant location (point A) from the tooltip for all the machining conditions, as indicated in Figure 6.2. The micro-EDM process was used to drill blind holes on the rear side of turning inserts to embed the thermocouple at point A. The measured temperature at point A and the measured sticking contact area (Chapter 5, section 5.2.1) are used for inverse estimation of the tool tip temperature using CFD-based numerical simulations in the later part of the study.

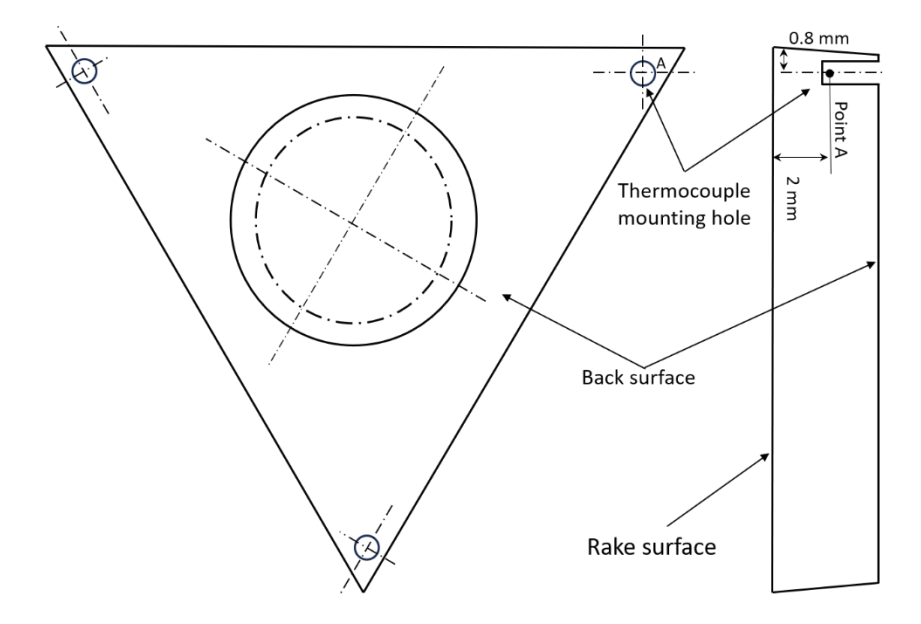


Figure 6.2. Schematic illustration of thermocouple mounting holes

The temperature measured by the embedded thermocouple during the turning operation under dry, compressed air and wet conditions are depicted in Figure 6.3. It is evident that the plain tool experiences a higher temperature compared to the textured tool, irrespective of the machining conditions. In dry condition a significant drop of 10.8 % is witnessed, followed by 7.6 % in compressed air and 4.2 % in wet condition. This indicates the effectiveness of the textured tools in adverse conditions. The major causes of this temperature drop are restricted tool-chip contact area and enhanced heat dissipation through the rake face. Micro-pillar textured tools are capable of inducing higher curling to the flowing chips, which mitigates the adhering tendency of the freshly formed chip underside to the rake surface. This aids in suppressing the additional heat generation in the seizure zone. Further, the increased

surface area due to the fabrication of micro-pillars on the rake face enhances convective heat transfer from the tool to the surrounding air/CF.

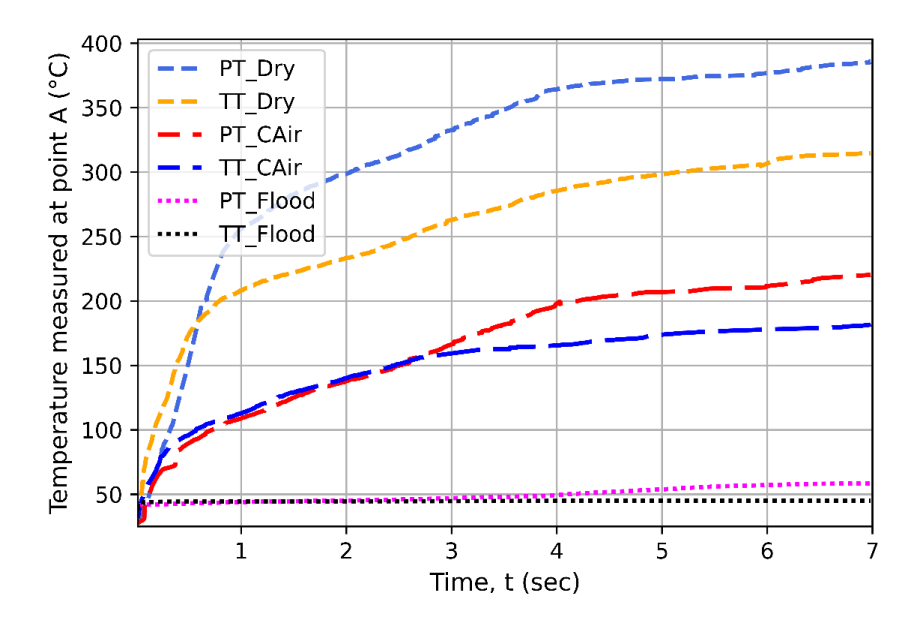


Figure 6.3: Measured tool temperature at a distant point A under various machining conditions

### 6.4.2. Analysis of cutting tool temperature using CFD

This section discusses the inverse estimation of tool tip temperature based on CFD analysis performed on the cutting tool inserts. The working model and the boundary conditions, as depicted in Figure 6.1, form the basis of this analysis. A uniform heat flux is applied to the experimentally obtained sticking contact area (Chapter 5, section 5.2.1), such that the simulated temperature becomes equal to the experimental tool temperature measured at a distant location A (refer to Figures 6.2 and 6.3). To ensure the accuracy of the results, a mesh convergence study is performed to negate the effect of element size, the findings of which are compiled in Figure 6.4. An element size of 30  $\mu$ m was used for the tool insert and the control volume, while a finer element size of 10  $\mu$ m was used for face meshing of the rake face due to the 20  $\mu$ m depth of the textures. These element sizes have been chosen as a trade-off between accuracy and computational time. The total elements for the plain and textured tools were 49,86,623 and 65,51,084, respectively.

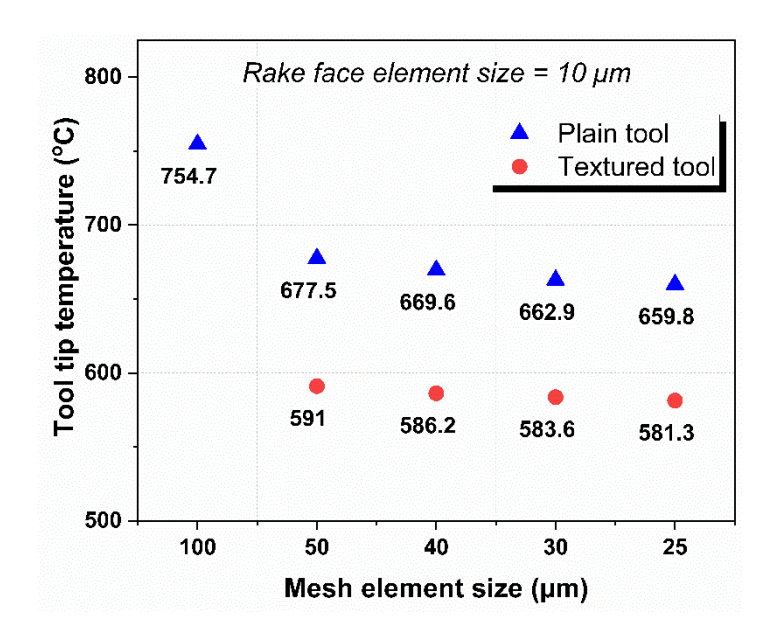


Figure 6.4. Mesh convergence results for maximum tool temperature of plain and textured tools

#### (a) Inverse estimation of tool tip temperature

Based on the inverse temperature estimation approach mentioned above, heat flux in the range of 15 to 22 W/mm<sup>2</sup> matched the experimental temperature, depending on the machining condition. Figure 6.5 shows the temperature contours of the tool section under various machining conditions. The experimentally obtained temperature is indicated by point A, which forms the reference for the study to fix the input heat flux over the experimentally obtained contact area on the rake face. The temperature at point B indicates the inversely estimated tool tip temperature. It can be observed that the estimated tool tip temperature for plain tools is significantly higher than the textured tools, irrespective of the machining condition. This resonates with the measured temperatures at point A. In dry condition, the tool tip temperature of the texture tool dropped by 7.5 % compared to the plain tool, while the temperature drop at point A for the same condition is about 10.8 %. A slightly higher temperature drop at the distant point A than at the tooltip (point B) suggests that the increased surface area due to the development of micro-pillars on the rake face enhances the convective heat dissipation through the rake face and hence a higher temperature drop in the textured tools. However, this trend does not hold true for compressed air and wet conditions. This is because an external source like compressed air or cutting fluid has superior heat dissipation capability, making the textures less effective in these cases. However, the textured tools have shown a significant temperature drop of 8.1 % and 13.3 % at point A for compressed air and flood conditions, respectively. Therefore, it can be concluded that under dry condition, tool temperature is controlled by low toolchip contact area and enhanced heat dissipation, whereas, for compressed air and wet conditions, it is majorly because of the lower tool-chip contact area.

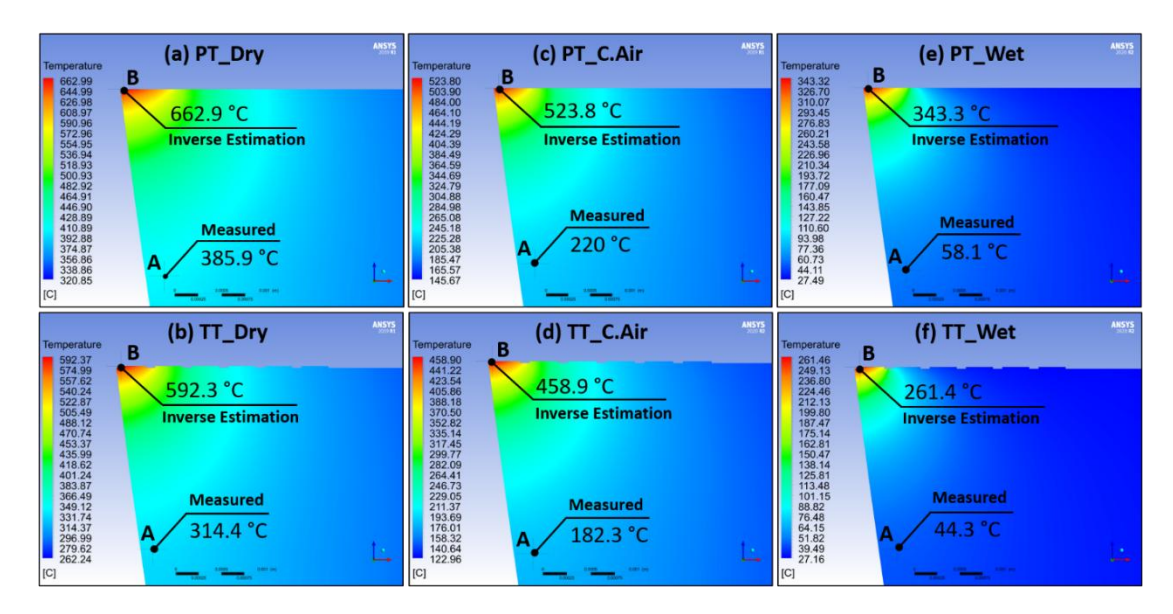


Figure 6.5: Temperature contours under dry, compressed air and wet conditions incorporating actual contact area: (a, c, e) Plain tools; (b,d,f) Textured tools

#### (b) Effect of micro-pillar texture size on tool temperature

Given the benefits associated with the micro-pillar textures developed on the rake face, it becomes necessary to study the effect of texture size on the tool temperature. From the basic knowledge of heat exchangers, it is well-known that long, closely-spaced fins of smaller diameter result in better heat dissipation from the hot body. However, the limitation associated with the existing manufacturing techniques to fabricate an array of micro-scale features makes this study challenging. Therefore, adopting a numerical approach becomes a feasible solution. The study in Chapter 4 revealed that increasing the depth of micro-pillars beyond 55 µm adversely affected its performance due to severe work material accumulation in between the textures. This restricts the use of higher-depth texture, which otherwise would enhance convective heat transfer. Moreover, the model developed in this study takes the tool-chip contact area as input, which is a function of texture shape and size. Thus, it should not be altered. Therefore, to explore the effect of texture size on tool temperature, the micro-pillar size was altered beyond the tool-chip contact area. Since textured tools were found to be most effective in improving convective heat transfer under dry conditions, only dry conditions are explored in the further part of the study.

Figure 6.6 indicates the effect of texture depth on the cutting tool temperature under dry condition. The diameter and pitch of the micro-pillar are kept constant at  $300 \mu m$ 

and 100  $\mu m$  respectively. It can be observed that increasing the depth of micro-pillars resulted in lower tool temperature due to improved convective heat transfer from the increased surface area of the rake face to the surrounding air. A temperature drop of 2.9 % is achieved by increasing the texture depth from 20  $\mu m$  to 100  $\mu m$ .

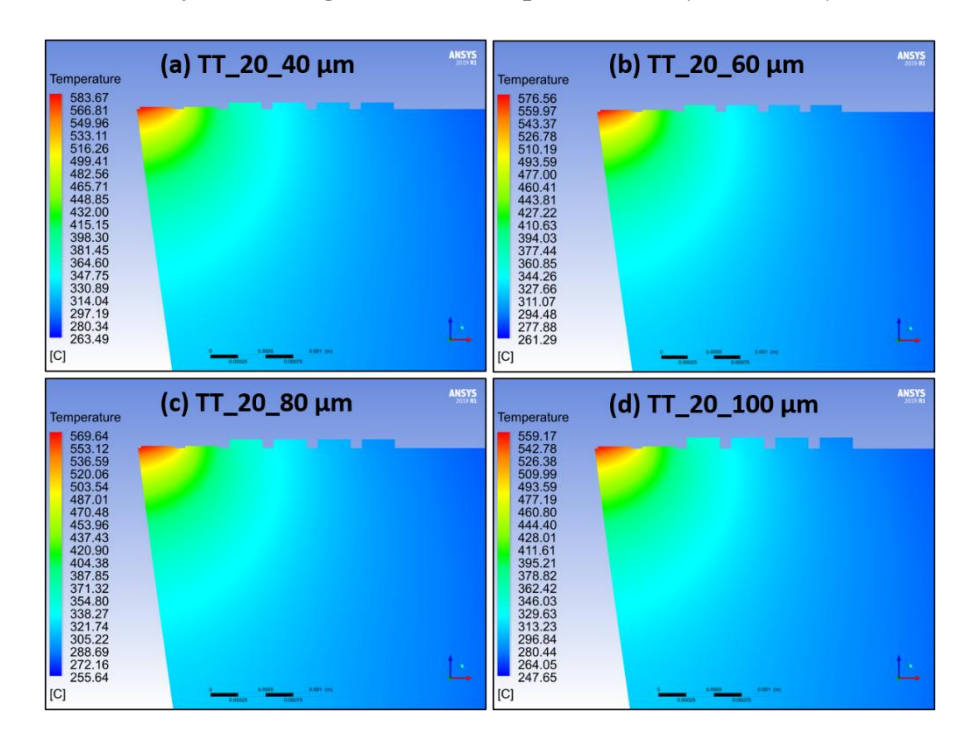


Figure 6.6: Temperature contours for textured tools with varying micro-pillar depth from 40  $\mu m$  to 100  $\mu m$  beyond the contact area under dry condition (Dia = 300  $\mu m$ , Pitch = 100  $\mu m$ )

The effect of change in diameter beyond the contact area at a constant depth and pitch of 100  $\mu$ m each is presented in Figure 6.7. Negligible improvement is observed in tool temperature. This is because the gap between two successive micro-pillars (pitch) is unaltered, which increases the number of micro-pillars but shifts them away from the machining region, thus making them ineffective.

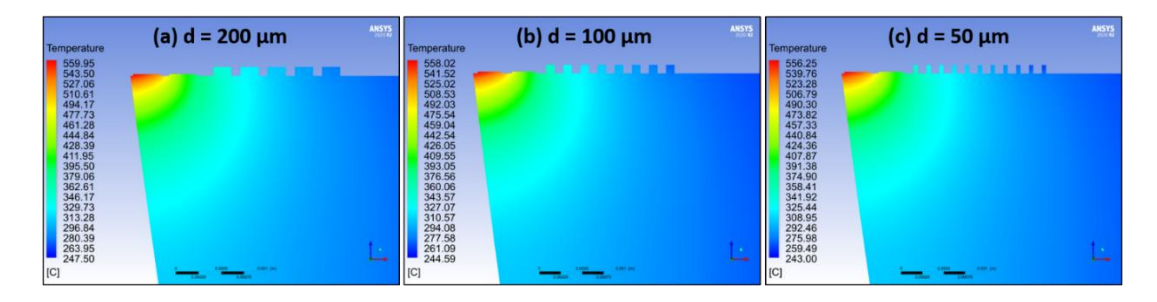


Figure 6.7: Temperature contours for textured tools with varying micro-pillar diameter from 200  $\mu$ m to 50  $\mu$ m beyond the contact area under dry condition (Depth = 100  $\mu$ m, Pitch = 100  $\mu$ m)

The effect of pitch variation at a constant diameter of 50  $\mu m$  and depth of 100  $\mu m$  on tool temperature is present in Figure 6.8. On decreasing the pitch from 200  $\mu m$  to 50  $\mu m$  a temperature drop of 2.3 % is witnessed. This is because a smaller pitch increases the number of micro-pillars in the confined region of interest, providing a larger surface area for heat dissipation. However, further reducing the pitch to 25  $\mu m$  adversely increased the tool temperature. This is probably due to extremely constrained passage between the micro-pillars, which would restrict the free flow of surrounding air through the textures up to the high-temperature region.

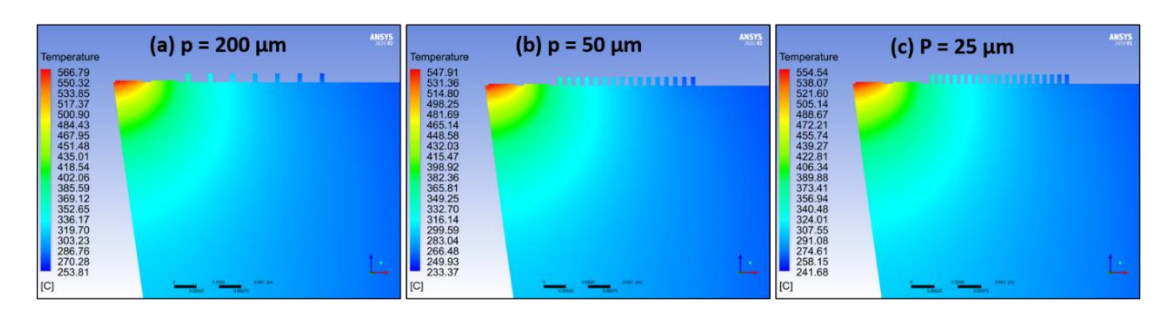


Figure 6.8: Temperature contours for textured tools with varying micro-pillar pitch from 200  $\mu$ m to 25  $\mu$ m beyond the contact area under dry condition (Depth = 100  $\mu$ m, dia = 50  $\mu$ m)

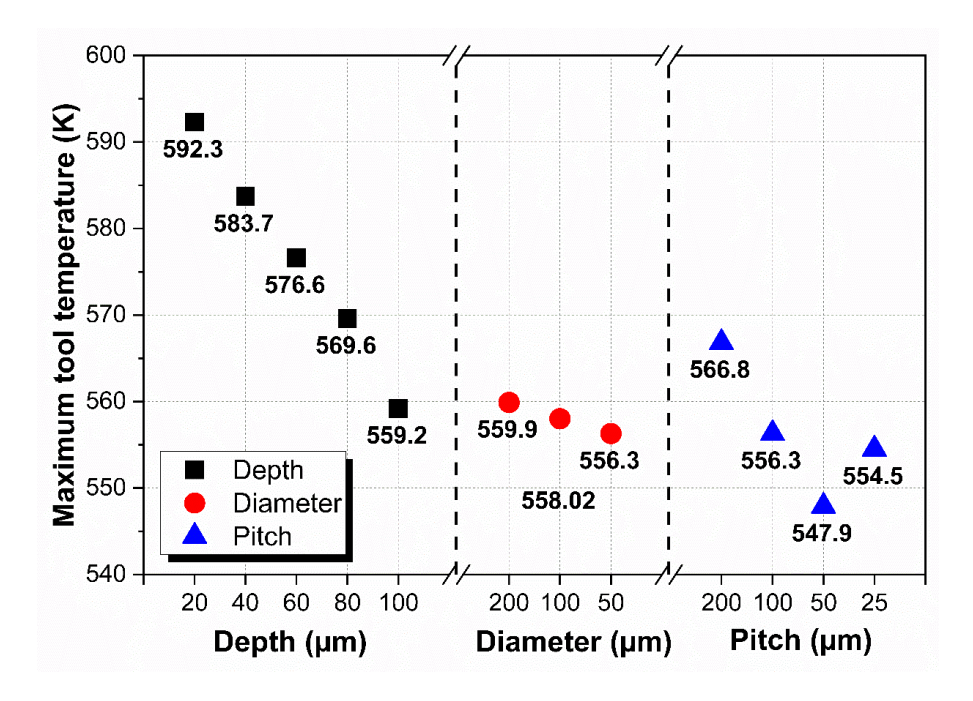


Figure 6.9: Effect of variation in micro-pillar depth, diameter and pitch beyond the contact area on the tool temperature under dry condition

These effects of variation in micro-pillar depth, diameter, and inter-micro-pillar gap tool temperature are compiled in Figure 6.9. An overall reduction of 5.1 % in tool tip temperature is achieved by increasing the texture depth from 20  $\mu$ m to 100  $\mu$ m and

decreasing the diameter and pitch from 300  $\mu m$  to 50  $\mu m$  and 200  $\mu m$  to 50  $\mu m$ , respectively.

### 6.5. Chapter conclusions

This chapter examines the heat dissipation capability of micro-pillar textures fabricated using  $R\mu EDM$  on tungsten carbide inserts while turning Ti6Al4V alloys. CFD-based numerical simulation determined the cutting tool temperature under Wet, dry and compressed air conditions using tool-chip contact area data from experiments. The key findings are:

- Reduced heat influx to the tool due to reduced contact at the tool-chip interface
  and enhanced heat dissipation from the increased surface area provided by the
  arrayed micro-pillar were the prime contributors to reduced tool temperature.
- Closely spaced (50  $\mu$ m) micro-pillars of smaller diameter (50  $\mu$ m) and higher depth (100  $\mu$ m) beyond the tool chip contact area reduced the peak tool temperature by 5.1 % compared to large, widely spaced and lower depth micro-pillars. However, the inter-micro-pillar gap should not be too low to hinder the flow of fluid through it, as observed in the 25  $\mu$ m pitch gap.

# CHAPTER 7 SUMMARY, CONCLUSION AND FUTURE SCOPE

This chapter summarises the findings of the thesis work, the aim of which was to "Explore the potential of a novel texture pattern on the rake face of cutting tools in restricting the tool/chip contact area and enhancing heat dissipation during the machining of a titanium alloy under sustainable dry and near-dry environments." In the end, it also recommends some critical issues that can be studied in the future.

### 7.1. Summary

The need to adopt sustainable approaches in machining is studied, which reveals the use of dry and near-dry environments as a sustainable alternative to flood lubrication and cooling systems. However, machining without cutting fluids has its challenges. Further different ways for enhancement of this sustainably viable approach are explored. Surface texturing of the cutting tools is found to improve the machining operation. A detailed review of the existing research on tool surface texturing revealed certain research gaps, based on which the research objectives of this thesis are defined.

**Objective 1:** Design and development of a novel texture pattern on cutting tool inserts

A new texture pattern design is proposed based on the limitations of the existing designs. This isotropic nature of the pattern can reduce directional dependency. The gaps between the micro-pillars promote air/cutting fluid penetration into the seizure zone, and the increased surface area of the rake face enhances heat dissipation.

Successful fabrication of micro-pillar arrays is demonstrated in Chapter 3 using reverse micro electrical discharge machining. During the fabrication process, spark frequency, discharge gap and surface morphology of the machined surface were analyzed to determine the suitable voltage-capacitance combination of 110 V and 100 nF.

**Objective 2:** Performance analysis of developed textures under dry machining conditions

Orthogonal machining is performed on a Ti6Al4V tube using plain and textured tools in a dry environment, the details and findings of which are presented in Chapter 4. A significant reduction in the sticking contact area on the rake face of textured tools is observed. A drop in the measured feed forces confirms the improvement in the frictional condition at the interface. Longer retention of cutting-edge sharpness is

determined in textured tools as concluded from the measured flank wear width. The chips produced are shorter, untangled and highly curled compared to plain tools. Textured tools aid in faster heat dissipation from the cutting region, as revealed by the preliminary tests performed using an external heat source. The tool tip temperature is estimated to be reduced to half for textured tools. Theoretical estimation of shear plane angle revealed the importance of contact length. A lower contact length, as observed in textured tools, gave a higher shear angle and lower total work rate.

The improved performance of the textured tools can be attributed to the disrupted chip momentum, which leads to tighter curling of the chips and the reduced chemical activeness of the freshly formed chip underside due to the enhanced capillary suction of the surrounding air at the interface.

Higher depths of micro-pillars resulted in excessive work-material accumulation between the micro-pillars, which deteriorated the overall performance of the textured tools. A depth in the range of 8  $\mu$ m to 30  $\mu$ m yielded superior results than the plain tools.

**Objective 3:** Performance analysis of developed textures under different machining conditions

Turning of a wrought and additively manufactured Ti6Al4V rod is performed using plain and textured tools under compressed air and MQL conditions. Dry and wet conditions are also examined for reference. These findings are presented in Chapter 5. The reasons for the better performance of the textured tools are similar to those discussed above with some additional contributors. The pressurized jet of air directed opposite to the chip flow direction continuously tries to uplift the chips from the rake face, further reducing the contact area at the interface. The added benefit of cutting fluids with the pressurized air in the MQL system further enhances the overall performance of the textured tools.

Two major but opposing mechanisms are observed in cutting forces results: First, the reduced chip/ tool contact area restricts the seizure zone to a smaller area, reducing the additional shearing of the chips in the secondary shear zone. This mechanism is directly reflected in measured feed forces; Second is the CF penetration beneath the chip and up to the cutting edge. Although this phenomenon is expected to reduce friction at the chip/tool interface, it also alters the flow stress of the work material due to quenching by the CF jet. This leads to a higher cutting force in wet and MQL conditions.

Overall, it can be concluded that compressed air condition performed far superior to dry condition, while MQL condition proved to be at par with the wet conditions.

#### **Objective 4:** *Numerical modeling of cutting tool temperature*

The tool-chip contact areas and tool temperature at a distant location obtained from the turning experiments are used to define the heat input on the rake face of cutting tools to perform a CFD-based numerical analysis. Chapter 6 presents the numerically estimated cutting tool temperature for different machining conditions. Two major reasons are observed for the reduced temperature of the textured tool: First, the reduced tool-chip contact area, which limits the heat entering the tools; Second, enhanced heat dissipation through the increased surface area of the tool's rake face.

Higher depth of the micro-pillars yielded lower tool temperature, but as concluded from Chapter 4, higher depth would lead to larger work-material accumulation. Therefore, it is proposed to have a lower texture depth in the tool chip sticking contact area to promote chip curling, whereas a higher texture depth beyond this region shall enhance heat dissipation. Closely placed micro-pillars of smaller diameter and higher depth beyond the tool chip contact area gave the lowest tool temperature.

#### 7.2. Conclusions

- The proposed micro-pillar texture pattern is successfully fabricated on the rake face of tungsten carbide inserts using reverse micro electrical discharge machining.
- The machinability of Ti6Al4V improved significantly in the presence of micropillars on the rake face. This can be primarily attributed to disturbed chip flow momentum, enhanced heat dissipation, and deeper air/cutting fluid penetration.
- Textured tools are highly capable of reducing the dependency on flood cooling and lubrication, as demonstrated by their performance under near-dry conditions.

It is expected the knowledge gained from this fundamental study will lead to the development of advanced cutting tools.

#### 7.3. Future scope

The current study can be further extended in the future on these lines:

Textured tools have shown better implementation of dry and near-dry machining.
 However, a scientific study on the sustainable assessment of textured tools is

- necessary. Life cycle assessment of the machining process shall further highlight the importance of textured tools as a sustainable alternative.
- The effect of shape and size of the micro-pillars have been investigated but beyond the tool-chip contact area. Its experimental investigation is very challenging; therefore, a finite element approach would reveal better insights into the effect of texture shape and size on its machining performance.
- Uncoated tools are used in this study to gain fundamental insight on the proposed texture pattern. However, coated tools are more practical in industries, therefore exploring coated micro-pillars is an avenue for further research.

#### References

- [1] World Bank. Manufacturing, value added (% of GDP). World Development Indicators 2022:1–18. http://data.worldbank.org/indicator/NV.IND.MANF.ZS.
- [2] World Economic Forum. Reducing the carbon footprint of the manufacturing industry through data sharing. World Economic Forum 2022. https://www.weforum.org/impact/carbon-footprint-manufacturing-industry/.
- [3] United States Environmental Protection Agency. Sustainable Manufacturing 2024. https://www.epa.gov/sustainability/sustainable-manufacturing.
- [4] Jayal AD, Badurdeen F, Dillon OW, Jawahir IS. Sustainable manufacturing: Modeling and optimization challenges at the product, process and system levels. CIRP J Manuf Sci Technol 2010;2:144–52. https://doi.org/10.1016/j.cirpj.2010.03.006.
- [5] Sustainable Development Goals. United Nations Department of Economic and Social Affairs 2012. https://sdgs.un.org/goals.
- [6] Trent EM (Edward M, Wright PKenneth. Metal cutting, 4th ed. 2000.
- [7] Klocke F, Eisenblaetter G. Dry cutting. CIRP Ann Manuf Technol 1997;46:519–26. https://doi.org/10.1016/S0007-8506(07)60877-4.
- [8] Narutaki N, Yamane Y, Tashima S, Kuroki H. A new advanced ceramic for dry machining. CIRP Ann Manuf Technol 1997;46:43–8. https://doi.org/10.1016/s0007-8506(07)60772-0.
- [9] Cheng C, Phipps D, Alkhaddar RM. Treatment of spent metalworking fluids. Water Res 2005;39:4051–63. https://doi.org/10.1016/j.watres.2005.07.012.
- [10] Debnath S, Reddy MM, Yi QS. Environmental friendly cutting fluids and cooling techniques in machining: A review. J Clean Prod 2014;83:33–47. https://doi.org/10.1016/j.jclepro.2014.07.071.
- [11] Bart JCJ, Gucciardi E, Cavallaro S. Environmental life-cycle assessment (LCA) of lubricants. Biolubricants 2013:527–64. https://doi.org/10.1533/9780857096326.527.
- [12] Bennett EO. Water based cutting fluids and human health. Tribol Int 1983;16:133–6. https://doi.org/10.1016/0301-679X(83)90055-5.
- [13] Hannu T, Suuronen K, Aalto-Korte K, Alanko K, Luukkonen R, Järvelä M, et al. Occupational respiratory and skin diseases among Finnish machinists: Findings of a large clinical study. Int Arch Occup Environ Health 2013;86:189–97. https://doi.org/10.1007/s00420-012-0754-8.
- [14] Lawal SA, Choudhury IA, Nukman Y. Application of vegetable oil-based metalworking fluids in machining ferrous metals A review. Int J Mach Tools Manuf 2012;52:1–12. https://doi.org/10.1016/j.ijmachtools.2011.09.003.
- [15] Metalworking Fluids: Safety and Health Best Practices Manual. Occupational Safety and Health Adminstration (OSHA) 1999. https://www.osha.gov/SLTC/metalworkingfluids/metalworkingfluids\_manual.html.

- [16] Osman KA, Ünver HÖ, Şeker U. Application of minimum quantity lubrication techniques in machining process of titanium alloy for sustainability: a review. International Journal of Advanced Manufacturing Technology 2019;100:2311–32. https://doi.org/10.1007/s00170-018-2813-0.
- [17] Lawal SA, Choudhury IA, Nukman Y. A critical assessment of lubrication techniques in machining processes: A case for minimum quantity lubrication using vegetable oilbased lubricant. J Clean Prod 2013;41:210–21. https://doi.org/10.1016/j.jclepro.2012.10.016.
- [18] Boswell B, Islam MN, Davies IJ, Ginting YR, Ong AK. A review identifying the effectiveness of minimum quantity lubrication (MQL) during conventional machining. International Journal of Advanced Manufacturing Technology 2017;92:321–40. https://doi.org/10.1007/s00170-017-0142-3.
- [19] Ezugwu EO, Wang ZM. Titanium alloys and their machinability A review. J Mater Process Technol 1997;68:262–74. https://doi.org/10.1016/S0924-0136(96)00030-1.
- [20] Yang X, Liu CR. Machining titanium and its alloys. Machining Science and Technology 1999;3:107–39. https://doi.org/10.1080/10940349908945686.
- [21] Cui C, Hu BM, Zhao L, Liu S. Titanium alloy production technology, market prospects and industry development. Mater Des 2011;32:1684–91. https://doi.org/10.1016/j.matdes.2010.09.011.
- [22] Rack HJ, Qazi JI. Titanium alloys for biomedical applications. Materials Science and Engineering C 2006;26:1269–77. https://doi.org/10.1016/j.msec.2005.08.032.
- [23] Machado AR, J Wallbank J. Machining of Titanium and its Alloys—a Review. Proc Inst Mech Eng B J Eng Manuf 1990;204:53–60. https://doi.org/10.1243/PIME\_PROC\_1990\_204\_047\_02.
- [24] Komanduri R, Reed WR. Evaluation of carbide grades and a new cutting geometry for machining titanium alloys. Wear 1983;92:113–23. https://doi.org/10.1016/0043-1648(83)90011-X.
- [25] Khanna N, Davim JP. Design-of-experiments application in machining titanium alloys for aerospace structural components. Measurement (Lond) 2015;61:280–90. https://doi.org/10.1016/j.measurement.2014.10.059.
- [26] Goindi GS, Sarkar P. Dry machining: A step towards sustainable machining Challenges and future directions. J Clean Prod 2017;165:1557–71. https://doi.org/10.1016/j.jclepro.2017.07.235.
- [27] Airao J, Nirala CK, Bertolini R, Krolczyk GM, Khanna N. Sustainable cooling strategies to reduce tool wear, power consumption and surface roughness during ultrasonic assisted turning of Ti-6Al-4V. Tribol Int 2022;169. https://doi.org/10.1016/j.triboint.2022.107494.
- [28] Rahman Rashid RA, Sun S, Wang G, Dargusch MS. An investigation of cutting forces and cutting temperatures during laser-assisted machining of the Ti-6Cr-5Mo-5V-4Al beta titanium alloy. Int J Mach Tools Manuf 2012;63:58–69. https://doi.org/10.1016/j.ijmachtools.2012.06.004.

- [29] Kaynak Y, Lu T, Jawahir IS. Cryogenic machining-induced surface integrity: A review and comparison with dry, mql, and flood-cooled machining. Machining Science and Technology 2014;18:149–98. https://doi.org/10.1080/10910344.2014.897836.
- [30] Lu P, Wood RJK. Tribological performance of surface texturing in mechanical applications-a review. Surf Topogr 2020;8. https://doi.org/10.1088/2051-672X/abb6d0.
- [31] Durairaj S, Guo J, Aramcharoen A, Castagne S. An experimental study into the effect of micro-textures on the performance of cutting tool. International Journal of Advanced Manufacturing Technology 2018;98:1011–30. https://doi.org/10.1007/s00170-018-2309-y.
- [32] Ma J, Duong NH, Lei S. 3D numerical investigation of the performance of microgroove textured cutting tool in dry machining of Ti-6Al-4V. International Journal of Advanced Manufacturing Technology 2015;79:1313–23. https://doi.org/10.1007/s00170-015-6937-1.
- [33] Kawasegi N, Kawashima T, Morita N, Nishimura K, Yamaguchi M, Takano N. Effect of texture shape on machining performance of textured diamond cutting tool. Precis Eng 2019;60:21–7. https://doi.org/10.1016/j.precisioneng.2019.07.007.
- [34] Fang Z, Obikawa T. Cooling performance of micro-texture at the tool flank face under high pressure jet coolant assistance. Precis Eng 2017;49:41–51. https://doi.org/10.1016/j.precisioneng.2017.01.008.
- [35] Sawant MS, Jain NK, Palani IA. Influence of dimple and spot-texturing of HSS cutting tool on machining of Ti-6Al-4V. J Mater Process Technol 2018;261:1–11. https://doi.org/10.1016/j.jmatprotec.2018.05.032.
- [36] Kumar Mishra S, Ghosh S, Aravindan S. Machining performance evaluation of Ti6Al4V alloy with laser textured tools under MQL and nano-MQL environments. J Manuf Process 2020;53:174–89. https://doi.org/10.1016/j.jmapro.2020.02.014.
- [37] Sugihara T, Enomoto T. Development of a Cutting Tool with a Textured Surface for Dry Cutting of Aluminum Alloys. International Journal of Automation Technology 2009;3:199–203. https://doi.org/10.20965/ijat.2009.p0199.
- [38] Xie J, Luo MJ, He JL, Liu XR, Tan TW. Micro-grinding of micro-groove array on tool rake surface for dry cutting of titanium alloy. International Journal of Precision Engineering and Manufacturing 2012;13:1845–52. https://doi.org/10.1007/s12541-012-0242-9.
- [39] Sugihara T, Enomoto T. Performance of cutting tools with dimple textured surfaces: A comparative study of different texture patterns. Precis Eng 2017;49:52–60. https://doi.org/10.1016/j.precisioneng.2017.01.009.
- [40] Gajrani KK, Suresh S, Sankar MR. Environmental friendly hard machining performance of uncoated and MoS2 coated mechanical micro-textured tungsten carbide cutting tools. Tribol Int 2018;125:141–55. https://doi.org/10.1016/j.triboint.2018.04.031.
- [41] Kishawy HA, Salem A, Hegab H, Hosseini A, Balazinski M. Micro-textured cutting tools: Phenomenological analysis and design recommendations. CIRP Annals 2021;70:65–8. https://doi.org/10.1016/j.cirp.2021.04.081.

- [42] Kishawy HA, Salem A, Hegab H, Hosseini A, Elbestawi M. An analytical model for the optimized design of micro-textured cutting tools. CIRP Annals 2022;71:49–52. https://doi.org/10.1016/j.cirp.2022.04.067.
- [43] Kümmel J, Braun D, Gibmeier J, Schneider J, Greiner C, Schulze V, et al. Study on micro texturing of uncoated cemented carbide cutting tools for wear improvement and built-up edge stabilisation. J Mater Process Technol 2015;215:62–70. https://doi.org/10.1016/j.jmatprotec.2014.07.032.
- [44] Smart EF, Trent EM. Coolants and Cutting Tool Temperatures. 1975:187–95. https://doi.org/10.1007/978-1-349-01986-1\_22.
- [45] Wright PK. Frictional interactions in machining: Comparisons between transparent sapphire and steel cutting tools. Metals Technology 1981;8:150–60. https://doi.org/10.1179/030716981803275406.
- [46] Rowe GW, Smart EF. The importance of oxygen in dry machining of metal on a lathe. British Journal of Applied Physics 1963;14:924–6. https://doi.org/10.1088/0508-3443/14/12/325.
- [47] Mazurkiewicz M, Kubala Z, Chow J. Metal machining with high-pressure water-jet cooling assistance-a new possibility. Journal of Manufacturing Science and Engineering, Transactions of the ASME 1989;111:7–12. https://doi.org/10.1115/1.3188736.
- [48] Diaz N, Choi S, Helu M, Chen Y, Jayanathan S, Yasui Y, et al. Machine Tool Design and Operation Strategies for Green Manufacturing 2010.
- [49] Dudzinski D, Devillez A, Moufki A, Larrouquère D, Zerrouki V, Vigneau J. A review of developments towards dry and high speed machining of Inconel 718 alloy. Int J Mach Tools Manuf 2004;44:439–56. https://doi.org/10.1016/S0890-6955(03)00159-7.
- [50] Devillez A, Schneider F, Dominiak S, Dudzinski D, Larrouquere D. Cutting forces and wear in dry machining of Inconel 718 with coated carbide tools. Wear 2007;262:931–42. https://doi.org/10.1016/j.wear.2006.10.009.
- [51] Sreejith PS, Ngoi BKA. Dry machining: Machining of the future. J Mater Process Technol 2000;101:287–91. https://doi.org/10.1016/S0924-0136(00)00445-3.
- [52] Ulutan D, Ozel T. Machining induced surface integrity in titanium and nickel alloys: A review. Int J Mach Tools Manuf 2011;51:250–80. https://doi.org/10.1016/j.ijmachtools.2010.11.003.
- [53] Sharma AK, Tiwari AK, Dixit AR. Effects of Minimum Quantity Lubrication (MQL) in machining processes using conventional and nanofluid based cutting fluids: A comprehensive review. J Clean Prod 2016;127:1–18. https://doi.org/10.1016/j.jclepro.2016.03.146.
- [54] Kamata Y, Obikawa T. High speed MQL finish-turning of Inconel 718 with different coated tools. J Mater Process Technol 2007;192–193:281–6. https://doi.org/10.1016/j.jmatprotec.2007.04.052.
- [55] Kishawy HA, Dumitrescu M, Ng EG, Elbestawi MA. Effect of coolant strategy on tool performance, chip morphology and surface quality during high-speed machining of

- A356 aluminum alloy. Int J Mach Tools Manuf 2005;45:219–27. https://doi.org/10.1016/j.ijmachtools.2004.07.003.
- [56] Sharma AK, Tiwari AK, Dixit AR. Effects of Minimum Quantity Lubrication (MQL) in machining processes using conventional and nanofluid based cutting fluids: A comprehensive review. J Clean Prod 2016;127:1–18. https://doi.org/10.1016/j.jclepro.2016.03.146.
- [57] Korkmaz ME, Gupta MK, Çelik E, Ross NS, Günay M. A sustainable cooling/lubrication method focusing on energy consumption and other machining characteristics in high-speed turning of aluminum alloy. Sustainable Materials and Technologies 2024;40. https://doi.org/10.1016/j.susmat.2024.e00919.
- [58] Sharma KA, Tiwari AK, Dixit AR. Improved Machining Performance with Nanoparticle Enriched Cutting Fluids under Minimum Quantity Lubrication (MQL) Technique: A Review. Mater Today Proc 2015;2:3545–51. https://doi.org/10.1016/j.matpr.2015.07.066.
- [59] Syam Sundar L, Singh MK, Sousa ACM. Investigation of thermal conductivity and viscosity of Fe3O4 nanofluid for heat transfer applications. International Communications in Heat and Mass Transfer 2013;44:7–14. https://doi.org/10.1016/j.icheatmasstransfer.2013.02.014.
- [60] Peng DX, Kang Y, Hwang RM, Shyr SS, Chang YP. Tribological properties of diamond and SiO2 nanoparticles added in paraffin. Tribol Int 2009;42:911–7. https://doi.org/10.1016/j.triboint.2008.12.015.
- [61] Lee K, Hwang Y, Cheong S, Choi Y, Kwon L, Lee J, et al. Understanding the role of nanoparticles in nano-oil lubrication. Tribol Lett 2009;35:127–31. https://doi.org/10.1007/s11249-009-9441-7.
- [62] Amrita M, Srikant RR, Sitaramaraju A V. Performance evaluation of nanographite-based cutting fluid in machining process. Materials and Manufacturing Processes 2014;29:600–5. https://doi.org/10.1080/10426914.2014.893060.
- [63] Gupta A, Kumar R, Kumar Kansal H, Garg H. Effect of nanoparticles mixing-ratio of Al2O3-MWCNT hybrid nano-cutting fluid during MQL turning. Materials and Manufacturing Processes 2024;39:43–54. https://doi.org/10.1080/10426914.2023.2187825.
- [64] Khanna N, Agrawal C, Pimenov DY, Singla AK, Machado AR, da Silva LRR, et al. Review on design and development of cryogenic machining setups for heat resistant alloys and composites. J Manuf Process 2021;68:398–422. https://doi.org/10.1016/j.jmapro.2021.05.053.
- [65] Yildiz Y, Nalbant M. A review of cryogenic cooling in machining processes. Int J Mach Tools Manuf 2008;48:947–64. https://doi.org/10.1016/j.ijmachtools.2008.01.008.
- [66] Kaynak Y, Gharibi A. Cryogenic Machining of Titanium Ti-5553 Alloy. Journal of Manufacturing Science and Engineering, Transactions of the ASME 2019;141. https://doi.org/10.1115/1.4042605.

- [67] Dhananchezian M. Study the machinability characteristics of Nicked based Hastelloy C-276 under cryogenic cooling. Measurement (Lond) 2019;136:694–702. https://doi.org/10.1016/j.measurement.2018.12.072.
- [68] Khanna N, Agrawal C, Dogra M, Pruncu CI. Evaluation of tool wear, energy consumption, and surface roughness during turning of inconel 718 using sustainable machining technique. Journal of Materials Research and Technology 2020;9:5794–804. https://doi.org/10.1016/j.jmrt.2020.03.104.
- [69] Wang Y, Han L, Liu K, Gan Y, Dai M, Liu H. Optimization of jet parameters for minimizing surface roughness in cryogenic milling of Ti-6Al-4V. Journal of Manufacturing Science and Engineering, Transactions of the ASME 2021;143. https://doi.org/10.1115/1.4049034.
- [70] Yang Z, Zhu L, Zhang G, Ni C, Lin B. Review of ultrasonic vibration-assisted machining in advanced materials. Int J Mach Tools Manuf 2020;156. https://doi.org/10.1016/j.ijmachtools.2020.103594.
- [71] Machado AR, da Silva LRR, Pimenov DY, de Souza FCR, Kuntoğlu M, de Paiva RL. Comprehensive review of advanced methods for improving the parameters of machining steels. J Manuf Process 2024;125:111–42. https://doi.org/10.1016/j.jmapro.2024.07.044.
- [72] Arefin S, Zhang XQ, Kumar AS, Neo DWK, Wang Y. Study of chip formation mechanism in one-dimensional vibration-assisted machining. J Mater Process Technol 2021;291. https://doi.org/10.1016/j.jmatprotec.2020.117022.
- [73] Sharma V, Pandey PM. Optimization of machining and vibration parameters for residual stresses minimization in ultrasonic assisted turning of 4340 hardened steel. Ultrasonics 2016;70:172–82. https://doi.org/10.1016/j.ultras.2016.05.001.
- [74] Willert M, Zielinski T, Rickens K, Riemer O, Karpuschewski B. Impact of ultrasonic assisted cutting of steel on surface integrity. Procedia CIRP 2020;87:222–7. https://doi.org/10.1016/j.procir.2020.02.009.
- [75] Attia H, Tavakoli S, Vargas R, Thomson V. Laser-assisted high-speed finish turning of superalloy Inconel 718 under dry conditions. CIRP Ann Manuf Technol 2010;59:83–8. https://doi.org/10.1016/j.cirp.2010.03.093.
- [76] Ahn JW, Woo WS, Lee CM. A study on the energy efficiency of specific cutting energy in laser-assisted machining. Appl Therm Eng 2016;94:748–53. https://doi.org/10.1016/j.applthermaleng.2015.10.129.
- [77] Ding H, Shin YC. Laser-assisted machining of hardened steel parts with surface integrity analysis. Int J Mach Tools Manuf 2010;50:106–14. https://doi.org/10.1016/j.ijmachtools.2009.09.001.
- [78] Panjehpour A, Soleymani Yazdi MR, Shoja-Razavi R. An experimental investigation of pulsed laser-assisted machining of AISI 52100 steel. Opt Laser Technol 2014;63:137–43. https://doi.org/10.1016/j.optlastec.2014.03.018.

- [79] Farahnakian M, Razfar MR. Experimental study on hybrid ultrasonic and plasma aided turning of hardened steel AISI 4140. Materials and Manufacturing Processes 2014;29:550–6. https://doi.org/10.1080/10426914.2014.892612.
- [80] Deswal N, Kant R. Hybrid turning process by interacting ultrasonic vibration and laser energies. Materials and Manufacturing Processes 2023;38:570–6. https://doi.org/10.1080/10426914.2022.2065014.
- [81] Taylor FW. On the Art of Cutting Metals. Transactions of the American Society of Mechanical Engineers 1906;28:31–279. https://doi.org/10.1115/1.4060388.
- [82] Groover MP. Fundamentals of Modern Manufacturing: Material, Processes, and Systems. John Wiley & Sons; 2010.
- [83] Jianxin D, Tongkun C, Xuefeng Y, Jianhua L. Self-lubrication of sintered ceramic tools with CaF2 additions in dry cutting. Int J Mach Tools Manuf 2006;46:957–63. https://doi.org/10.1016/j.ijmachtools.2005.07.047.
- [84] Jaffery SI, Mativenga PT. Assessment of the machinability of Ti-6Al-4V alloy using the wear map approach. International Journal of Advanced Manufacturing Technology 2009;40:687–96. https://doi.org/10.1007/s00170-008-1393-9.
- [85] Machado AR, da Silva LRR, de Souza FCR, Davis R, Pereira LC, Sales WF, et al. State of the art of tool texturing in machining. J Mater Process Technol 2021;293. https://doi.org/10.1016/j.jmatprotec.2021.117096.
- [86] Sugihara T, Enomoto T. Development of a cutting tool with a nano/micro-textured surface-Improvement of anti-adhesive effect by considering the texture patterns. Precis Eng 2009;33:425–9. https://doi.org/10.1016/j.precisioneng.2008.11.004.
- [87] Enomoto T, Sugihara T. Improving anti-adhesive properties of cutting tool surfaces by nano-/micro-textures. CIRP Ann Manuf Technol 2010;59:597–600. https://doi.org/10.1016/j.cirp.2010.03.130.
- [88] Sugihara T, Enomoto T. Improving anti-adhesion in aluminum alloy cutting by micro stripe texture. Precis Eng 2012;36:229–37. https://doi.org/10.1016/j.precisioneng.2011.10.002.
- [89] Sugihara T, Enomoto T. Crater and flank wear resistance of cutting tools having micro textured surfaces. Precis Eng 2013;37:888–96. https://doi.org/10.1016/j.precisioneng.2013.05.007.
- [90] Enomoto T, Sugihara T, Yukinaga S, Hirose K, Satake U. Highly wear-resistant cutting tools with textured surfaces in steel cutting. CIRP Ann Manuf Technol 2012;61:571–4. https://doi.org/10.1016/j.cirp.2012.03.123.
- [91] Siju AS, Gajrani KK, Joshi SS. Dual textured carbide tools for dry machining of titanium alloys. Int J Refract Metals Hard Mater 2021;94. https://doi.org/10.1016/j.ijrmhm.2020.105403.
- [92] Mishra SK, Ghosh S, Aravindan S. 3D finite element investigations on textured tools with different geometrical shapes for dry machining of titanium alloys. Int J Mech Sci 2018;141:424–49. https://doi.org/10.1016/j.ijmecsci.2018.04.011.

- [93] Mishra SK, Ghosh S, Aravindan S. Characterization and machining performance of laser-textured chevron shaped tools coated with AlTiN and AlCrN coatings. Surf Coat Technol 2018;334:344–56. https://doi.org/10.1016/j.surfcoat.2017.11.061.
- [94] Gajrani KK, Suvin PS, Kailas SV, Rajurkar KP, Sankar MR. Machining of hard materials using textured tool with minimum quantity nano-green cutting fluid. CIRP J Manuf Sci Technol 2021;35:410–21. https://doi.org/10.1016/j.cirpj.2021.06.018.
- [95] Koshy P, Tovey J. Performance of electrical discharge textured cutting tools. CIRP Ann Manuf Technol 2011;60:153–6. https://doi.org/10.1016/j.cirp.2011.03.104.
- [96] Kawasegi N, Ozaki K, Morita N, Nishimura K, Yamaguchi M. Development and machining performance of a textured diamond cutting tool fabricated with a focused ion beam and heat treatment. Precis Eng 2017;47:311–20. https://doi.org/10.1016/j.precisioneng.2016.09.005.
- [97] Ma J, Ge X, Qiu C, Lei S. FEM assessment of performance of microhole textured cutting tool in dry machining of Ti-6Al-4V. International Journal of Advanced Manufacturing Technology 2016;84:2609–21. https://doi.org/10.1007/s00170-015-7918-0.
- [98] Xie J, Luo MJ, Wu KK, Yang LF, Li DH. Experimental study on cutting temperature and cutting force in dry turning of titanium alloy using a non-coated micro-grooved tool. Int J Mach Tools Manuf 2013;73:25–36. https://doi.org/10.1016/j.ijmachtools.2013.05.006.
- [99] Arulkirubakaran D, Senthilkumar V, Kumawat V. Effect of micro-textured tools on machining of Ti-6Al-4V alloy: An experimental and numerical approach. Int J Refract Metals Hard Mater 2016;54:165–77. https://doi.org/10.1016/j.ijrmhm.2015.07.027.
- [100] Obikawa T, Kamio A, Takaoka H, Osada A. Micro-texture at the coated tool face for high performance cutting. Int J Mach Tools Manuf 2011;51:966–72. https://doi.org/10.1016/j.ijmachtools.2011.08.013.
- [101] Mishra SK, Ghosh S, Aravindan S. Performance of laser processed carbide tools for machining of Ti6Al4V alloys: A combined study on experimental and finite element analysis. Precis Eng 2019;56:370–85. https://doi.org/10.1016/j.precisioneng.2019.01.006.
- [102] Kothari CR. Research methodology: Methods and techniques. Second rev. New Age International; 2004.
- [103] Flick U. Introducing Research Methodology: A Beginner's Guide to Doing a Research Project. Sage; 2015.
- [104] Kishore H, Nirala CK, Agrawal A. Feasibility demonstration of μEDM for fabrication of arrayed micro pin-fins of complex cross-sections. Manuf Lett 2020;23:14–8. https://doi.org/10.1016/j.mfglet.2019.11.005.
- [105] Kishore H, Nirala CK, Agrawal A. Exploring AZ31B magnesium alloy for innovative micro products by reverse- $\mu$ EDM. Mater Lett 2022;328. https://doi.org/10.1016/j.matlet.2022.133109.

- [106] Raza S, Nadda R, Nirala CK. Analysis of Discharge Gap using Controlled RC based Circuit in μEDM Process. Journal of The Institution of Engineers (India): Series C 2022;103:21–7. https://doi.org/10.1007/s40032-021-00711-w.
- [107] Arulkirubakaran D, Senthilkumar V, Kumawat V. Effect of micro-textured tools on machining of Ti-6Al-4V alloy: An experimental and numerical approach. Int J Refract Metals Hard Mater 2016;54:165–77. https://doi.org/10.1016/j.ijrmhm.2015.07.027.
- [108] Bergmann B, Denkena B, Schaper F. Thermomechanical tool loading and chip formation in oxygen-free titanium cutting. CIRP J Manuf Sci Technol 2023;45:253–9. https://doi.org/10.1016/j.cirpj.2023.06.016.
- [109] Siju AS, Waigaonkar SD. Effects of rake surface texture geometries on the performance of single-point cutting tools in hard turning of titanium alloy. J Manuf Process 2021;69:235–52. https://doi.org/10.1016/j.jmapro.2021.07.041.
- [110] Abukhshim NA, Mativenga PT, Sheikh MA. Heat generation and temperature prediction in metal cutting: A review and implications for high speed machining. Int J Mach Tools Manuf 2006;46:782–800. https://doi.org/10.1016/j.ijmachtools.2005.07.024.
- [111] Elkaseer A, Lambarri J, Sarasua JA, Cascón I. On the development of a chip breaker in a metal-matrix polycrystalline diamond insert: Finite element based design with ns-laser ablation and machining verification. J Micro Nanomanuf 2017;5. https://doi.org/10.1115/1.4036933.
- [112] Fang YJ, Fang XD, Basu A. a 3-D Kinematic Model of Complex Chip Curling With Chip Breaker Tools in Metal Cutting. Part I: Analytical Modelling. ASME International Mechanical Engineering Congress and Exposition, Proceedings (IMECE) 1997;1997-W:177–82. https://doi.org/10.1115/IMECE1997-1150.
- [113] Wallbank J. Structure of built-up edge formed in metal cutting. Metals Technology 1979;6:145–53. https://doi.org/10.1179/030716979803276426.
- [114] Rowe GW, Spick PT. A New Approach to Determination of the Shear-Plane Angle in Machining. Journal of Engineering for Industry 1967;89:530–8. https://doi.org/10.1115/1.3610103.
- [115] Godlevski VA, Volkov A V., Latyshev VN, Maurin LN. The kinetics of lubricant penetration action during machining. Lubrication Science 1997;9:127–40. https://doi.org/10.1002/ls.3010090203.
- [116] Jawahir IS, van Luttervelt CA. Recent Developments in Chip Control Research and Applications. CIRP Ann Manuf Technol 1993;42:659–93. https://doi.org/10.1016/S0007-8506(07)62531-1.
- [117] Nakayama K, Arai M. Comprehensive Chip Form Classification Based on the Cutting Mechanism. CIRP Ann Manuf Technol 1992;41:71–4. https://doi.org/10.1016/S0007-8506(07)61155-X.
- [118] Jayal AD, Balaji AK. Tribological and thermal effects of cutting fluid application in machining with coated and grooved cutting tools. American Society of Mechanical Engineers, Manufacturing Engineering Division, MED 2005;16–1:513–20. https://doi.org/10.1115/IMECE2005-82963.

- [119] Puertas Arbizu I, Luis Pérez CJ. Surface roughness prediction by factorial design of experiments in turning processes. J Mater Process Technol 2003;143–144:390–6. https://doi.org/10.1016/S0924-0136(03)00407-2.
- [120] He CL, Zong WJ, Zhang JJ. Influencing factors and theoretical modeling methods of surface roughness in turning process: State-of-the-art. Int J Mach Tools Manuf 2018;129:15–26. https://doi.org/10.1016/j.ijmachtools.2018.02.001.
- [121] Niketh S, Samuel GL. Drilling performance of micro textured tools under dry, wet and MQL condition. J Manuf Process 2018;32:254–68. https://doi.org/10.1016/j.jmapro.2018.02.012.
- [122] Khanna N, Zadafiya K, Patel T, Kaynak Y, Rahman Rashid RA, Vafadar A. Review on machining of additively manufactured nickel and titanium alloys. Journal of Materials Research and Technology 2021;15:3192–221. https://doi.org/10.1016/j.jmrt.2021.09.088.
- [123] Li G, Chandra S, Rahman Rashid RA, Palanisamy S, Ding S. Machinability of additively manufactured titanium alloys: A comprehensive review. J Manuf Process 2022;75:72–99. https://doi.org/10.1016/j.jmapro.2022.01.007.
- [124] Majeed M, Khan HM, Rasheed I. Finite element analysis of melt pool thermal characteristics with passing laser in SLM process. Optik (Stuttg) 2019;194. https://doi.org/10.1016/j.ijleo.2019.163068.
- [125] Cai C, Radoslaw C, Zhang J, Yan Q, Wen S, Song B, et al. In-situ preparation and formation of TiB/Ti-6Al-4V nanocomposite via laser additive manufacturing: Microstructure evolution and tribological behavior. Powder Technol 2019;342:73–84. https://doi.org/10.1016/j.powtec.2018.09.088.
- [126] Gong H, Rafi K, Gu H, Starr T, Stucker B. Analysis of defect generation in Ti-6Al-4V parts made using powder bed fusion additive manufacturing processes. Addit Manuf 2014;1:87–98. https://doi.org/10.1016/j.addma.2014.08.002.
- [127] Gu D, Hong C, Meng G. Densification, microstructure, and wear property of in situ titanium nitride-reinforced titanium silicide matrix composites prepared by a novel selective laser melting process. Metall Mater Trans A Phys Metall Mater Sci 2012;43:697–708. https://doi.org/10.1007/s11661-011-0876-8.
- [128] Gu DD, Meiners W, Wissenbach K, Poprawe R. Laser additive manufacturing of metallic components: Materials, processes and mechanisms. International Materials Reviews 2012;57:133–64. https://doi.org/10.1179/1743280411Y.0000000014.
- [129] Galindo-Fernández MA, Mumtaz K, Rivera-Díaz-del-Castillo PEJ, Galindo-Nava EI, Ghadbeigi H. A microstructure sensitive model for deformation of Ti-6Al-4V describing Cast-and-Wrought and Additive Manufacturing morphologies. Mater Des 2018;160:350–62. https://doi.org/10.1016/j.matdes.2018.09.028.
- [130] Gong H, Rafi K, Gu H, Janaki Ram GD, Starr T, Stucker B. Influence of defects on mechanical properties of Ti-6Al-4V components produced by selective laser melting and electron beam melting. Mater Des 2015;86:545–54. https://doi.org/10.1016/j.matdes.2015.07.147.

- [131] Rafi HK, Karthik N V., Gong H, Starr TL, Stucker BE. Microstructures and mechanical properties of Ti6Al4V parts fabricated by selective laser melting and electron beam melting. J Mater Eng Perform 2013;22:3872–83. https://doi.org/10.1007/s11665-013-0658-0.
- [132] Raval J, Kazi A, Randolph O, Guo X, Zvanut R, Lee C, et al. Machinability comparison of additively manufactured and traditionally wrought Ti-6Al-4V alloys using single-point cutting. J Manuf Process 2023;94:539–49. https://doi.org/10.1016/j.jmapro.2023.03.041.
- [133] Nguyen HD, Pramanik A, Basak AK, Dong Y, Prakash C, Debnath S, et al. A critical review on additive manufacturing of Ti-6Al-4V alloy: Microstructure and mechanical properties. Journal of Materials Research and Technology 2022;18:4641–61. https://doi.org/10.1016/j.jmrt.2022.04.055.
- [134] Chan KS, Koike M, Mason RL, Okabe T. Fatigue life of titanium alloys fabricated by additive layer manufacturing techniques for dental implants. Metall Mater Trans A Phys Metall Mater Sci 2013;44:1010–22. https://doi.org/10.1007/s11661-012-1470-4.
- [135] Sartori S, Bordin A, Moro L, Ghiotti A, Bruschi S. The Influence of Material Properties on the Tool Crater Wear When Machining Ti6Al4 v Produced by Additive Manufacturing Technologies. Procedia CIRP 2016;46:587–90. https://doi.org/10.1016/j.procir.2016.04.032.
- [136] Sartori S, Moro L, Ghiotti A, Bruschi S. On the tool wear mechanisms in dry and cryogenic turning Additive Manufactured titanium alloys. Tribol Int 2017;105:264–73. https://doi.org/10.1016/j.triboint.2016.09.034.
- [137] Bordin A, Bruschi S, Ghiotti A, Bucciotti F, Facchini L. Comparison between wrought and EBM Ti6Al4V machinability characteristics. Key Eng Mater 2014;611–612:1186–93. https://doi.org/10.4028/www.scientific.net/KEM.611-612.1186.
- [138] Bordin A, Sartori S, Bruschi S, Ghiotti A. Experimental investigation on the feasibility of dry and cryogenic machining as sustainable strategies when turning Ti6Al4V produced by Additive Manufacturing. J Clean Prod 2017;142:4142–51. https://doi.org/10.1016/j.jclepro.2016.09.209.
- [139] Polishetty A, Shunmugavel M, Goldberg M, Littlefair G, Singh RK. Cutting Force and Surface Finish Analysis of Machining Additive Manufactured Titanium Alloy Ti-6Al-4V. Procedia Manuf 2017;7:284–9. https://doi.org/10.1016/j.promfg.2016.12.071.
- [140] Li G, Rashid RAR, Ding S, Sun S, Palanisamy S. Machinability Analysis of Finish-Turning Operations for Ti6Al4V Tubes Fabricated by Selective Laser Melting. Metals (Basel) 2022;12. https://doi.org/10.3390/met12050806.
- [141] Stephenson DA. Tool-work thermocouple temperature measurements—theory and implementation issues. Journal of Manufacturing Science and Engineering, Transactions of the ASME 1993;115:432–7. https://doi.org/10.1115/1.2901786.
- [142] Santos MC, Araújo Filho JS, Barrozo MAS, Jackson MJ, Machado AR. Development and application of a temperature measurement device using the tool-workpiece thermocouple method in turning at high cutting speeds. International Journal of

- Advanced Manufacturing Technology 2017;89:2287–98. https://doi.org/10.1007/s00170-016-9281-1.
- [143] Chen WC, Tsao CC, Liang PW. Determination of temperature distributions on the rake face of cutting tools using a remote method. International Communications in Heat and Mass Transfer 1997;24:161–70. https://doi.org/10.1016/S0735-1933(97)00002-X.
- [144] Dearnley PA. New technique for determining temperature distribution in cemented carbide cutting tools. Metals Technology 1983;10:205–14. https://doi.org/10.1179/030716983803291578.
- [145] Oezkaya E, Beer N, Biermann D. Experimental studies and CFD simulation of the internal cooling conditions when drilling Inconel 718. Int J Mach Tools Manuf 2016;108:52–65. https://doi.org/10.1016/j.ijmachtools.2016.06.003.
- [146] López De Lacalle LN, Angulo C, Lamikiz A, Sánchez JA. Experimental and numerical investigation of the effect of spray cutting fluids in high speed milling. J Mater Process Technol 2006;172:11–5. https://doi.org/10.1016/j.jmatprotec.2005.08.014.
- [147] Singh R, Sharma V. CFD based study of fluid flow and heat transfer effect for novel turning tool configured with internal cooling channel. J Manuf Process 2022;73:164–76. https://doi.org/10.1016/j.jmapro.2021.10.063.
- [148] Fang Z, Obikawa T. Turning of Inconel 718 using inserts with cooling channels under high pressure jet coolant assistance. J Mater Process Technol 2017;247:19–28. https://doi.org/10.1016/j.jmatprotec.2017.03.032.
- [149] Li T, Wu T, Ding X, Chen H, Wang L. Design of an internally cooled turning tool based on topology optimization and CFD simulation. International Journal of Advanced Manufacturing Technology 2017;91:1327–37. https://doi.org/10.1007/s00170-016-9804-9.